A.D. MDLXII

UNIVERSITY OF SASSARI

DEPARTMENT OF BIOMEDICAL SCIENCES

Ph.D. Course in Life Sciences and Biotechnologies

Curriculum Biochemistry, Physiology and Molecular Biology

XXIX cycle

CORDINATOR: PROF. LEONARDO ANTONIO SECHI

LRRK2 effect on dopamine receptor trafficking – implication in Parkinson's disease

Tutor:
Dr. Ciro Iaccarino

Ph.D. student:
Mauro Rassu

Academic year 2015/2016

Index

Abstract

Parkinson disease (PD) is the second most common neurodegenerative disorder affecting 4 million people worldwide. It is characterized by the loss of dopaminergic neurons in the Substantia Nigra pars compacta (SNpc) and by the presence of cytoplasmic inclusion bodies (Lewy bodies, LB). Cell death leads to a profound depletion of dopamine neurotransmitter involved mainly in the control of the movement. Mutations in LRRK2 (leucine-rich repeat kinase 2) gene (PARK8; OMIM #609007) are responsible for one of the autosomal-dominant forms of Parkinson's disease. LRRK2 is a protein of 2527 amino acids composed by different functional domains: ankyrin, leucine-rich repeat (LRR), Roc (Ras in complex proteins), COR domain (C-terminal of Roc), protein kinase catalytic domain and a WD40 domain. LRRK2 mutations associated with PD have been identified in different protein domains. These observations, along with the lack of deletion or truncation mutants with dominant inheritance, suggest a gain of function mechanism. Up to date, the LRRK2 biological function is largely unknown. LRRK2 appears to be localized in different intracellular districts that play a critical role in the control of vesicular trafficking: ER, Golgi apparatus and associated vesicles, cytoskeleton, lipid raft and lysosomes. Although, some discrepancies between different experimental approaches, the involvement of LRRK2 in the regulation of vesicle trafficking appears quite consistent both in animal and cellular models. In neurons, vesicle trafficking is a complex process regulating multiple different cellular functions, in addition to the neurotransmitter release or re-uptake, such as the localization and levels of membrane receptors, changes in plasma membrane composition at the cell surface and, not least, organelle biogenesis.

This research focuses on LRRK2 role in the regulation of D1 and D2 dopamine receptors trafficking. Considering the relevance of dopamine receptor trafficking in DA neuronal physiology, this research may have a strong implication in the discovery of the pathological mechanisms underlying the PD onset and development. This work indicates that PD-associated mutant G2019S LRRK2 impairs dopamine receptor D1 internalization, leading to an alteration in signal transduction. Moreover, the mutant forms of LRRK2 affect dopamine receptor D2 turnover by decreasing the rate of the receptor trafficking from the Golgi complex to the cell membrane. Collectively, these findings are consistent with the conclusion that LRRK2 influences the motility of neuronal vesicles and the neuronal receptor trafficking. These findings have important implications to clarify the complex role that LRRK2 plays in neuronal physiology and the possible pathological mechanisms that may lead to neuronal death in PD.

Mauro Rassu: "LRRK2 effect on dopamine receptor trafficking – implication in Parkinson's disease".
Ph.D. Course in Life Sciences and Biotechnologies – University of Sassari.

Chapter 1

Introduction

1.1 Parkinson's disease

Parkinson's disease (PD) is a chronic, neurodegenerative, progressive disease, described for the first time in 1817 in the *Essay on the Shaking Palsy* by the English medical doctor James Parkinson. PD is the second most common neurodegenerative disorder after Alzheimer disease and affect approximately 20/100000 cases per year in the population over 50 years, up to 120/100000 new cases per year among the over 70 years old[1]. In about 95% of PD cases, no an apparent genetic cause (sporadic PD) in the pathogenesis of PD can be detected, but in the remaining 5% it seems hereditary. Stronger differences in incidence are observed among different ethnic groups, probably due to the disease etiology linked to environmental risk factors or genetic susceptibility. The average age onset is around 60 years, even if the 4% of the patients show an early disease development (before 50 years). Unfortunately, since the clinical symptoms appear only when more than 50-60% of the neurons of the Substantia Nigra pars compacta (SNpc) are damaged and the striatal levels of dopamine are strongly reduced[1], it is currently possible that the disease arises before the symptomatology therefore there is a high percentage of people, apparently healthy, that are developing PD.

The cardinal motor features that describe PD are resting tremor, bradykinesia, postural instability and muscle rigidity.

The PD clinical symptoms are due by a progressive and profound loss of dopaminergic neurons in the Substantia Nigra pars compacta (SNpc). These neurons project mainly to the striatum (i.e., putamen and caudate nucleus). The loss of the nigrostriatal dopaminergic neurons causes a profound depletion of dopamine in the striatum that is responsible of the trigger and control of movement (figure 1).
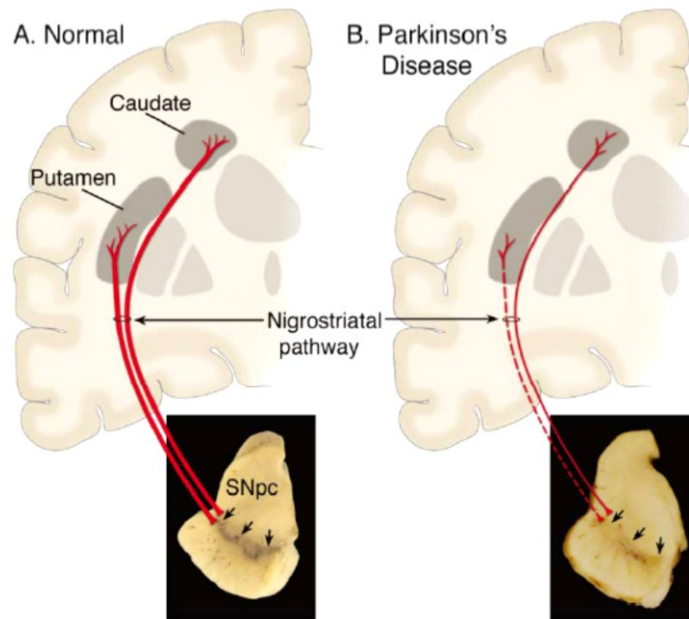

Figura 1. Schematic representation of the Nigrostriatal pathway. In red the Nigrostriatal pathway. It is composed of dopaminergic neurons whose cell bodies are located in the SNpc. These neurons projections to striatum (A) in physiological conditions and (B) in PD conditions; Down is shown the (A) SNpc in normal conditions and (B) the depigmentation of SNpc caused by the loss of dopaminergic neurons in PD patients[1].

PD is the most common form of Parkinsonism. In some cases the differential diagnosis among PD and other Parkinsonism forms is easy, in other cases more difficult. The main forms of Parkinsonism syndromes are described in table 1.

Up to date, the 80% of patients have a PD diagnosis "possible or probable". The final diagnosis need the post mortem analysis to highlight the loss of dopaminergic neurons, the depigmentation of SNpc and presence of Lewy Body (spherical eosinophilic cytoplasmic protein aggregates composed of numerous proteins, including α-synuclein, parkin, ubiquitin, and neurofilaments[2, 3]) in the surviving neurons. LBs are not specific for PD, they are also found in Alzheimer disease, in a condition called "dementia with LB disease" and as an incidental pathologic finding in people of

advanced age at a greater frequency than the prevalence of PD[4]. In life, the diagnosis of PD is made through the analysis of the clinical features, but definite diagnosis requires the identification of both LB and SNpc dopaminergic neuron loss. This permit to distinguish PD to others parkinsonism forms[1, 5].

Parkinsonism syndromes

Primary Parkinsonism
    Parkinson disease (sporadic, familial)
Secondary Parkinsonism
    Drug-induced: dopamine antagonists and depletors
    Hemiatrophy-hemiparkinsonism
    Hydrocephalus: normal pressure hydrocephalus
    Hypoxia
    Infectious: postencephalitic
    Metabolic: parathyroid dysfunction
    Toxin: Mn, CO, MPTP, cyanide
    Trauma
    Tumor
    Vascular: multiinfarct state
Parkinson-plus Syndromes
    Cortical-basal ganglionic degeneration
    Dementia syndromes: Alzheimer disease, diffuse Lewy body disease, frontotemporal dementia
    Lytico-Bodig (Guamanian Parkinsonism-dementia-ALS)
    Multiple system atrophy syndromes: striatonigral degeneration, Shy-Drager syndrome, sporadic olivopontocerebellar degeneration (OPCA), motor neuron disease-parkinsonism
    Progressive pallidal atrophy Progressive supranuclear palsy
Familial Neurodegenerative Diseases
    Hallervorden-Spatz disease
    Huntington disease
    Lubag (X-linked dystonia-parkinsonism)
    Mitochondrial cytopathies with striatal necrosis
    Neuroacanthocytosis
    Wilson disease

MPTP, 1-methyl-4-phenyl-1,2,3,6-tetrahydropyridine; ALS, amytrophic lateral sclerosis.

Table 1. The main forms of Parkinsonism syndromes[1].

1.2 Dopamine and dopamine receptors

Dopamine synthesis and metabolism

Dopamine (DA) with adrenaline and noradrenaline, are the catecholamine neurotransmitter class. Even though DA is an important brain neurotransmitter, a significant part of the DA is not produced in the brain but by the mesenteric organs[6].

Dates back 60 years ago the discovery of the physiological functions of 3-hydroxytyramine (DA)[7]. The two-step of DA synthesis begin in the cytosol of catecholaminergic neurons. The first step is the hydroxylation of L-tyrosine at the phenol ring by tyrosine hydroxylase (TH) to generate DOPA. DOPA is subsequently decarboxylated to DA by aromatic amino acid decarboxylase (AADC, also known as DOPA decarboxylase). Moreover, a cytochrome P450-mediated pathway has been shown to exist in rat in vivo[8, 9]. In this pathway decarboxylation forerun hydroxylation; tyrosine is decarboxylated to tyramine and then is hydroxylated by Cyp2D proteins (figure 2)[9]. Another pathway of DA synthesis is operated by tyrosinase via hydroxylation. Eumelanins and phaeomelanins are normally synthetize by tyrosinase, but it has been shown that tyrosinase have a central role in TH-negative mice for catecholamine synthesis[10]. After synthesis, in catecholaminergic neurons, the vesicular monoamine transporter 2 (VMAT2), by secondary active transport, operates the DA accumulation into synaptic vesicles[11] (figure 2). In vesicles, the oxidation of DA is stabilized by the acidic pH[12] and this prevents oxidative stress in the cytosol[13].

Upon excitation of dopaminergic neurons, the membrane of the synaptic vesicles melts with the presynaptic element cell membrane. In this way dopamine is released into the synaptic cleft to bind the postsynaptic DA receptors or the regulatory presynaptic DA autoreceptors[14, 15]. Successively, extracellular DA has to be removed from the synaptic cleft to stop the signaling pathway. DA can be recycled after reuptake by dopaminergic neurons or be degraded after uptake by glial cells. The neuronal reuptake is operated by the dopamine transporter (DAT) at level of the presynaptic element and accumulates into synaptic vesicles by VMAT2[16]. The DA that remains in the cytosol is quickly depredated by monoamine oxidase (MAO) to prevent

ROS formation. MAO enzyme catalyzes the oxidative deamination of DA to produce hydrogen peroxide and 3,4 -dihydroxyphenylacetaldehyde (DOPAL). DOPAL can be inactivated in two major pathways, by reduction to the alcohol 3,4-dihydroxyphenylethanol (DOPET) via alcohol dehydrogenase (ADH) or by oxidation to the carboxylic acid 3,4-dihydroxyphenylacetic acid (DOPAC) via aldehyde dehydrogenase (ALDH). Under normal conditions, the majority of DOPAL is oxidized to the carboxylic acid DOPAC[17].

In the synaptic cleft DA can be recovered by glial cells. Glial cells quickly degrade DA by MAO and also by catechol-O methyl transferase (COMT). COMT catalyze the metalation reaction by the transfer of the methyl groups from S-adenosylmethionine (SAM) to hydroxyl groups of various catecholic compounds. MAO reaction produces DOPAC that in subsequently converted in homovanilic acid (HVA), one of the most important products of the degradation of DA (figure 2). It has been shown that there is COMT activity in glial cells but no COMT activity in the dopaminergic nigro-striatal neurons[18, 19].
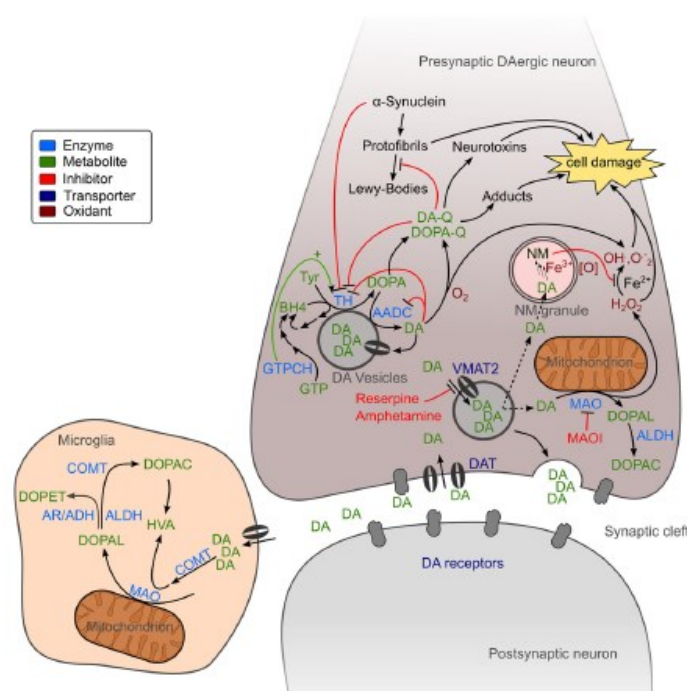

Figure 2. Neuronal DA metabolism. See text for details[19].

Dopaminergic system and dopamine receptors in the brain

Three major dopaminergic pathways have been identified in the mammalian brain; the nigrostriatal (originating in the A9 area), mesolimbic-mesocortical (originating in the A10 area) and tuberoinfundibular (originating in the A8 area)[20, 21]. These different pathways are known to be important for various vital functions regulated by the central nervous system. The nigrostriatal pathway is primary involved in the control of the motor functions. The mesolimbic-mesocortical pathway is mainly involved in the control of the behavior. The tuberoinfundibular is mainly involved in the control of the endocrine system[22-25].

Based on their structural, pharmacological, and biochemical properties, dopamine receptors have been classified as D1-like dopamine receptors D1 and D5 or D2-like dopamine receptors D2, D3, and D4[26-28]. It is know that the D1-like dopamine receptors (D1 and D5) activate the $G\alpha_{s/olf}$ family of G proteins to produce cAMP by stimulation of the adenylate cyclase. D1-like dopamine receptor are located exclusively on the plasma membrane of the postsynaptic neurons in the dopaminergic transmission. The D2-like dopamine receptors (D2, D3, and D4) interact with the $G\alpha_{i/o}$ family of G proteins to induce inhibition of adenylate cyclase. In contrast to the D1-like dopamine receptors, D2 and D3 dopamine receptors are postsynaptic and presynaptic in the dopaminergic synaptic transmission[29-31]. The D1- and D2-like dopamine receptors are also different at the level of genetic structure, presence of splice variants, G protein coupling agonists, selective agonists and antagonists and their brain distribution (table2).

Dopamine receptor subtype	D1-like		D2-like		
	D1	**D5**	**D2**	**D3**	**D4**
Gene symbol	*DRD1*	*DRD5*	*DRD2*	*DRD3*	*DRD4*
Chromosome gene map locus	5q35.1	4p16.1	*11q23.1*	3q13.3	11p15.5
Numbers of introns in the coding region	None	None	6	5	3
Pseudogenes	None	*DRD5P1, DRD5P2*	None	None	None
Presence of splice variants	None	None	D2S, D2L	Yes	Yes
Number of aminoacids	446	477	D2S, 414; D2L, 443	400	387
Molecular weight	49,300	52,951	D2S, 47,347; D2L, 50,619	44,225	41,487
G protein coupling agonists	$G\alpha_s$, $G\alpha_{olf}$	$G\alpha_s$, $G\alpha_q$	$G\alpha_i$, $G\alpha_o$	$G\alpha_i$, $G\alpha_o$	$G\alpha_i$, $G\alpha_o$
Effector pathway	↑cAMP	↑cAMP	↓cAMP, ↑K+ channel, ↓Ca2+ channel	↓cAMP	↓cAMP
Selective agonists	Fenoldopam, SKF-38393, SKF-81297	None	Bromocriptine, pergolide, cabergoline, ropinirole	7-OH-DPAT, pramipexole, rotigotine, (+)-PD-128907	A-412997, ABT-670, PD-168,077
Selective antagonist	SCH-23390, SCH-39166, SKF-83566	None	Haloperidol, spiperone, raclopride, sulpiride, risperidone	Nafadotride, GR 103,691, GR 218,231, SB-277011A	A-381393, FAUC 213, L-745,870, L-750,667
mRNA distribution in the brain	Caudate-putamen, nucleus accumbens, olfactory tubercle	Hippocampus, hypothalamus	Caudate-putamen, nucleus accumbens, olfactory tubercle	Olfactory tubercle, hypothalamus, nucleus accumbens	Frontal cortex, medulla, midbrain

Table 2. Basic genetic, structural and pharmacological properties of dopamine receptor subtypes [25, 32].

Dopamine receptors have different expression patterns in the brain. D1 dopamine receptors have been found at a high level of density in the nigrostriatal, mesolimbic, and mesocortical areas, as well as the striatum, nucleus accumbens, substantia nigra, olfactory bulb, amygdala, and frontal cortex. On the contrary dopamine receptor D1 is expressed at lower levels in the hippocampus, cerebellum, thalamic areas and hypothalamic areas. D5 dopamine receptors have been found at low levels of density in different brain regions, such as pyramidal neurons of the prefrontal cortex, the premotor cortex, the cingulated cortex, the entorhinal cortex, substantia nigra, hypothalamus and the hippocampus. A very low level of expression has also been observed in the MSNs of the caudate nucleus and nucleus accumbens[23, 29, 33, 34]. At the cellular level, the large spiny neurons of neostriatum in primates, that are typically cholinergic interneurons, only express D5 receptors[35]. Highest levels of dopamine receptors D2 have been detected in the striatum, nucleus accumbens and in the olfactory tubercle D2 receptors are also expressed at detectable levels in the substantia nigra, ventral tegmental area, hypothalamus, cortical areas, septum, amygdala, and hippocampus[23, 28, 36, 37]. The dopamine receptors D3 are more limited in distribution, the highest level of expression have been found in the limbic areas, such as in the shell of the nucleus accumbens, the olfactory tubercle, and the islands of Calleja[23, 38]. At lower levels, the dopamine receptors D3 have been found in the striatum, the substantia nigra pars compacta, the ventral tegmental area, the hippocampus, the septal area, and in various cortical areas. Dopamine receptors D4 have been found a lower level of density in the frontal cortex, amygdala, hippocampus, hypothalamus, globus pallidus, substantia nigra pars reticulata, and thalamus[23, 31].

Dopamine receptors and locomotor activity

Different experimental evidence shows that the dopaminergic system is involved in the control of locomotor activity across species[39]. Locomotor activity is at least regulated by dopamine receptors D1, D2 and D3[23, 40]. The activation of dopamine receptors D1 has a moderate stimulatory effect on locomotor activity. The roles of the dopamine receptors D2 and D3 are much more complex than D1 dopamine receptors due to their presynaptic and postsynaptic localization[23, 40]. Presynaptic autoreceptors are important

for the negative feedback mechanism involved in neuronal synthesis and release of the neurotransmitter in response to synaptic cleft neurotransmitter levels[23, 40, 41]. Presynaptic D2-like autoreceptors stimulation gives rise to a decrease in dopamine release and consequently a decrease in locomotor activity. On the contrary, an activation of postsynaptic receptors stimulates locomotor activity. Since D2-like autoreceptors are more sensitive to dopamine than D2-like postsynaptic receptors, dopamine can induce a biphasic effect that is resumed in a decrease in locomotor activity at low dopamine doses and locomotor activation at high dopamine doses. Moreover, dopamine receptor D2 has two splice variants D2L and D2S, with different synaptic distributions. D2S is mainly presynaptic and D2L is mainly postsynaptic. Consequently, the effects of the postsynaptic and presynaptic D2 dopamine receptors are probably determined by the different contributions of these isoforms[42, 43]. Different pharmacological[44, 45] and genetic studies in dopamine receptor D3 knockout mice[40, 46] show that D3 autoreceptors can also play a role in the regulation of tonically released dopamine, in a synergic manner with D2S autoreceptor in regulating the neuronal firing rate, synthesis and release of dopamine[43]. Dopamine receptor D3 probably has a moderate inhibitory function on locomotor activity due to autoreceptors and postsynaptic receptors activity[40, 46]. The roles played by dopamine receptors D4 and D5, that are expressed at lower level in the primary motor regions of the brain, appear to be not very important in the control of locomotor activity[23, 31, 40]. It is obvious that both the postsynaptic D1- and D2-like dopamine receptors are essential for the completely manifestation of locomotor activity[47].

Dopamine receptors signaling and trafficking

G protein-coupled receptors (GPCRs) are seven transmembrane (TM) proteins representing the largest and most expressed cell surface receptors. They play important roles in a broad array of cellular functions and in diseases and represent the targets for a large fraction of existing drugs[48-50]. GPCRs, upon ligand binding, induce dissociation of G proteins into their Gα and Gβγ components and ultimately modulate the activity of enzyme or ion channel effectors[51-53]. In the canonical view of G protein-coupled receptor (GPCR) signaling, the agonist binds the receptor in its binding site in

the extracellular or transmembrane regions of the receptor. Subsequently the conformation of the GPCR receptor changes and operates as a guanine nucleotide exchange factor, catalyzing the exchange of the GDP in GTP on the Gα subunit. Than the Gα and Gβγ subunits dissociate from each other and from the GPCR receptor[54]. Subsequently, signal transduction cascades are activated directly or by generating second messengers (such as cyclic AMP, diacylglycerol (DAG) and inositol-1,4,5-trisphosphate (Ins(1,4,5)P3) that modulate downstream effectors, such as protein kinase A (PKA) and protein kinase C (PKC). The Gβγ subunits, after their release from the heterotrimeric G protein complex, can bind and regulate other downstream effectors, such as ion channels and PLCβ. G protein-mediated signaling can be terminated by GPCR phosphorylation by GPCR kinases (GRKs) and concomitant association with arrestins. Subsequently, close to the GPCR-arrestin complex is assembled an AP2-clathrin complex to drive GPCR internalization into endosomes and receptor desensitization. The mitogen-activated protein kinase extracellular signal-regulated kinase (ERK) pathway can also be activated not only via the main signal transduction cascades but also through the interaction of the GPCR-arrestin complex. Following internalization, the endosomes containing GPCR receptors can melt with lysosome to be ultimately degraded, or can be recycled in the recycling endosomes pool and go back to the cell surface in the functional process of resensitization[53, 55, 56]. This general model can be applied to dopamine receptors (table 2 and figure 3).

Dopaminergic modulation of ATP in cAMP and cAMP in AMP conversion, operated by the adenylyl cyclase and phosphodiesterase respectively, results in the regulation of protein kinase A (PKA) and potentially other exchange proteins activated by cAMP[25, 57]. PKA substrates such as Protein phosphatase 1 regulatory subunit 1B (DARPP-32/PPP1R1B) have been extensively studied over the last 30 years. When phosphorylated on Thr34 by PKA, DARPP-32 is a negative regulator of protein phosphatase 1 (PP1). In contraposition, phosphorylation of DARPP-32 on Thr75 by cyclin-dependent kinase 5 (CDK5), in response to dopamine receptor D1 activation, results in PKA inhibition[55, 58].
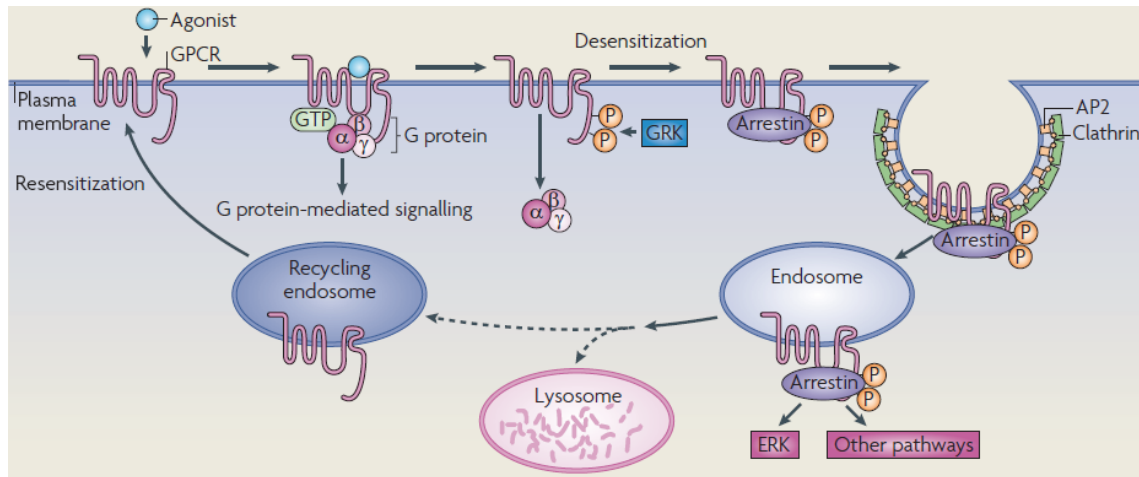
Figura 3. Canonical mechanisms for GPRC's signaling and trafficking[53].

Furthermore, other important dopamine signaling pathways have also been discovered, including the modulation of the Akt-GSK3 signaling pathway[59] and the activation of the PAR4 signaling pathway[60].

Receptor–Receptor Interactions: Homomeric and heteromeric dopamine receptors

Dopamine receptors can physically interacts with its own type or other receptors in the plasma membrane of neurons, to form homomers or heteromers respectively, or high-order receptor oligomers[61-64]. In a receptor mosaic model view, each receptor represents a single tile inside the mosaic; furthermore, receptors in the mosaic have different features and properties compared to each single receptor that compose the mosaic[64-66].

In the brain, the dopamine receptors D1 and D2 are the most abundant dopamine receptor expressed. For reason of brevity in this paragraph it will be explained only the interaction D1-D2, and D1-D3 heteromers for their implication in movement disorders. See table 3 for more information about dopamine receptors heteromer interactions.

The physiological relevance of dopamine receptor D1–D2 heterodimers is supported by the co-expression of D1 and D2 receptors in small populations of medium spiny neurons (MSNs) of the nucleus accumbens (NAc) in the mouse[67] and in other regions

of the basal ganglia[68]. Dopamine receptors D1 and D2 can form heteromeric receptor complexes through electrostatic interactions among a specific glutamic acid residues in the carboxyl-tail of the dopamine receptor D1 and an arginine residues in the third intracellular loop of the dopamine receptor D2[69]. The expression of dopamine receptors D1-D2 heteromers has been reported to exist at presynaptic but not at postsynaptic terminals of MSNs. Up to now, different data suggest that neurons expressing dopamine receptors D1-D2 heteromers may have a unique physiological function compared to the neurons expressing dopamine receptor monomers at local level and distal level[70, 71]. Dopamine receptors D1-D2 heteromers can stimulate calcium signaling, by Gq/11 and phospholipase C (PLC) activation, resulting in the activation of calcium calmodulin kinase IIa (CaMKII)[72-74] and increased expression of brain-derived neurotrophic factor (BDNF) in NAc and ventral tegmental area (VTA)[70, 73, 75]. Evidence suggests an implication of dopamine receptors D1-D2 heteromers in drugs addiction and schizophrenia[70, 76].

Dopamine receptors D1-D3 heteromers have been found by different techniques in the striatonigral pathway of rat striatum[77, 78]. Data show that upon DA denervation and intermittent L-Dopa therapy, dopamine receptor D3 is overexpressed in the dopamine receptor D1-GABA pathway. The dopamine receptor D3 overexpression can consequently contribute to the dopamine receptor D1 sensitization and development of L-Dopa-induced dyskinesias[79, 80]. The dopamine receptor D1-D3 interaction has been reported to determine a receptor D3 stimulation and an increase of dopamine receptor D1 response[77, 78]. It was proposed that dopamine receptor D1-D3 heteromer can operate a reinforcing of the dopamine receptor D1 signaling in turning affecting motor functions and can contribute to dyskinesia in PD patients[78, 81].

Heteromer	Physicial interaction		Functional evidence
	In vitro	In vivo	
D1-D2	Co-IP, NLS FRET rat striatal neurons radioligand binding	Co-IP rat STR, PFC FRET in situ rat CP, NAc, GP	Novel Gq-coupling resulting in intracellular calcium release and BDNF expression, signaling blocked by D1R and D2R antagonists, GSK-3b inactivation.
D2-D4	BRET D2R and D4.4, no heteromer between D2R and D4.7 variant	Colocalization in mouse STR	Potentiation of ERK activation when D2R and D4R coexpressed but not with D4.7 variant, knock-in mice expressing D4.7 variant show no synergistic increase in striatal ERK activation.
D1-D3	BRET, FRET	Co-IP rat STR	Agonist-induced D1R cytoplasmic sequestration abolished by D3R coexpression, D3R stimulation enhanced D1R agonist affinity and potentiated D1R-mediated behaviors.
D2-D3	Co-IP	Colocalization STR	In the presence of excess D3R, the properties of partial D2R agonists transformed to antagonists.
D2-D5	FRET, NLS	Colocalization, rat cortex, VP, CP	Gq-coupling resulting in intracellular calcium release followed by extracellular calcium influx.
A1-D1	Co-IP	Co-IP rat NAc	A1R promoted D1R G protein uncoupling and dampened receptor signaling.
A2-D2	Co-IP, FRET, BRET	Colocalization inSTR	A2R promoted D2R G protein uncoupling and dampened receptor signaling.
D1-NMDA	BRET	Co-IP rat HIP, STR PSD, PFC, pulldown assay rat HIP	Uncoupling the heteromer with a disrupting peptide upregulated NMDA-mediated LTP in rat HIP and promoted working memory.
D2-NMDA		Co-IP rat STR PSD, pull-down assay STR	Heteromer formation induced by cocaine disrupted the CaMKII/NR2B interation and reduced NMDA receptor-mediated currents.
D2-5HT2A	Co-IP, FRET, BRET	Colocalization in STR	5HT2AR-mediated PLC activation was synergistically enhanced by D2R activation, D2R-mediated AC inhibition was attenuated by 5HT2AR activation.
D1-H3	BRET	Co-IP rat STR	D1R mandatory for H3R-induced ERK activation, D1R- and H3R-induced ERK activation blocked by antagonists for either receptor.
D2-H3	BRET	Co-IP rat STR	H3R agonists dampened D2R receptor function and D2R-induced locomotor activity

Table 3. Physical and Functional Evidence for Dopamine Receptor Heteromers. Abbreviations: 5HT2AR, 5HT2A receptor; A1R, adenosine A1 receptor; A2R, adenosine A2 receptor; AC, adenylyl cyclase; ADHD, attention-deficit hyperactivity disorder; BDNF, brain-derived neurotrophic factor; BRET, bioluminescent resonance energy transfer; CaMKII, calcium calmodulin kinase II; Co-IP, coimmunoprecipitation; CP, caudate putamen; D1R, dopamine D1 receptor; D2R, dopamine D2 receptor; D3R, dopamine D3 receptor; D4R, dopamine D4 receptor; ERK, extracellular signal-related kinase; FRET, fluorescent resonance energy transfer; GP, globus pallidus; GSK-3b, glycogen synthase kinase 3b; H3R, histamine H3 receptor; HIP, hippocampus; LTP, long-term potentiation; mGlu5, metabotropic glutamate receptor 5; NAc, nucleus accumbens; NR2B, NMDA receptor subunit 2B; PLC, phospholipase C; PFC, prefrontal cortex; PSD, postsynaptic density; STR, striatum; VP, ventral pallidum[70].

1.3 Current treatments of Parkinson disease

In these last years, PD treatment has become articulated due to the presence of new drugs and treatments (figure 4). Treatments for PD include pharmacotherapy, functional stereotaxic neurosurgery (deep brain stimulation), and supportive therapy such as physiotherapy, speech therapy, and dietary measures. All treatments available until 2016 are of symptomatic nature. No therapy is currently available that slows down the progression of PD or even prevents its manifestation[82].

L-Dopa

The first and the most efficient treatment established to recover the dopaminergic deficit was L-Dopa always in fixed combination with a decarboxylase inhibitor. L-Dopa is the physiological precursor of dopamine and unlike dopamine it is permeable at the blood brain barrier. According to present knowledge, L-Dopa does not influence the progression of the disease. The effects of L-Dopa are dose-dependent. L-Dopa adverse reactions depend mostly on its oxidative metabolism and its potential capability to produce reactive oxygen species. Treatment with L-Dopa is recommended in all stages of the disease. The uptake of L-Dopa starts from the duodenum into the blood and from the blood to the brain competing with the uptake mechanism for neutral amino acids. Once in the CNS, L-Dopa is converted in dopamine by a neuronal L-Dopa decarboxylase in the dopaminergic neurons. Therefore, dopamine is transported in the synaptic vesicles. When the impulse reach the dopaminergic neurons, vesicles fuse with plasma membrane and dopamine is released into synaptic cleft leading to its physiological effect[83-86].

Dopamine agonists

Ten dopamine agonists (five ergot- and five non-ergotderivates) are usable for the treatment of PD. Ergot dopamine agonists include bromocriptine, cabergoline, adihydroergocriptine, lisuride, and pergolide. The non-ergot derivates include piribedil, pramipexole, ropinirole, apomorphine and rotigotine. Usually, dopamine agonists are provided in the advanced PD stages since they may increase the risk of cognitive

impairment or dementia development. However the anti-Parkinson efficacy is limited and motor complications are not completely prevent[87, 88].

<u>MAO and COMT inhibitors</u>

The duration of the effect of L-Dopa can be prolonged blocking degrading enzymes of L-Dopa and dopamine. Usually, COMT inhibition (entacapone, opicapone or tolcapone) is associated with an increased stability of levodopa plasma level, suppressing peaks of levodopa concentrations associated with motor complications[82]. MAO-B inhibitors (rasagiline, safinamide, selegiline) can amplify the effect of L-Dopa. However, clinical studies concerning the efficacy of this therapeutic drugs have produced controversial results.
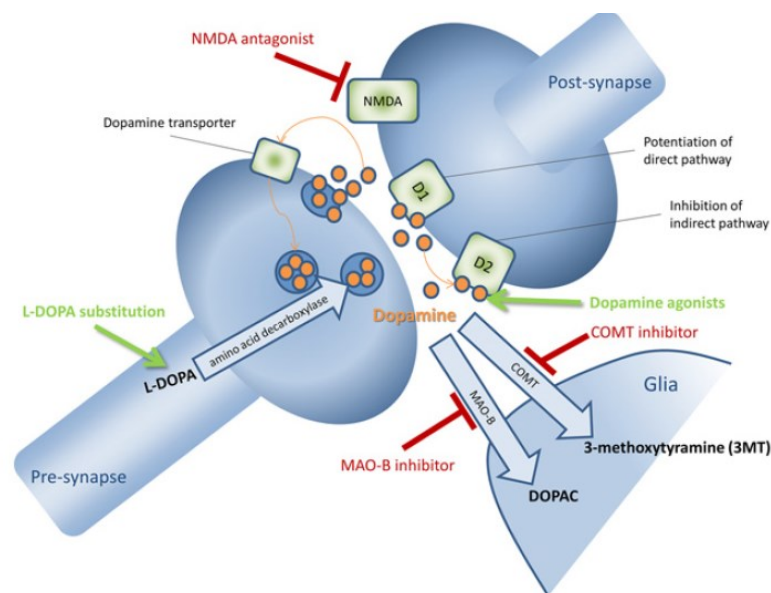

Figura 4. Pharmacology of dopaminergic transmission. Dopamine is released into the synaptic cleft, where it can bind to post-synaptic D1-like (D1 and D5) and D2-like (D2, D3, and D4) receptors. Dopamine can be metabolized in glia cells to 3-methoxytyramine (3MT) by the catechol-O-methyl transferase (COMT) or to 3,4-dihydroxyphenylacetic acid (DOPAC) by monoamine oxidase B (MAO-B). Dopamine is also reuptaken into the pre-synapse by dopamine transporters. Drugs are L-Dopa, D1-, and D2-like dopamine agonists, MAO-B- and COMT-inhibitors[82].

1.4 Etiology

To date the etiology of PD is unknown. PD has a complex and multi-factorial etiology, involving genetic and environmental factors. However, the molecular details of the degeneration are unknown. Nevertheless, the discovery of PD related genes has lit a new light on the cellular mechanisms related to PD neurodegeneration.

Environmental factors

Epidemiological analyses show that pesticide exposition (Paraquat, Rotenone), lifestyle (diet, habit, occupation), metal exposure (Al, Cu, Fe, Hg, Mn, Pb, Zn), chemical and industrial products (MPTP, organic solvents), trauma and viral infections can increase the risk of PD development[89].

An example of how an exogenous toxin can mimic the clinical and pathological symptoms of PD is the MPTP (1-methyl-4-phenyl-1,2,3,6,-tetrahydropyridine or meperidine) intoxication[90]. In 1982 MPTP was discovered as dopaminergic neurotoxin when drug users developed a rapidly progressive parkinsonian syndrome as a result of intravenous self-administration of a street preparation of 1-methyl-4-phenyl-4-propionoxypiperidine (MPPP), an analog of the narcotic Demerol contaminated by MPTP[90]. In humans and monkeys, MPTP produces a severe parkinsonian syndrome, L-Dopa responsive, characterized by all the PD symptoms including the cardinal symptoms of PD.

In the brain, by crossing the blood brain barrier, MPTP is converted in to 1-methyl-4-fhenyl-2,3-didropiridine (MPTP+) by monoamine oxidase B (MAO-B) in glial cells, serotoninergic neurons and in each neuron that contain MAO-B enzyme. Subsequently, MPTP+ is converted in 1-metil-4-fenilpiridinio (MPP+), probably by spontaneous oxidation, and released in the extracellular space. MPP+ is transported in dopaminergic neurons through its high affinity for the dopamine transporter (DAT). Inside neurons MPP+ can follow at least three routes: (i) it can bind the vesicular monoamine transporter-2 (VMAT2)[91], which translocates MPP+ into synaptosomal vesicles; (ii) it can be concentrated within the mitochondria[92] and (iii) it can remain in the cytosol to interact with the cytosolic enzymes[93]. In the mitochondria MPP+ exerts

is toxic mechanism binding and blocking the complex I, which interrupts the transfer of electrons to ubiquinone (figure 5). This perturbation enhances reactive oxygen species (ROS) production and decreases ATP synthesis leading to a neuronal dead via apoptosis[1, 90]. The MPTP related Parkinsonism supports the environmental hypothesis of PD etiology and the MPTP-treated animals can be an interesting models for PD studies. Other substances like rotenone, 6-hydroxydopamine (6-OHDA) and paraquat were identified PD causative and currently used in toxin-based animal models of PD[94].

In addition to toxins, other environmental factors, which can be considered as risk factors rather than causative elements, are lifestyle and habits. Repetitive or simple violent traumas can provoke a Parkinson-like progressive syndrome as the one frequently observed among boxers that take the name of "Pugilistic Parkinson Syndrome". Another two risk factors are age and sex, males are more affected than women (in a 1,5:1 ratio). In humans, neuronal and SNpc neuromelanin loss increases around 60 years, coinciding with the average age of PD onset. Since neuromelanin has a protective effect in neurons against free radicals and toxins, the decrease in this pigment may predispose the brain of aged people to Parkinson[95].

Finally, an infective etiology has been hypothesized; clinical manifestations of PD-like syndromes have been observed in patients affected by a viral encephalitis propagated in 1920[96, 97].
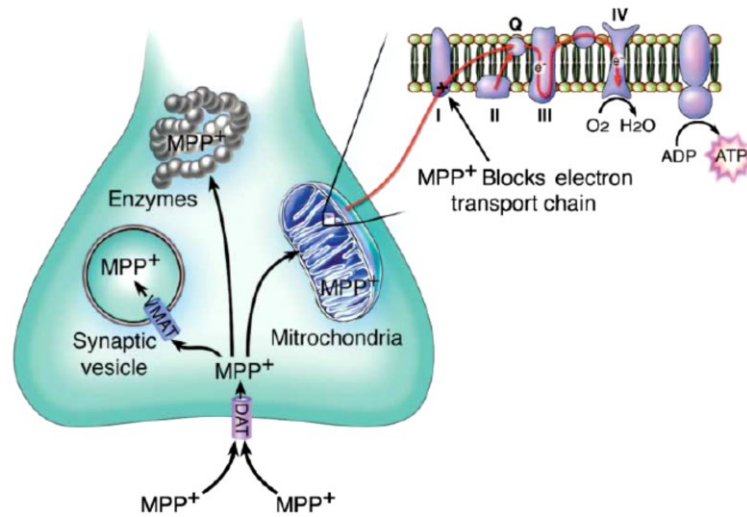
Figure 5. Schematic representation of MPP+ intracellular pathway[1].

Genetic factors

Until the end of the 19th century, PD has been considered a sporadic disease, even though the 10-30% of PD patients presented a first line relative affected by the disease. Leroux in 1880 identified recurring PD cases in the same family, corroborating the hypothesis that hereditary factors could be related to pathology[98, 99]. However, in the last 20 years, the identification of gene mutations related to PD and risk factors, has proved the importance of genetic factors in the pathogenesis of the disease, even if less than 10% of the cases are familiar. Until now, 19 mendelian transmission forms and several risk factors have been related to PD (table 4)[100].

Locus	Chromosome	Gene	Inheritance	Probable Function
PARK1/PARK4	4q21	SNCA	Dominant	Presynaptic protein, Lewy body, lipid and vesicle dynamics
PARK2	6q25.2-q27	PARK	Recessive	Ubiquitin E3 ligase, mitophagy
PARK3	2p13	-	Dominant	Unknown
PARK5	4p14	UCH-L1	Dominant	Ubiquitin C-terminal hydrolase
PARK6	1p35-36	PINK1	Recessive	Mitochondrial kinase
PARK7	1p36	DJ1	Recessive	Oxidative stress
PARK8	12q12	LRRK2	Dominant	Kinase signaling, cytoskeletal dynamics, protein translation
PARK9	1p36	ATP13A2	Recessive	Unknown
PARK10	1p32	-	-	Unknown
PARK11	2q36-37	GIGYF2	Dominant	IGF-I signaling
PARK12	Xq21-q25	-	X-linked	Unknown
PARK13	2p12	HTRA2	Dominant	Mitochondrial serine protease
PARK14	22q13.1	PLA2G6	Recessive	Phospholipase enzyme
PARK15	22q11.2-qter	FBXO7	Recessive	Ubiquitin E3 ligase
PARK16	1q32	Unknown	Unknown	Unknown
PARK17	16q11.2	VPS35	Dominant	Exocyst complex member
PARK18	3q27.1	EIF4G1	Dominant	Translation factor activity, RNA binding
PARK19	1p31.3	DNAJC16	Recessive	Unknown

Table 4. Loci involved in monogenic forms of Parkinson's disease (PD).

Alpha synuclein (PARK1/PARK4)

Using traditional linkage mapping, the point mutation A53T in the SNCA gene was discovered in the large Italian-American family Contursi and subsequently identified in three Greek families with familial PD[101]. A decade later, the same mutation was discovered in two Korean and one Swedish family[102, 103]. Subsequently to the discovery that SNCA mutations are involved in a rare familial form of PD, Spillantini and colleagues demonstrated that α-synuclein is a major constituent of Lewy bodies[104]. Mutations in SNCA are rare. Until now, five point mutations are discovered (A30P, E46K, H50Q, G51D, A53T) and related to autosomal dominant inheritance forms of PD. Moreover, triplications of the complete gene were discovered[105]. Triplication of the SNCA gene was discovered in 2003 and reported in several PD families[106-108]. The gene SNCA is located on the chromosome 4q21 consists of six exons[109] and encodes a small 140 amino acid protein[110] organized in three distinct domains: an N-terminal amphipathic region (AA 1-60) consisting in six repeats of eleven amino acid with consensus sequence KTKEGV[111]. A central hydrophobic NAC domain (non-amiloid-β component of plaque, AA 60-95) necessary for homomeric interactions[112]. Finally an acidic unfolded C-terminal region (AA 96-140)[113]. Monomeric α-synuclein can form conformers, including oligomers, protofibrils and fibrils, and they have been found in Lewy bodies. All the five point mutations are located in the amphipathic domain and can modify the homomeric interaction kinetic[114]. Until now the normal function of α-synuclein remains poorly understood. The α-synuclein is mainly found in the cytosol where can bind the lipid rafts in an interaction that is required for its association with the synapse[115]. Data show that α-synuclein interacts with members of the Rab and SNARE families, suggesting a role in vesicular trafficking[100, 116-118].

Parkin (PARK2)

The year following the discovery of the SNCA gene as PD causative, in a Japanese PD patient group was discovered a protein associated to an early-onset form of PD (AR-JP). PARK gene is one of the largest genes in the human genome, mapping on the 6q25.2-q27 chromosome, with a length of 1.38 Mb[119]. Numerous point mutations and exon rearrangements (to date 147) have been found in PARK gene in various ethnic

groups[100, 120]. Parkin protein is an E3 ubiquitin ligase of 465 amino acids organized in different domains: an N-terminal ubiquitin like domain, a central linker region and C-terminal RING domain consisting of two RING finger motifs separated by a RING domain[98, 121]. The ubiquitin-like domain of E3 ubiquitin ligases can bind unfolded proteins to be degraded by the ubiquitin-proteasome system[122]. A serious neuronal loss in the substantia nigra is related to PARK2 PD form, with occasional tau pathology and rare Lewy Bodies in postmortem brains[123-125] probably due to the young age of Parkin disease onset[126]. The loss of the ubiquitin ligases activity, due to mutations in the RING domain, can cause an accumulation of unubiquitinated proteins. It has been proposed that the overexpression of Parkin could protect from toxic forms of α-synuclein by Lewy Body formations[98]. The E2 enzyme associated with Parkin is UbcH7 and the mutation T240R in the first RING domain disrupt this interaction[127]. It has been demonstrated that when mitochondria are damaged, PINK1 (another gene associated with AR-JP), phosphorylates Parkin. Subsequently, Parkin translocates to the surface of demented mitochondria to ubiquitinate mitochondrial membrane proteins[128, 129]. The majority of Parkin mutations are linked to dysfunctions in the mitochondrial quality control, suggesting a role of the mitochondria in the pathogenesis of PD[100].

PTEN-induced kinase 1, PINK-1 (PARK6)

After different studies, the locus PARK6 was mapped on the chromosome 1p35-p36 in a large Italian family presenting a mendelian form of PD with recessive inheritance[130]. In 2004, Valente and colleagues identified two mutations in the PTEN-induced putative kinase 1 (PINK1) gene: the G309D missense mutation and a W437X truncating mutation[131]. The PINK1 gene is assembled in height exons and encode for a 581 amino acid protein consisting of an N-terminal 34 amino acid mitochondrial targeting motif, a conserved serine–threonine kinase domain and a C-terminal auto regulatory domain. The majority of the mutations in the PINK1 gene are located in the region encoding for the kinase domain, suggesting the importance of PINK1 enzymatic activity in PD pathogenesis[121]. PINK1 related PD is a fast onset and slow progression Parkinsonism form responsive to L-Dopa treatment[132]. It has been demonstrated that PINK1 can co-localize and phosphorylate the mitochondrial chaperone TRAP1 protein[133]. As

mentioned PINK1 phosphorylates Parkin to regulate mitophagy[129, 134]. In a general view, when mitochondria are damaged, mitochondrial membrane potential is reduced and PINK1 is recruited and binds the mitochondrial membrane. Parkin is then recruited to induce mitophagy via ubiquitination[135-137]. It is controversial the function of TRAP1 in this pathway[138].

Dj-1 (PARK7)

Mutations in the Dj-1 gene were first reported in two European family and associated with an autosomal recessive form of PD[139]. Dj-1 gene is composed of height exons and encodes for a 189 amino acid ubiquitary protein first identified as oncogene[140]. DJ-1-linked PDs are rare, L-Dopa responsive, and indistinguishable from Parkin or PINK1 linked PD [141]. However, about 10 different point mutations and exonic deletions have been described[142]. Dj-1 has been reported against oxidative stress like a chaperone oxidative stress sensor[143, 144]. The DJ-1 protein forms dimeric structures[145], and it appears that most of Dj-1 PD linked mutants (L166P, E64D, M26I, and D149A) heterodimerize with wild-type DJ-1[146]. However, the mutated proteins are not correctly folded and unstable, affecting Dj-1 neuroprotective function and antioxidant activity[147, 148]. DJ-1 also can function as redox-dependent chaperone to inhibit α-synuclein aggregation and subsequent Lewy Body formation. Recently, DJ-1 has been linked to the Parkin/PINK1 pathway by the transcriptional regulation of PINK1[149].

Vacuolar protein sorting 35-VPS-35 (PARK17)

In 2011, Zimprich and colleagues using next generation sequencing identified the VPS35 gene in an Austrian family with 16 members affected by late-onset autosomal dominantly inherited parkinsonism. Later, the mutation D620N, was validated by Sanger[100, 150]. Simultaneously, Vilarino-Guell and colleagues, using next generation sequencing, identified the D620N mutation as a cause of PD in a large Swiss family[151]. VPS35 mutations are a rare cause of PD concerning 1% of familial parkinsonism and 0.2% of sporadic PD[150, 152]. VPS35 linked PD is characterized by bradykinesia, resting tremor and is responsive to levodopa therapy comparable to idiopathic disease[153]. VPS35 gene was mapped on the 16q11.2 locus and encodes for a highly conserved 796

amino acid protein. The yeast homologous of Vps35 has been well characterized and it has been shown to compose the retromer complex with other 4 Vps proteins (Vps5, Vps17, Vps26, Vps29). The retromer complex is involved in retrograde transport of proteins to the trans-Golgi network[154]. VPS35 is a helical solenoid like protein, such as other proteins involved in coated vesicle trafficking[155]. The VPS35 human homolog have been found to be involved in the same endosome–trans-Golgi network pathway as the yeast Vps35[156]. A recent study links the D620N mutation to dysfunction of the retromer complex, generating a redistribution of the retromer endosomes to the perinuclear region in cell lines and PD patient-derived fibroblasts. Moreover, the D620N mutant alters the cathepsin D trafficking, a protein implicated in the α-synuclein degradation[100].

1.5 Leucine rich repeat kinase 2 – (LRRK2)

PARK8 locus have been associated for the first time to PD by Funayama and colleague in the 2002[157] in a large Japanese family presenting a dominant autosomal Parkinsonism without Lewy Body. After two years, two groups independently have identified in PARK8 locus the LRRK2 gene (Leucine-rich repeat kinase 2)[158, 159]; subsequently many pathological mutations have been identified and associated with PD. Mutations in LRRK2 gene are the most frequently cause of familiar PD. In 2014 Nalls and colleagues associated LRRK2 as a risk locus implied in sporadic PD[160].

General characteristic and structural domains of LRRK2

The gene encoding for LRRK2 is located on chromosome 12.q12 and is composed by 51 exons. LRRK2 is a 286-kDa multidomain protein exhibiting both GTPase and kinase activities that belongs to the Roco protein family of G proteins protein. LRRK2 has 7 functional conserved domains (figure 6)[161-163]:

- An "armadillo repeats" domain;

- An "ankyrin repeats" domain;

- A leucine-rich repeats (LRR) domain;

- A Roc domain with GTPase activity;

- A carboxy terminal of Roc domain (COR);

- A Kinase domain, homologous with MAP-kinase-kinase-kinase (MAPKKK);
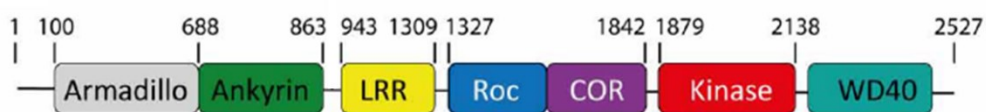
- A C-terminal WD-40 repeat domain.

Figure 6. Domain structure of LRRK2[163].

The Armadillo Repeats domain is a motif of 42 amino acid, composed by three α-helixes and was firstly identified in the "Armadillo" protein of Drosophila, whose human homologue is the β-catenin. The Armadillo domain forms a versatile molecular interaction domain like a platform available for different protein[164].

The Ankyrin Repeats domain is a 7 ankyrin repeats motif, which forms helix-loop-helix structures that ends in a loop or hairpin (figure 7). This motif is common in a high number of prokaryotic and eukaryotic proteins like cytoskeletal proteins, transcription factors, signaling proteins and cell cycle regulators[165].

LRR domain is made of an 11 amino acid conserved motif LxxLxLxxNxL (Leucines can be replaced by isoleucine, valine or phenylalanine). These repeats are formed by a β-strand followed by an α-helix that line up side-by side to form an arch-like structure (figure 7). LRR domains participate in the interactions with different proteins through binding to their extended solvent-accessible surface[166, 167].
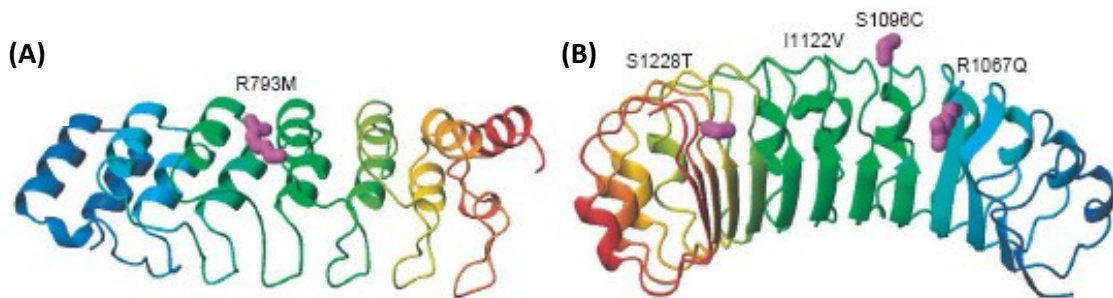
Figura 7. Homology models of (A) the ankyrin repeat domain and (B) the leucine-rich repeat (LRR) domain of LRRK2[166].

The WD40 repeat domain (known as β-transducin repeat) has a high conserved tridimensional structure and form a seven-blade propeller-like structure. Each repeat is composed by four antiparallel β-sheet and together these repeats form a circular bladed propeller-like structure. The predicted WD40 domain of LRRK2 contains seven WD40 repeats (figure 8), to form an interaction platform for protein-protein reversible interactions. Proteins containing WD40 domains have been found in all eukaryote proteins with different functions including the Gβ subunit of heterotrimeric G proteins,

transcriptional regulators, protein phosphatase subunits, RNA processing complexes, cytoskeletal assembly proteins, and proteins involved in vesicle formation and trafficking. Different experimental results suggest an important role for the WD40 domain in the intramolecular regulation of LRRK2 activity[166, 168].
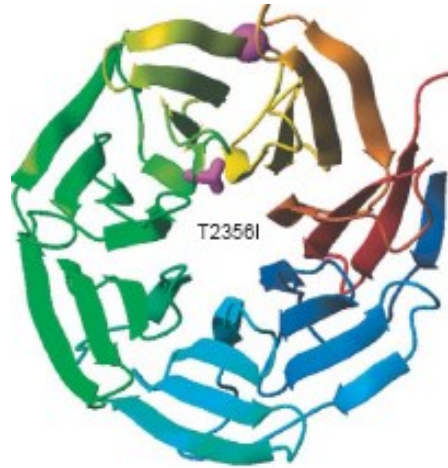

Figure 8. Homology models of the WD40 repeat domain[166].

LRRK2 and Roco proteins are serine/threonine specific kinases. Gilsbach colleagues proposed a structure of the LRRK2 kinase domain based on *Dictyostelium discoideum* Roco4 (figure 9) in its active and inactive state[169]. Dictyostelium Roco4 has the same domain architecture of LRRK2, but is biochemically and structurally more easily worked than LRRK2. The Roco4 kinase structure consists of a canonical, two lobed kinase structure. The N-terminal lobe is composed of anti-parallel β sheets and contains the conserved αC-helix. The C-terminal lobe consists of α-helices and contains the activation loop with the conserved N-terminal DFG motif. The ATP binding site is formed by a cleft between those lobes and forms the catalytic site of the kinase. The formation of a polar contact between Roco4 K1055 from the β3-strandand E1078 from the αC-helix is essential for correct positioning of the αC-helix. The DFG motif is essential for catalysis: the Aspartic acid is essential to interact with ATP directly or via coordination of a magnesium ion; the Phenylalanine takes hydrophobic contacts to the αC-helix and the HxD motif and is responsible for the correct positioning of the DFG motif[169, 170].
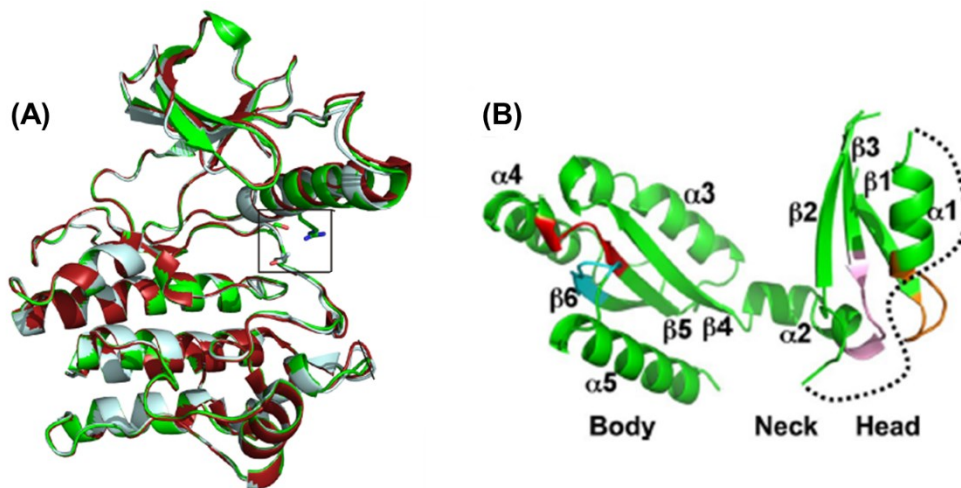
Figure 9. Models of the (A) kinase domain of *Dictyostelium discoideum ROCO4* and (B) Roc domain of LRRK2[170, 171].

The putative GTPase domain of LRRK2 is a member of the ROCO family. In the ROCO proteins predicted GTPase (Roc) domain is always in tandem with the COR domain. This Roc–COR structure is conserved throughout evolution, suggesting the functional interdependence of the two domains[170]. Deng and colleagues suggested that the structure of the LRRK2 Roc domain (figure 9) displays a homodimer with extensive domain-swapping. Each monomer contains five α-helices and six β-strands with loops in between, showing three subdomains: head, neck, and body. The head domain is composed by β1, α1, β2, and β3. The loop between α2 and β2, such as that between β2 and β3, are not folded. The neck domain consist of a bent helix α2. The body domain is structured with β4, α3, β5, α4, β6, and α5 with loops in between. In the same paper, Deng and colleagues, suggest that LRRK2 Roc domain structure revealed an inverted dimer or rather the N-terminal of one domain interacts with the C-terminal of the other[171]. In contrast, the *C. tepidum* Roc-COR domain structure showed that the COR domain is the dimerization domain and that Roco proteins that are not able to dimerize are not able to hydrolyze GTP[172].

Using size-exclusion column chromatography and native gel analysis, Greggio and colleagues and Sen and colleagues proved that recombinant LRRK2 expressed in HEK293FT cells exists as monomer, dimer and higher order oligomers, but only the

dimeric form has significant kinase activity[173, 174]. The existence of LRRK2 dimer in cells was also confirmed by several other groups of researchers[175-177].

Guaitoli and colleagues proposed a high-resolution structure model for LRRK2 (figure 10). This model suggest that there are close contacts of the kinase domain with the N-terminal ankyrin and LRR repeat domains. In the model, the kinase-ankyrin module localizes in a position close to the LRR domain and the α0-helix connecting the LRR and the Roc G-domain. In this model the dimerization domain is represented by the COR domain[163].
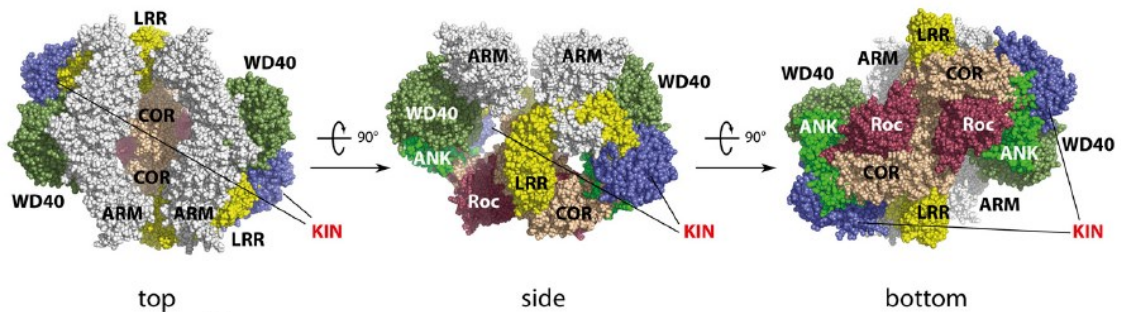
Figure 10. LRRK2 high-resolution homodimer structure model[163].

This LRRK2 structure is in contrast with the Deng model in which the dimerization domain is displayed by the Roc domain. In a general view there is the possibility that LRRK2 has a differential conformational structure and there are different possible conformations of a more dynamic molecule[178].

It has been shown that the G-domain of LRRK2 is a GTP-binding protein and that GTP binding is essential for the regulation of kinase activity[176, 179]. Until now, the activation mechanism of LRRK2 is unknown. In a general model (figure 11), LRRK2 activity is regulated by at least three different ways: dimerization, intramolecular activation, and binding of the substrates. After dimerization, LRRK2 can switch from an inactive state (GDP binding) to an active state (GTP binding). Subsequently, LRRK2 conformation changes; this change is imparted to the others domains of the protein. Subsequently the activation loops of the two-kinase protomers are auto phosphorylated and

activated. The GTPase reaction is also critically dependent on dimerization. In this way, the intramolecular GTPase reaction functions as a stopwatch for the activation and function of Roco proteins. The N- and C-terminal segments of LRRK2 regulate the intramolecular signaling cascade and are important for kinase activity, oligomerization, localization and determine the specificity of the Roco proteins[170, 180].
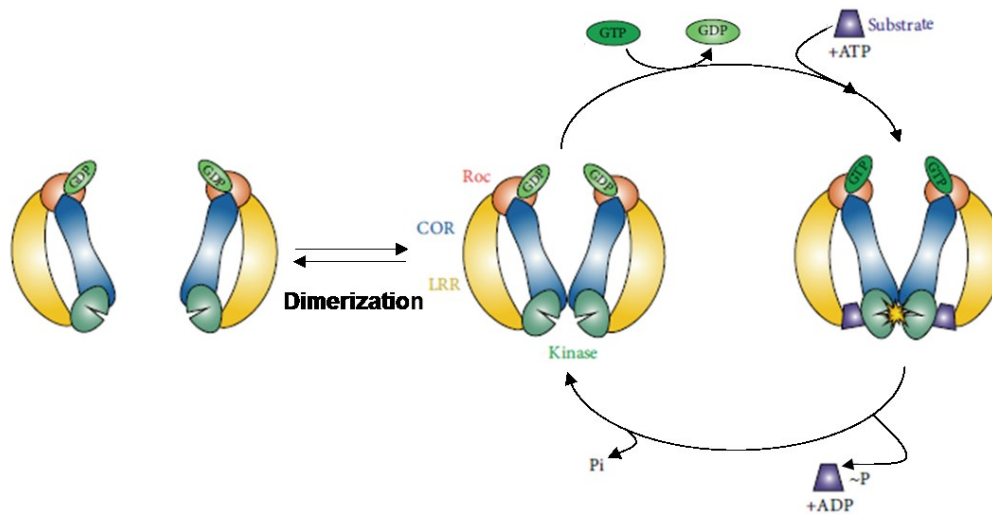

Figure 11. Proposed model of the activation mechanism of LRRK2 modified. Modified from[180].

Mutations in LRRK2 gene and their implication in PD

Up to now, more than 100 distinct missense and non-sense mutations have been reported in LRRK2[100, 181]; however, only a small number of these mutation are related with PD (R1441C/G/H, Y1699C, S1761R, I2012T, G2019S and I2020T)[182-186]. These pathogenic modifications are located in exons encoding the Roc domain, COR domain, or kinase domains of the protein. Phenotypically, LRRK2 mutation patients are fundamentally indistinguishable from sporadic PD presenting a late onset around 60 years of age, with a slow progression and responsive to levodopa therapy[187].

The most studied mutation, G2019S, affects the kinase domain and is common in various populations: it has been identified in up to 42% of familial cases, depending on the ethnic group[182, 188]. It is frequent in North African, Middle Eastern, Ashkenazi Jewish PD patients and North African Berber populations (35–40% of PD patients are G2019S carriers). G2019S mutation was found in sporadic cases of PD in approximately

2% in Northern European and US populations and up to 10% of sporadic cases worldwide. The penetrance of the G2019S mutation depends on the age from 28% at 59 years to 74% at 79 years of age[100]. As mentioned, the G2019S mutation is located in the kinase domain of LRRK2, determining an approximatively twofold increase in its kinase activity[189-191]. Another mutation, the I2020T, was found in the kinase domain and isolated in a Japanese family[192], but the effect of this mutation on LRRK2 kinase activity and cellular toxicity remains poorly understood[193-196]. The R1441C, R1441G and R1441H mutations are located in the GTPase domain of LRRK2; the R1441G mutation are founded in > 40% of familial PD cases in the Basque population[197, 198]. The Y1699C mutation is located between the GTPase and kinase domains, and have been reported 25 affected subjects in a large PD affected family in UK[199]. The R1441C/G/H and Y1699C mutations show a decrease in GTP hydrolysis[200-202], but the impact on the kinase function of LRRK2 remains controversial[198].

LRRK2 functions in physiological and pathological conditions

Up to now, although the extensive studies performed, the physiological role of LRRK2 remains elusive. LRRK2 is ubiquitously expressed in various tissues. LRRK2 is expressed throughout the brain, including the olfactory bulb, striatum, cortex, hippocampus, midbrain, brainstem, and cerebellum[203, 204]. Gene expression analysis suggests that LRRK2 is expressed in peripheral organs such as kidney, lung, spleen and peripheral blood mononuclear cells and immune cells[205-208]. The subcellular localization of LRRK2 is fundamentally cytosolic with an important component associated with the membranes, Golgi apparatus, mitochondria, lysosomes, endoplasmic reticulum, microtubules and cytoskeleton structures[203]. LRRK2 has been implicated in different cellular pathways, including cytoskeletal dynamics, autophagy, mitochondrial homeostasis, vesicular trafficking, protein aggregation and protein translation (figure 12).
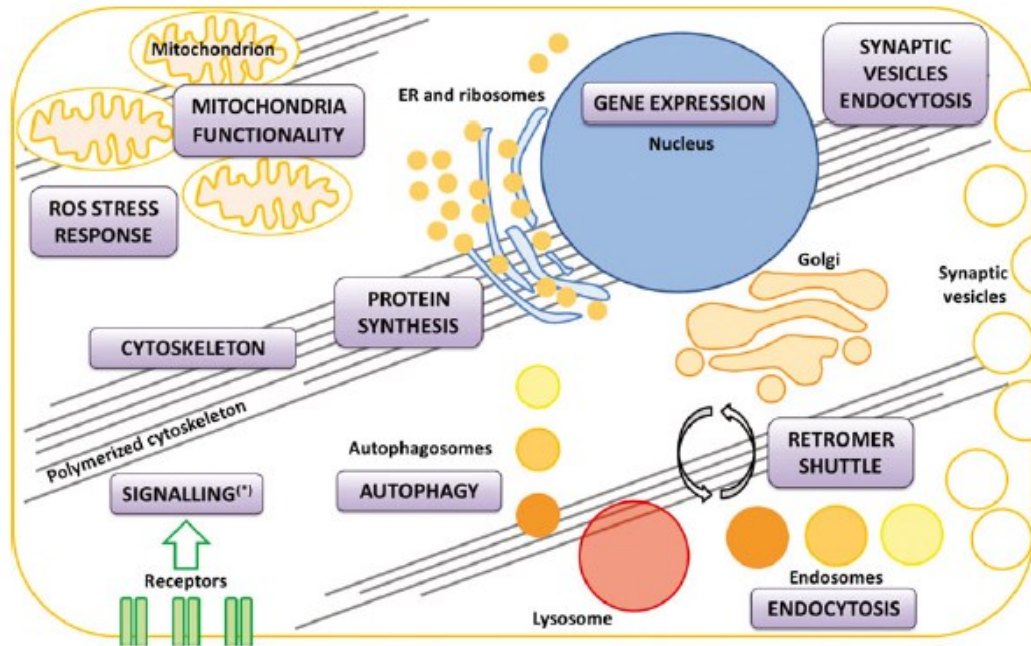
Figure 12. Implication of LRRK2 in cellular functions[198].

LRRK2 and cytoskeleton dynamics

Microtubules are cytoskeletal structures that are involved in different cellular functions such as neuronal polarity, neuronal morphology and transporting cargo proteins[209]. One of the most significant effects of LRRK2 mutants on the cytoskeleton is the impairment in neurite outgrowth[210-212]. However, it is not clear if this is due to LRRK2 mediated changes in tubulin phosphorylation, tubulin acetylation, MAP phosphorylation and/or microtubule associated protein kinase regulation. In vitro experiments in HEK293 cells revealed that LRRK2 colocalize with β-tubulin[193]. It has been reported that LRRK2 can phosphorylates bovine brain β-tubulin and phosphorylation was significantly increased G2019S pathological mutant[213]. Experimental evidence shows a functional interaction between LRRK2 and the microtubule-associated protein tau[214]. Kawakami and colleagues proved that LRRK2 mediates tau phosphorylation at threonine 181 in vitro[211, 215].

LRRK2 and autophagy

It has been reported that blocking macroautophagy the toxicity of overexpressed LRRK2 G2019S was reduced[216]. Although there is experimental evidence on the involvement of LRRK2 in autophagy, the current data are not sufficient and sometimes controversial for a LRRK2 accurate implication in this pathway, suggesting the possibility that LRRK2 may have different roles in different cell types or different physiological conditions. An age dependent biphasic alteration in macroautophagy has been observed in kidneys of LRRK2 knockout animal models, in which autophagy was enhanced at young age and reduced at old age. In this study there was an increased ratio of LC3-II/LC3-I in young animals and an opposite ratio was reported in older animals[198, 217]. On the contrary, another study reported a generalized increase in LC3-II in 12 to 20 months animals[218]. Recently Manzoni and colleagues reported that in H4 glioma cell line and in primary astrocytes the LRRK2 kinase activity is involved in the non-canonical control of macroautophagy, working in parallel with the mTOR/ULK1 pathway and dependent on PI3P and Beclin-1 activity[198, 219].

LRRK2 and mitochondrial dysfunctions

Mitochondria have essential functions for cellular homeostasis. Fibroblasts from LRRK2 G2019S PD patients display abnormal mitochondrial morphology[220]. It has been demonstrate that an increase in mitophagy and altered calcium levels were observed in primary mouse cortical neurons expressing LRRK2 G2019S or LRRK2 R1441C mutants[198, 221]. It has been shown that endogenous LRRK2 directly interacts with the fission regulator dynamin-related protein (Drp1) at the mitochondrial membrane, increases Drp1 phosphorylation and activation leading to mitochondrial fission[222, 223]. This LRRK2-Drp1 dependent mitochondrial fragmentation is enhanced by overexpressing wild type LRRK2 or G2019S mutant form[222, 224]. LRRK2 also interacts with the mitochondrial fusion regulators mitofusin protein 1/2 (Mfn1/2) and the dynamin-like 120 kDa protein (OPA1) modulating their activities; PD patients carrying the G2019S mutation have reduced levels of mature OPA1[225, 226]. Iaccarino and colleagues have demonstrated that mutant LRRK2 toxicity in human (SH-SY5Y) and murine (ETNA embryonic neuronal precursors) neuronal cells is mediated by the

mitochondria-dependent apoptotic pathway[227]. These observations suggest that LRRK2 might be involved in the control of mitochondria homeostasis.

LRRK2 and vesicular trafficking

LRRK2 is associated with membranous structures and vesicles as well as Golgi complex in mammalian brain and Golgi fragmentation was observed in mice overexpressing LRRK2 wild-type or G2019S[210, 228, 229, 228]. As mentioned a subcellular localization study performed in primary cortical neurons and rodent brains showed that LRRK2 co-localizes to Golgi apparatus and Golgi-associated vesicles, endoplasmic reticulum (ER), lysosomes and mitochondria, and in a lesser extent, to vesicle markers like synaptotagmin[203]. Different experimental evidence suggests that LRRK2 has a functional role in the vesicle trafficking control, and alteration in synaptic vesicle trafficking seems a common pathological mechanism in PD[230, 231]. LRRK2 has been implicated in the regulation of synaptic endocytosis with Rab5b; LRRK2 overexpression remarkably reduced synaptic vesicle endocytosis, and this phenotype was rescued by the introduction of Rab5b[232]. In mammalian cells, has been demonstrated that LRRK2 interacts with members of the dynamin GTPase superfamily Dnm1, Dnm2 and Dnm3, which play an important in clathrin-mediated endocytosis[225]. In Drosophila, Matta and colleagues demonstrated that LRRK2 phosphorylates EndophilinA (EndoA), resulting in an EndoA decreasing affinity for membranes. LRRK2 G2019S mutant prevented synaptic endocytosis and this phenotype was rescued by pharmacological inhibition of LRRK2 kinase activity[233]. Recently, the same group validated these data in mammalian cells, in which LRRK2 phosphorylate EndoA1, the neuron-specific EndoA isoform[234]. To clarify the physiological role of LRRK2 in synaptic vesicular trafficking, Piccoli and colleagues analysed, at presynaptic and postsynaptic levels, the cortical neurons in which LRRK2 was silenced by RNA interference. Electrophysiological analyses were performed and revealed that LRRK2 silencing modifies synaptic transmission. Moreover, LRRK2 silencing perturbs vesicle dynamics and distribution in the recycling pool, determining a significant decrease in docked vesicles, but an increase in the amount of recycling vesicle[235]. LRRK2 can regulate synaptic vesicle exocytosis by phosphorylating Snapin, and therefore regulating soluble NSF attachment protein

receptor (SNARE) complex activity and late endosomal transport[236]. Migheli and colleagues demonstrated that the expression of disease-associated LRRK2 mutants lead to alteration of dopamine receptor D1 trafficking both in animal and cellular models. In particular, expression of G2019S LRRK2 determines an increase of dopamine receptor D1 on membrane that parallels a decrease in the vesicle pool[237]. Two independent studies showed a genetic interaction between LRRK2 and Rab7L1[238, 239]; a genetic risk factor for sporadic PD. The expression of LRRK2 G2019S in primary neurons cause lysosomal swelling and accumulation of cation-independent mannose-6-phosphate receptor (C6-MPR), a component of the retromer complex[198, 238]. The C6-MPR is in general recycled between endolysosomes and the Golgi apparatus[240]. The C6-MPR accumulation was rescued either by the overexpression of VPS35 (another PD causative gene) component of the retromer or by the overexpression of Rab7L1[238]. Later, Rab7 was found in complex with LRRK2 to further the clearance of Golgi vesicles to degradation. In vivo models of LRRK2, while do not show significant typical PD-like alterations or relevant signs of neurodegeneration, some of them present different synaptic alterations[241] such as decreased DA release and re-uptake[242], impairment of dopamine D2 receptor signaling[243], impaired of dopamine reuptake[244], impaired synaptic vesicles endocytosis[234] and decreased extracellular dopamine levels, storage and uptake[198, 245]. Even though some results are quite contradictory or difficult to interpret, it is obvious a prominent role for LRRK2 in the tangled network of vesicular trafficking (figure 13). To date, LRRK2 appear to be involved in anterograde and/or retrograde vesicle trafficking between the ER and Golgi apparatus and/or Golgi and cell membrane and/or Golgi and lysosomes and/or endosome and endosome and/or endosome and lysosome trafficking in a dynamic process[233, 238, 246-249].
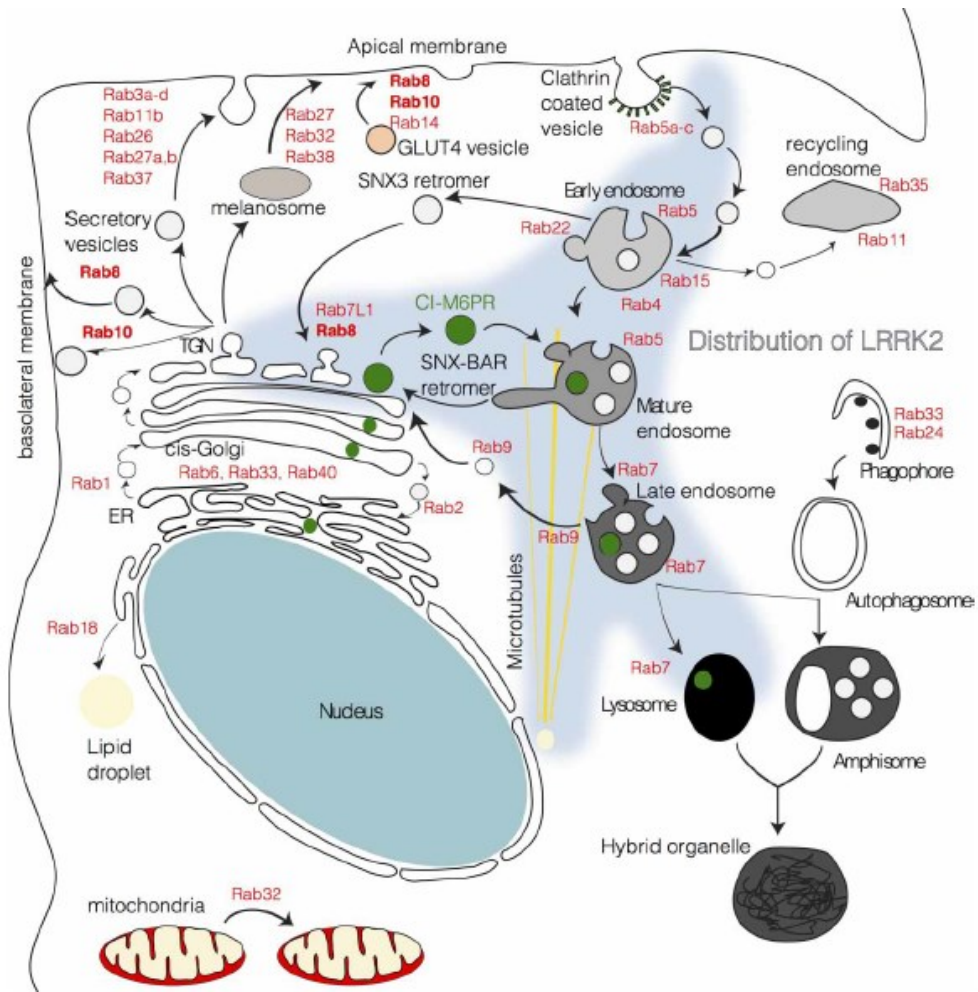
Figure 13. The localization of LRRK2 in cells supports a role in vesicular trafficking. The distribution of LRRK2 is represented as a shadow across multiple organelle compartments and associated with microtubules and the centrosome (in yellow)[178].

Chapter 2

Materials and methods

Tween® 20 (Polyethylene glycol sorbitan monolaurate), protease inhibitor cocktail, Dopamine hydrochloride, IGEPAL® CA-630 (Octylphenoxy poly(ethyleneoxy)ethanol), L-Glutathione reduced, Streptavidin–Agarose from Streptomyces avidinii, Collagen type IV, IBMX (3-Isobutyl-1-methylxanthine), Ro 20-1724 (4-(3-Butoxy-4-methoxybenzyl)imidazolidin-2-one), R-(−)-Apomorphine hydrochloride hemihydrate were obtained from Sigma-Aldrich (Milano, Italy). EZ-Link™ Sulfo-NHS-Biotin was from Thermo Fisher Scientific. LRRK2 inhibitors: CZC-25146 and GSK 2578215A from Calbiochem. The phosphate-buffered saline (PBS) solution was made using NaCl (137 mM), KCl (2.7 mM), Na2HPO4 (8.1 mM), KH2PO4 (1.47 mM) from Sigma and then adjusted to pH 7.4. Dulbecco's modified Eagle's medium (DMEM)–F12, Fetal Bovine Serum (FBS), Streptomycin/Penicillin, Geneticin-G418 were purchased from Life Technologies.

Animals

Male homozygous LRRK2 G2019S KI mice backcrossed on a C57Bl/6J background were raised at the University of Ferrara. Male non-transgenic wild-type (WT) mice were littermates obtained from the respective heterozygous breeding. Mice employed in the study were kept under regular lighting conditions (12 h light/dark cycle) and given food and water ad libitum. Experimental procedures involving the use of animals were approved by the Italian Ministry of Health (license 318/2013-B). Adequate measures were taken to minimize animal pain and discomfort.

Molecular biology techniques

Standard molecular biology techniques were performed in according to Joseph Sambrook and David W. Russell Molecular Cloning a Laboratory Manual[250].

Plasmid constructions

cDNA corresponding to human LRRK2 (accession no. NM_198578) was RT – PCR amplified from human lymphoblast mRNA and cloned as previously described in[227]. *Pac*I recognition site on LRRK2 cDNA was mutagenized by site-directed mutagenesis (forward TTGAGAAATTAATCAAACAGTGTTTG, reverse CAAACACTGTTTGATTAATTTCTCAA) without changing the amino acidic sequence. pShuttle2-LRRK2 (WT or R1441C or D1994A or G2019S) were obtained by digestions of cDNAs corresponding to human LRRK2 without *Pac*I restriction site with *Not*I and *Xba*I and subcloned in *Dra*I/*Xba*I cloning sites in pShuttle2 vector (Clontech). Expression cassettes containing LRRK2 cDNAs were excised from pShuttle2 and subcloned into pAdeno-X vector according to Adenoviral-X Expression System 1 (Clontech). Plasmids to generate DRD1 or DRD2 stable cell lines were obtained as previously described in[237]

Adenoviral delivery

Adenoviral particles were produced and titrated using the Adenoviral-X Expression System 1 (Clontech) according to manufacturer's instruction. Cells were transduced by adenoviral particles (10-30 pfu/cell) in DMEM-F12 and incubated at 37°C for 1 h. The transduced cells (usually more than 90% expressing LRRK2) were analysed 48h transduction.

Cell lines and SH-SY5Y stable clones

Human neuroblastoma SH-SY5Y cells (ATCC number CRL-2266) were grown in DMEM–F12, 10% Fetal Bovine Serum (FBS) at 37°C. The plasmid pcDNA3.1 containing cDNAs coding for DRD1-Flag or DRD2-Flag were transfected using Lipofectamine® LTX Reagent (Life Technologies) according to the manufacturer's protocol. The different SH-SY5Y clones were maintained under selection by 400 µg/mL of G418. Individual clones were picked after 14 days of selection, moved in a 96 well plate, and maintained under

selective medium until confluence growth. Different individual clones were analysed for DRD1 or DRD2 expression by western blot and immunofluorescence.

Adeno-X 293 cell line: Adenovirus 5-transformed Human Embryonic Kidney 293 cell line (HEK 293; ATCC, Rockville, MD, CRL 1573) were used to package and propagate the recombinant adenoviral-based vectors produced with the BD Adeno-X Expression System.

Biotin Protection/Degradation Assay (BPA)

$1x10^6$ -DRD1 SH-SY5Y or cells were grown in a collagen type IV (Sigma-Aldrich) coated 6-well plates. After 24 hours, cells were transduced by recombinant adenovirus and 48 later subjected to the biotin protection assay protocol as described in (25). Briefly, cells were treated with 0.3 mg/ml Sulfo-NHS-SS-Biotin for 30 min at 4°C. Cells were then washed in PBS 1X supplied with 1 mM MgCl2, 0.1 mM CaCl2, pH 8.2 and placed in DMEM–F12 pre-warmed medium for 15 min before treatment with 10µM Dopamine hydrochloride (or no treatment). After ligand treatment, plates were washed in PBS 1X containing 1 mM MgCl2, 0.1 mM CaCl2, pH 8.2, and remaining cell surface-biotinylated receptors were stripped in 75 mM NaCl, 1 mM MgCl2, 0.1 mM CaCl2, 50 mM reduced glutathione (GSH), 80 mM NaOH, 10% FBS pH 8.6 at 4 °C for 30 min. Cells were then washed in PBS 1X containing 1 mM MgCl2, 0.1 mM CaCl2, pH 8.2 and lysed by 150 mM NaCl, 1% NP40, 20mM Tris-HCl pH 7.5, protease inhibitor cocktail. Cellular debris were removed by centrifugation at 13,000xg. Cleared lysates were precipitated by Streptavidin-Agarose beads overnight at 4°C. Beads were washed 4 times with 20 mM, 150 mM NaCl, 1% IGEPAL, 20mM Tris-HCl pH 7.5. Samples were then resolved by SDS-PAGE.

Subcellular fractionation of cells or mouse tissues

Tissues from 4 months old LRRK2WT or LRRK2G2019S KI male mice were quickly dissected and frozen. Subcellular fractionation was conducted as described in (40). Briefly, striatum were homogenized in ice-cold homogenization-buffer (320 mM sucrose, 4 mM HEPES, pH 7.4, protease inhibitor cocktail (Sigma)). The homogenates were centrifuged at 1000xg for 10 min to produce the pellet containing nuclei and

large debris fraction (P1). The supernatant (S1) was further fractionated into pellet (P2 containing the membrane fraction) and supernatant (S2) by centrifugation at 10,000xg for 20 min. The S2 was ultracentrifuged at 100,000xg g to obtain the pellet (P3 containing the vesicle fraction). Protein content was determined using the Bradford protein assay. Equal amount of protein extracts were loaded into the SDS-PAGE.

Western blot analysis

Western blot analysis was performed as previously described[237]. Briefly, protein content was determined using the Bradford protein assay. Equal amounts of protein extracts were resolved by standard sodium dodecyl sulfate-polyacrylamide gel electrophoresis. Samples were electroblotted onto Protan nitrocellulose (GE Healthcare Life Sciences). Membranes were incubated with 3% low-fat milk in 1X PBS-Tween 0.05% solution with the indicated antibody: anti-LRRK2 (1:5000 MJFF2 c41-2 Epitomics), anti-Flag (1:2500 Sigma-Aldrich), anti-D1 dopamine receptor (1:2000 Sigma-Aldrich), anti-beta-actin (1:5000 Sigma-Aldrich), Phospho-p44/42 MAPK (Thr202/Tyr204) (1:1000 Cell Signalling) for 16 h at 4°C. Goat anti-mouse immunoglobulin G (IgG) peroxidase-conjugated antibody (1:2500 Millipore Corporation) or goat anti-rabbit IgG peroxidase-conjugated antibody (1:5000 Millipore Corporation) were used to reveal immunocomplexes by enhanced chemiluminescence using Pierce™ ECL Plus Western Blotting Substrate (Thermo Fischer Scientific).

Immunofluorescence

For cells: 1×10^5 SH-SY5Y-DRD1 or SH-SY5Y-DRD2 cells, grown on a cover-glass, were washed twice with PBS 1X and then fixed with 4% paraformaldehyde/PBS for 20 min. Cells were permeabilized with 0.1% Triton X-100 diluted in PBS. For tissue: after apomorphine hydrochloride (3mg/Kg) treatment mice were sacrificed. The brains were embedded in OCT freezing medium and 10 μm-thick sections were prepared by cryostat. All sections were fixed with 4% paraformaldehyde/PBS for 15 min and washed with 0.05% Tween-20 diluted in PBS. Non-specific binding was blocked with 5% bovine serum albumin, 0.05% Tween-20 diluted in PBS for 1 h at room temperature. Cells or tissue were incubated with primary antibodies: anti-LRRK2 (1:500 MJFF2 c41-2 Epitomics), anti-Flag (1:2500 Sigma-Aldrich), anti-alpha-synuclein

41

(1:500, Millipore), anti-D1 dopamine receptor (1:1000, Sigma-Aldrich), anti-H4 histone (1:5000, Sigma-Aldrich) diluted in blocking solution, overnight at 4°C. Samples were then washed with PBS, 0.05% Tween-20 diluted in PBS and incubated with secondary antibodies: Goat anti-Mouse IgG Secondary Antibody Alexa Fluor® 488 (Life Technologies), Goat anti-Mouse IgG Secondary Antibody Alexa Fluor® 647 (Life Technologies), Rabbit IgG Secondary Antibody Alexa Fluor® 488 (Life Technologies), Rabbit IgG Secondary Antibody Alexa Fluor® 647 (Life Technologies) and Rat IgG Secondary Antibody Alexa Fluor® 488 (Life Technologies) diluted 1:1000 in blocking solution for 1 hour at room temperature. Golgi staining was performed with anti-TGN46 antibody (Bio-Rad) and Donkey anti-Sheep IgG Alexa Fluor® 647 as secondary antibody were used. Before analysis, cells were mounted using Mowiol mounting medium and fluorescence was revealed with a Leica TCS SP5 confocal microscope with LAS lite 170 image software with a 63x magnification oil immersion objective and 3.50 digital zoom. Post analysis were performed using ImageJ NIH software.

Intracellular cAMP Determination

SH-SY5Y-DRD1 cells were incubated in sterile 96-well plate with a seeding density of 1×10^4 cells per well. Cells were cultured in DMEM-F12 10% FBS during 24 hours and transduced by adenovirus encoding LRRK2s for 48 hours. Medium was replaced by serum-free medium containing 10µM Dopamine hydrochloride, 500µM IBMX and 100µM Ro 20-1724 and incubated for different times. Intracellular cAMP levels measurement was performed using cAMP-Glo assay kit according to manufacturer's instruction (Promega Corporation). Luminescence was measured using the Victor™ X5 Multilabel Plate Reader (PerkinElmer)

Statistical analysis

The results are presented as means ± S.D. of n≥3 independent experiments. Statistical evaluation was conducted by one-way or two-way ANOVA and Bonferroni post test. Values significantly different from the relative control are indicated with an asterisk. *p<0,05; **p<0,01; ***p<0,001.

Chapter 3

Results

3.1 Characterization of SH-SY5Y cells stably expressing dopamine receptor D1 or D2 and LRRK2 adenoviral vectors

SH-SY5Y cells stably expressing dopamine receptor D1 or D2

To generate stable SH-SY5Y cell lines stably expressing dopamine receptor D1 (DRD1) or dopamine receptor D2 long isoform (DRD2L), pcDNA3.1-DRD1-3xFlag or pcDNA3.1-DRD2L-3xFlag plasmid constructs were transfected in SH-SY5Y cell lines using Lipofectamine® LTX with Plus™ Reagent (Life Thecnologies) as described in the manufacturer's instructions. After several weeks of selection by G418, single stable clones were isolated. Different individual clones were analysed for DRD1 or DRD2L expression by western blot and immunofluorescence (figure 14 B-C-D). As expected, DRD1 is largely localized on the cell membrane. On the contrary DRD2L is partially localized inside SH-SY5Y cells. This phenotype is comparable to published data obtained by independent groups that have generated similar DRD2L stable clones[251, 252]

Adenoviral delivery of LRRK2

As molecular tool to express LRRK2 WT or pathological mutants, recombinant LRRK2 adenoviral vectors were generated. The assembly of recombinant adenoviruses has been completed in few stages: first, the cDNA encoding for LRRK2 WT, R1441C or G2019S pathological mutants and D1994A kinase dead were cloned into pShuttle2 plasmid DNA. Second, the expression cassette was excised from recombinant

Mauro Rassu: "LRRK2 effect on dopamine receptor trafficking – implication in Parkinson's disease".
Ph.D. Course in Life Sciences and Biotechnologies – University of Sassari.

pShuttle2 plasmid DNA by digestion with I-*Ceu* I and PI-*Sce* I and ligated into Adeno-X and selected. Third, the recombinant adenoviral constructs were cleaved by *Pac*I to expose the inverted terminal repeats (ITR) and transfected into HEK-293 AdenoX cell lines. After 7–10 days, viruses were harvested and amplified by infecting packaging cells for three times to obtain high titer virus stock. The final yields were evaluated performing an end-point dilution assay. To characterize LRRK2 adenoviral expression vectors, recombinant adenoviruses were used to transduce SH-SY5Y cells with a scalar multiplicity of infection (M.O.I.). Forty-eight hours after transduction cells were lysed and protein extracts analysed by Western Blot. As shown in figure 14A all adenoviral preparations are able to produce a high level of expression of LRRK2 in SH-SY5Y cell lines.
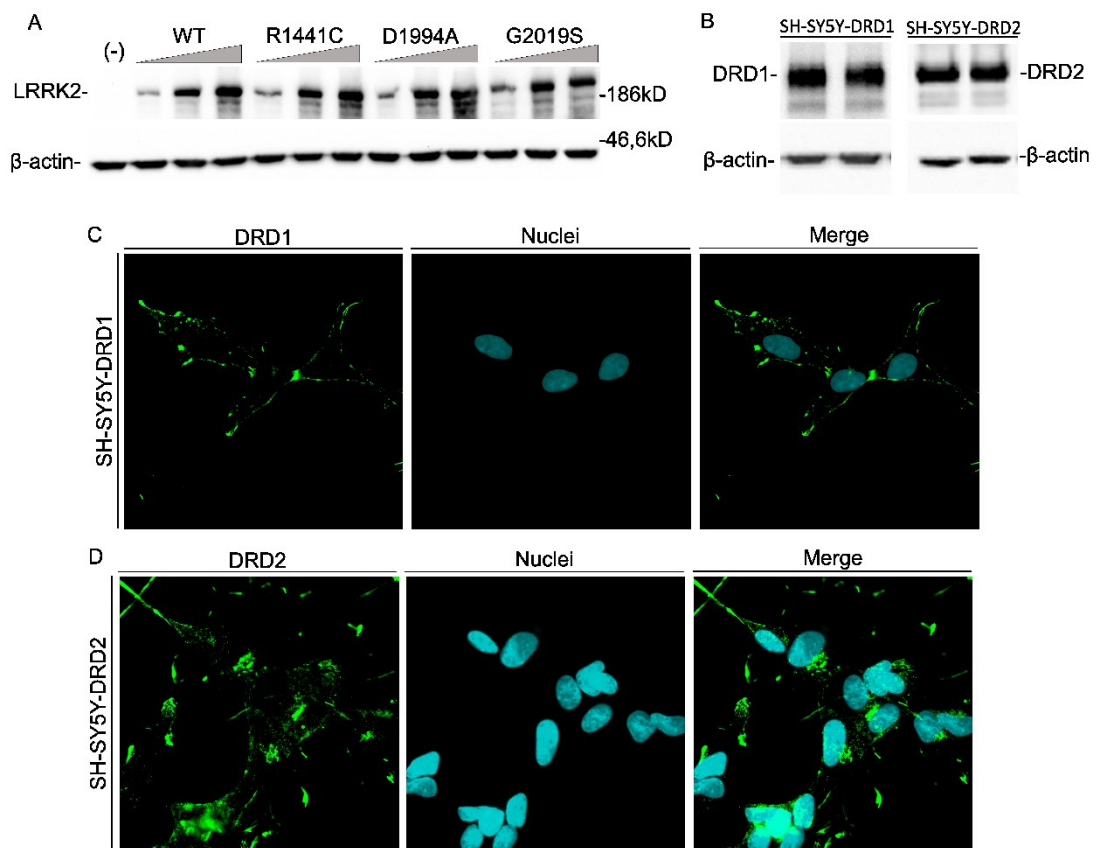
Figure14. Evaluation of LRRK2 expression level and SH-SY5Y stable clones analysis. (A) SH-SY5Y were transduced by increasing amount of recombinant adenoviruses (5-20-60 pfu/cell) and analyzed 48 hours after transduction. Cell lysates were subjected to reducing SDS-PAGE and western blot. The anti-LRRK2 antibody (MJFF2 c41-2) was used to visualize LRRK2 expression level and β-actin serves as controls for equal loading of samples. (B) SH-SY5Y stable clones were analyzed to evaluate the expression levels of DRD1 and DRD2L by SDS-PAGE and western blot using an anti-FLAG antibody and (C-D) by immunofluorescence using an anti-FLAG antibody and an Alexa Fluor-488 anti-mouse as a secondary antibody. Imagines were acquired by a DMI 6000 CS Leica florescent microscopy at 63x magnification.

3.2 LRRK2 affects DRD1 trafficking in cellular models

To investigate the role of LRRK2 in DRD1 trafficking, stable SH-SY5Y-DRD1 cells were transduced with the adenoviral vectors encoding for LRRK2 WT, R1441C or G2019S pathological mutants and D1994A dead kinase. The internalization of DRD1 was analysed upon DA (10µM) treatment, at different time points, by confocal microscopy. As shown in figure 15 A and 16 A, at basal conditions the receptor is mainly localized on the cell surface, both in not transduced cells or in cells overexpressing the different LRRK2 isoforms. Upon DA treatment (figure 15 B) DRD1 is rapidly internalized at five minutes as displayed by the presence of red dots inside the cells. On the contrary, LRRK2 G2019S mutant overexpression impairs the receptor internalization. This effect becomes even more evident after fifteen minutes of dopamine treatment (figure 15 B and 16B). After one hour of DA treatment, the DRD1 is almost completely recycled back to the membrane in untrasnsduced cells while some red dots are still visible in cells transduced by G2019S LRRK2. No significant effects on DRD1 internalization were obtained in cells expressing LRRK2 WT, R1441C mutant or D1994A kinase dead compared to negative control (figure 15 B-C-D and 16 B) or two different LRRK2 kinase inhibitors CZC-25146 or GSK 2578215A inhibitors (figure 17 only CZC-25146 treatment at 0 and 15 minutes is shown in A and B). The reduced internalization of DRD1 observed in the presence of G2019S LRRK2 after stimulation with dopamine, strongly indicates an alteration of endocytosis rather than an increase in recycling/exocytosis pathway.
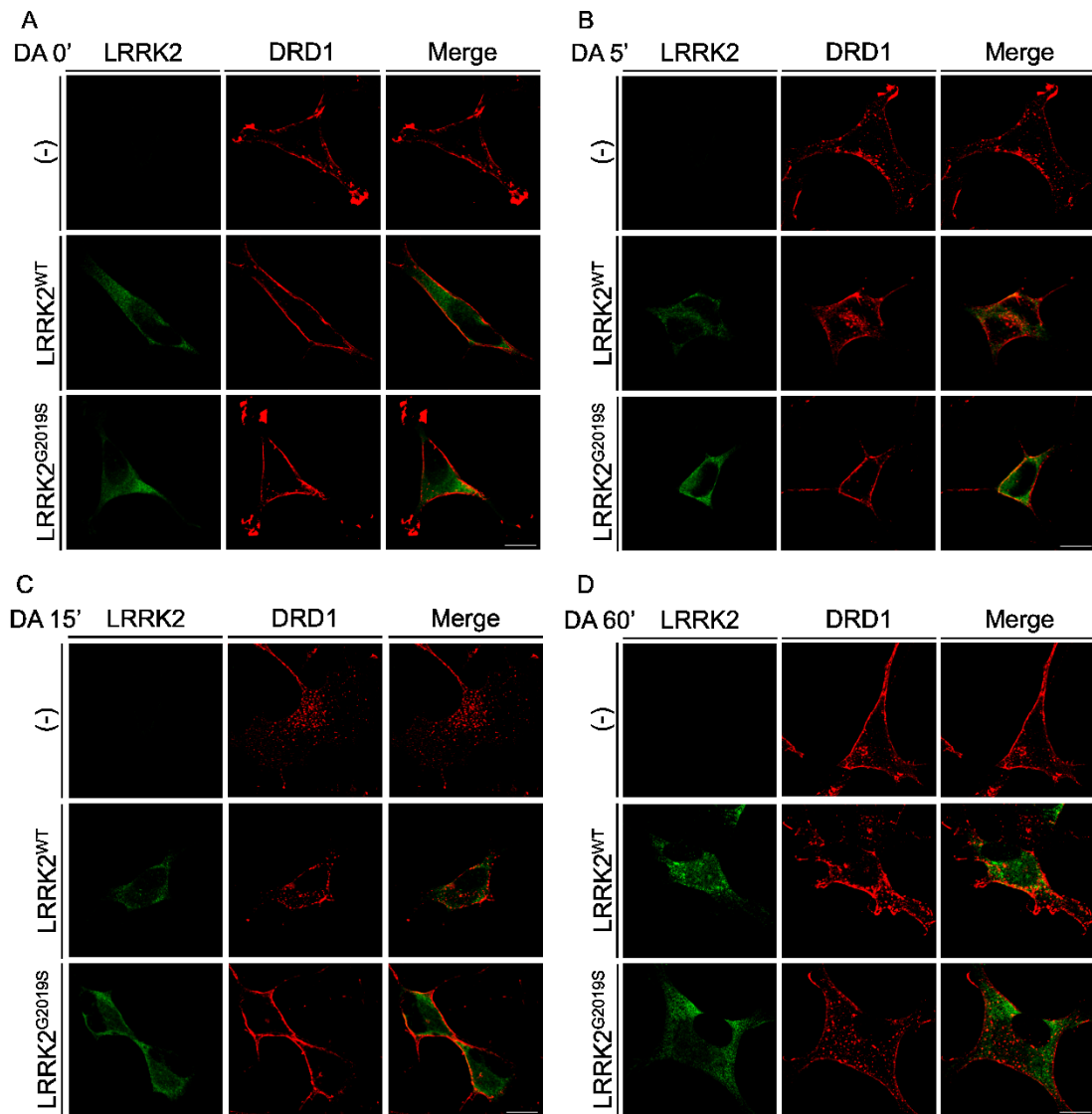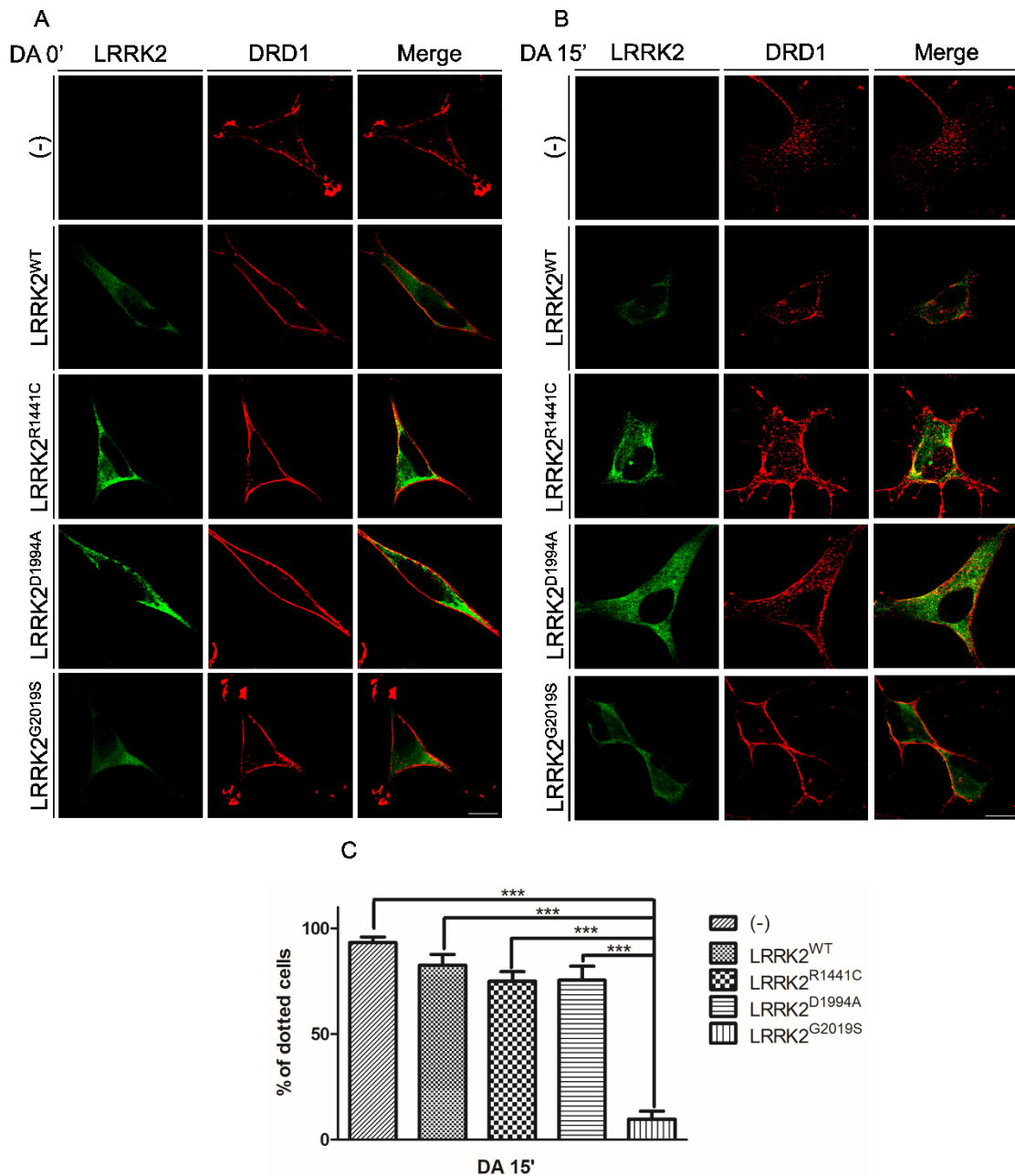
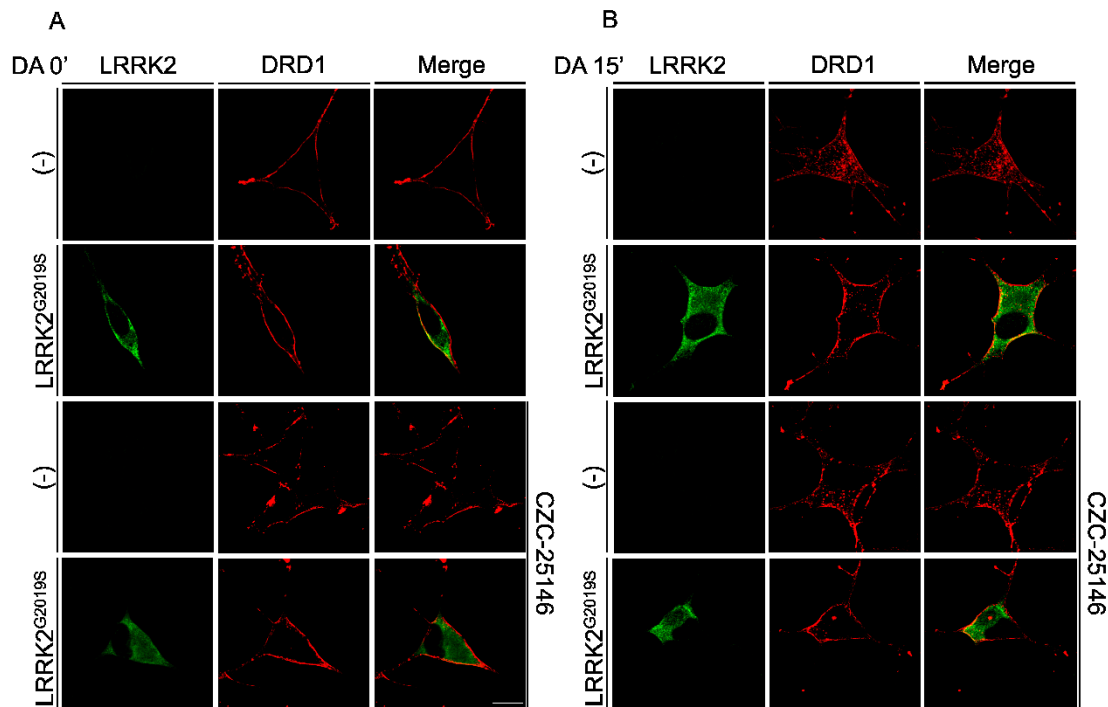**Figure 15. Analysis of DRD1 internalization upon dopamine treatment in SH-SY5Y-DRD1 cells untransduced or transduced by WT or mutant G2019S LRRK2**. (A-D) DRD1 localization at basal conditions (A) and upon 5-15-60 minutes (B-C-D) of dopamine (10μm) treatment of SH-SY5Y-DRD1 cells transduced by the different recombinant adenovirus for 48h. After agonist treatment the cells were fixed and incubated by the different primary antibodies (anti-FLAG for DRD1 and anti-LRRK2 (MJFF2) for LRRK2) and with Alexa647-conjugated secondary antibody (red) or Alexa488-conjugated secondary antibody (green) for DRD1 or LRRK2 respectively. Scale bars = 10μm.

Figure 16. Analysis of DRD1 internalization upon dopamine treatment in SH-SY5Y-DRD1 cells untransduced or transduced by WT, R1441C G2019S mutants or D1994A kinase dead LRRK2. DRD1 localization at basal conditions (A) and upon 15 minutes (B) of dopamine treatment of SH-SY5Y-DRD1 cells transduced by the different recombinant adenovirus for 48h. After dopamine (10μm) treatment the cells were fixed and incubated by the different primary antibodies (anti-FLAG for DRD1 and anti-LRRK2 (MJFF2) for LRRK2) and with Alexa647-conjugated secondary antibody (red) or Alexa488-conjugated secondary antibody (green) for DRD1 or LRRK2 respectively. Scale bars = 10μm. (C) The graph represents the percentage of cells with dots at 15' minutes of dopamine treatment and Two-way ANOVA analysis. ***$p < 0{,}001$.

Figure 17. Analysis of DRD1 internalization upon dopamine treatment and LRRK2 kinase inhibitors in SH-SY5Y-DRD1 cells untransduced or transduced by LRRK2 G2019S. DRD1 localization at basal conditions (A) and upon 15 minutes (B) of dopamine treatment of SH-SY5Y-DRD1 cells transduced by the different recombinant adenovirus for 48h. Cells were and treated with two different LRRK2 inhibitors (5µM overnight). After agonist treatment the cells were fixed and incubated by the different primary antibodies (anti-FLAG for DRD1 and anti-LRRK2 (MJFF2) for LRRK2) and with Alexa647-conjugated secondary antibody (red) or Alexa488-conjugated secondary antibody (green) for DRD1 or LRRK2 respectively.

To have a more quantitative evaluation of the alteration of DRD1 trafficking in the presence of G2019S LRRK2 a biotin degradation protection assay (BPA) was performed[253]. As shown in figure 18 A-B the kinetic of DRD1 internalization is strongly reduced in LRRK2 G2019S transduced cells compared to untransduced cells or cells transduced with LRRK2 WT upon 15 minutes of DA treatment. It is interesting to note the shift in DRD1 molecular weight upon agonist treatment, probably due to receptor phosphorylation. In fact, in absence of any phospho-specific antibody that recognize phospho-DRD1, the DRD1 shift has been largely used to measure the receptor phosphorylation/activation state[254].
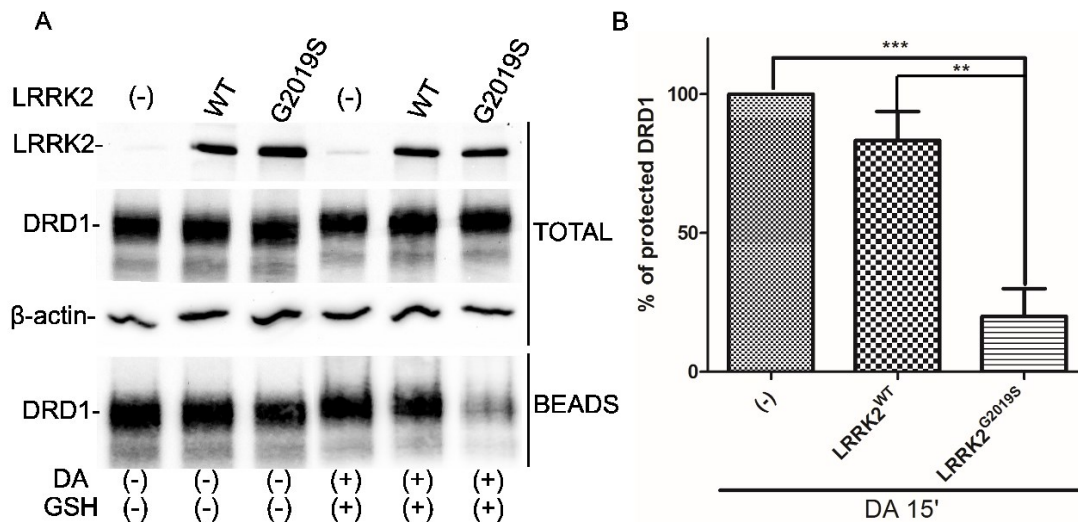
Figure 18. Evaluation of DRD1 intracellular and extracellular level by BPA upon dopamine treatment in SH-SY5Y-DRD1 cells untransduced or transduced by WT or G2019S LRRK2. (A) Cells stably expressing FLAG-tagged DRD1 were transduced by the different LRRK2 isoforms. 48h after transduction the cell membrane protein were labeled by biotin. After 15 minutes of dopamine treatment the cell surface-biotinylated receptors were stripped and the cell lysates subjected to immunoprecipitation by anti-biotin. Total and immunoprecipitated (beads) proteins were visualized by western blot using specific antibody for the indicated proteins. β-actin serves as controls for equal loading of samples. (B) Densitometric analysis of data obtained in (A) normalized by the untransduced cells and analyzed by two-way ANOVA test. **p<0,01; ***p<0,001.

As previously mentioned in the introduction chapter different experimental evidence suggests a potential role of synuclein in the control of vesicle trafficking[255]. The possible effect of synuclein overexpression on DRD1 trafficking upon DA treatment was analysed in the same experimental conditions performed in LRRK2 experiments. As shown in figure 19 A-B no significant effect in DRD1 trafficking is displayed by the overexpression of alpha synuclein WT or the pathological mutant A53T.
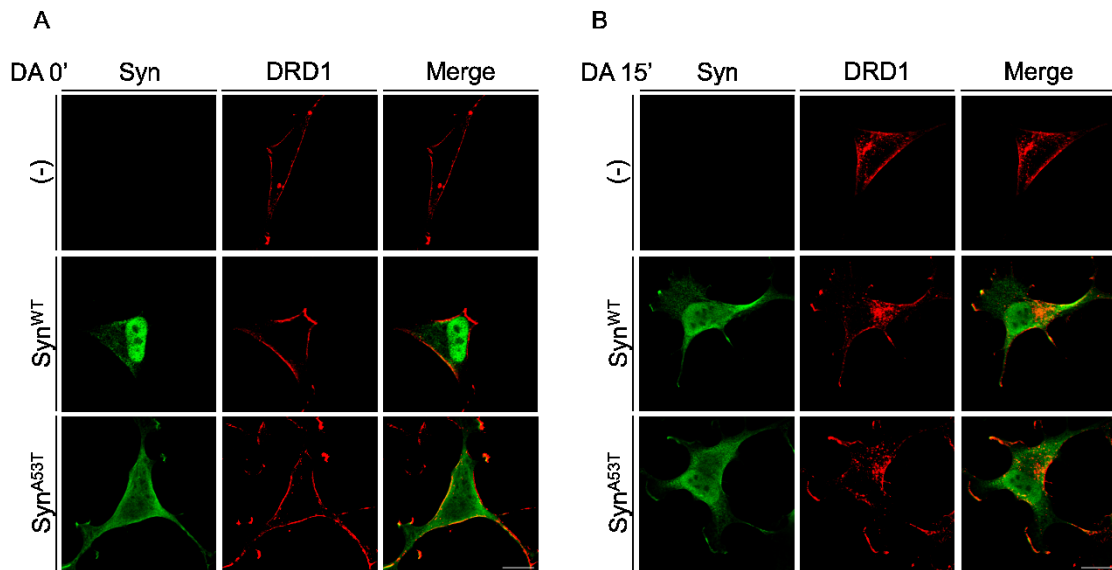
Figure 19. Analysis of DRD1 internalization upon dopamine treatment in SH-SY5Y-DRD1 cells untransduced or transduced by WT or A53T Alpha synuclein. DRD1 localization at basal conditions (A) and upon 15 minutes (B) of dopamine treatment of SH-SY5Y-DRD1 cells transduced or not by alpha-synuclein WT or A53T. After agonist treatment the cells were fixed and incubated with the different primary antibodies (anti-FLAG for DRD1 and anti-synuclein (Millipore) for alpha-synuclein) and with Alexa647-conjugated secondary antibody (red) or Alexa488-conjugated secondary antibody (green) for DRD1 or synuclein respectively. Scale bars = 10µm. No significative results were obtained after two-way ANOVA test analysis.

3.3 LRRK2 alters the dopamine D2 receptor trafficking

As mentioned, DRD1 is largely localized on the cell membrane whereas DRD2L is partially localized inside SH-SY5Y cells, likely linked to vesicle structures and Golgi apparatus. This phenotype matches with reports from other groups that used similar DRD2L stable clones[251, 252]. Moreover, in SH-SY5Y cells, the dopamine receptor trafficking differs between the different subtypes. DRD1 is recycled back to the plasma membrane while DRD2 is mainly degraded after receptor internalization upon agonist treatment[253].

First of all, to analyse the possible alteration in DRD2L localization the stable SH-SY5Y-DRD2L cells were transduced by the different LRRK2 isoforms. After 48 hours post-transduction intracellular DRD2L distribution was analysed by confocal microscopy. As shown in figure 20 A-B, the overexpression of LRRK2 pathological mutants causes a significant accumulation of DRD2L into the cells compared to LRRK2 WT, kinase dead and even more compared to not transduced cells. Co-staining by anti-TGN46 antibody detect the presence of DRD2L into the Golgi apparatus (figure 20 A).
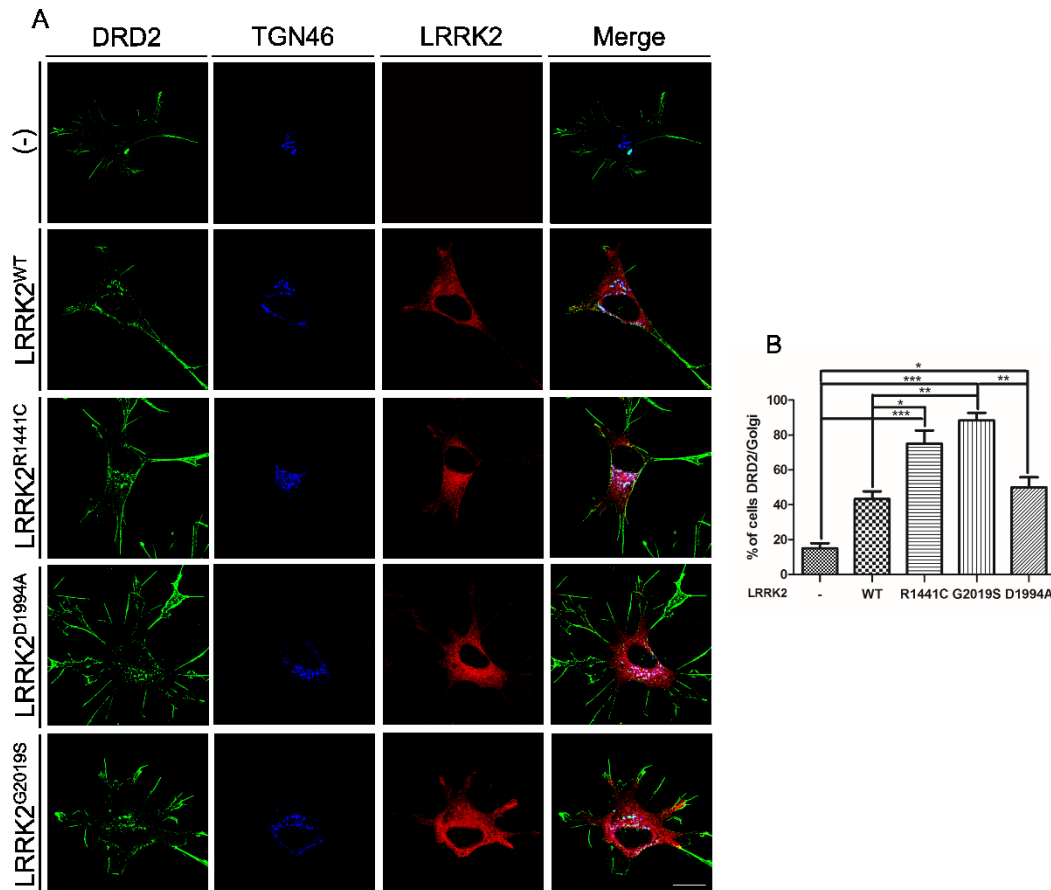
Figure 20. Analysis of LRRK2 effect on DRD2 cell localization. (A) SH-SY5Y cells stably expressing FLAG-tagged DRD2L were transduced by WT or G2019S LRRK2. 48h after transduction, the cells were fixed and incubated with the different primary antibodies (anti-FLAG for DRD2, anti-LRRK2 antibody (MJFF2 c41-2) for LRRK2 and anti-TGN46 antibody as trans-Golgi marker) and with Alexa488-conjugated secondary antibody (green), Alexa546-conjugated secondary antibody (red) and Alexa647-conjugated (blu) for DRD2, LRRK2 and trans-Golgi respectively. Scale bars = 10μm. (B) Quantification of data obtained in (A). One-way ANOVA analysis *p<0,1 **p<0,01; ***p<0,001.

To investigate if DRD2 Golgi localization results in an alteration in DRD2L total protein level in presence of LRRK2 overexpression, or if LRRK2 affect only the DRD2 Golgi localization without any chance in DRD2 total protein level, stable SH-SY5Y-DRD2L cells were transduced by the different LRRK2 isoforms. After forty-height hours the total DRD2L protein level was analysed by western blot. As shown in figure 21 A-B, the over-expression of LRRK2 mutants determines a slight but significant increase in DRD2L total protein level compared to LRRK2 WT and an important increase compared to untransduced cells. No change in DRD1 total level protein was detectable in the presence of any LRRK2 isoforms (figure 21 G). In a general view, the increased DRD2 protein total level can be linked to a higher transcription rate, an increase in protein synthesis or a DRD2 protein degradation inhibition. However no difference in DRD2

mRNA total levels, analysed by real time PCR, were detected 48 hours after adenoviral transduction, by any LRRK2 mutant, compared to untransduced cells (data not shown).

De novo protein synthesis was then analysed after short protein translation block by puromycin treatment. As shown in figure 21C and 21D, the level of DRD2L protein synthesis was comparable between the different experimental samples at early time points (1 or 2 hours), strongly indicating that LRRK2 expression does not alter DRD2 protein translation rate. However, at 3 hours is possible to detect significant differences in DRD2L level in the presence of G2019S LRRK2 that likely reflects an alteration in localization and/or degradative pathways. No differences on LRRK2 or beta-actin protein level were detected by this short puromycin treatment. Then, the DRD2 turnover was evaluated by blocking protein synthesis by puromycin treatment forty-height hours after transduction of SH-SY5Y-DRD2L cells by WT or G2019S LRRK2 recombinant adenovirus. As shown in figure 21 (E and F), the degradation rate is slower in G2019S LRRK2 cells than in untransduced cells. Roughly 50% of DRD2 is degraded in untransduced cells after 15 minutes of puromycin treatment compared to the roughly 20% decrease in cells transduced by G2019S LRRK2. Cells transduced by LRRK2 WT show an intermediate phenotype. Taken together, these data suggest that LRRK2 pathological mutants can affect the DRD2L trafficking between the Golgi and the plasma membrane that in turn may influence the DRD2L half-life. These results do not exclude also a direct fuction/involvement of LRRK2 in the autophagic-lysosomal pathways.
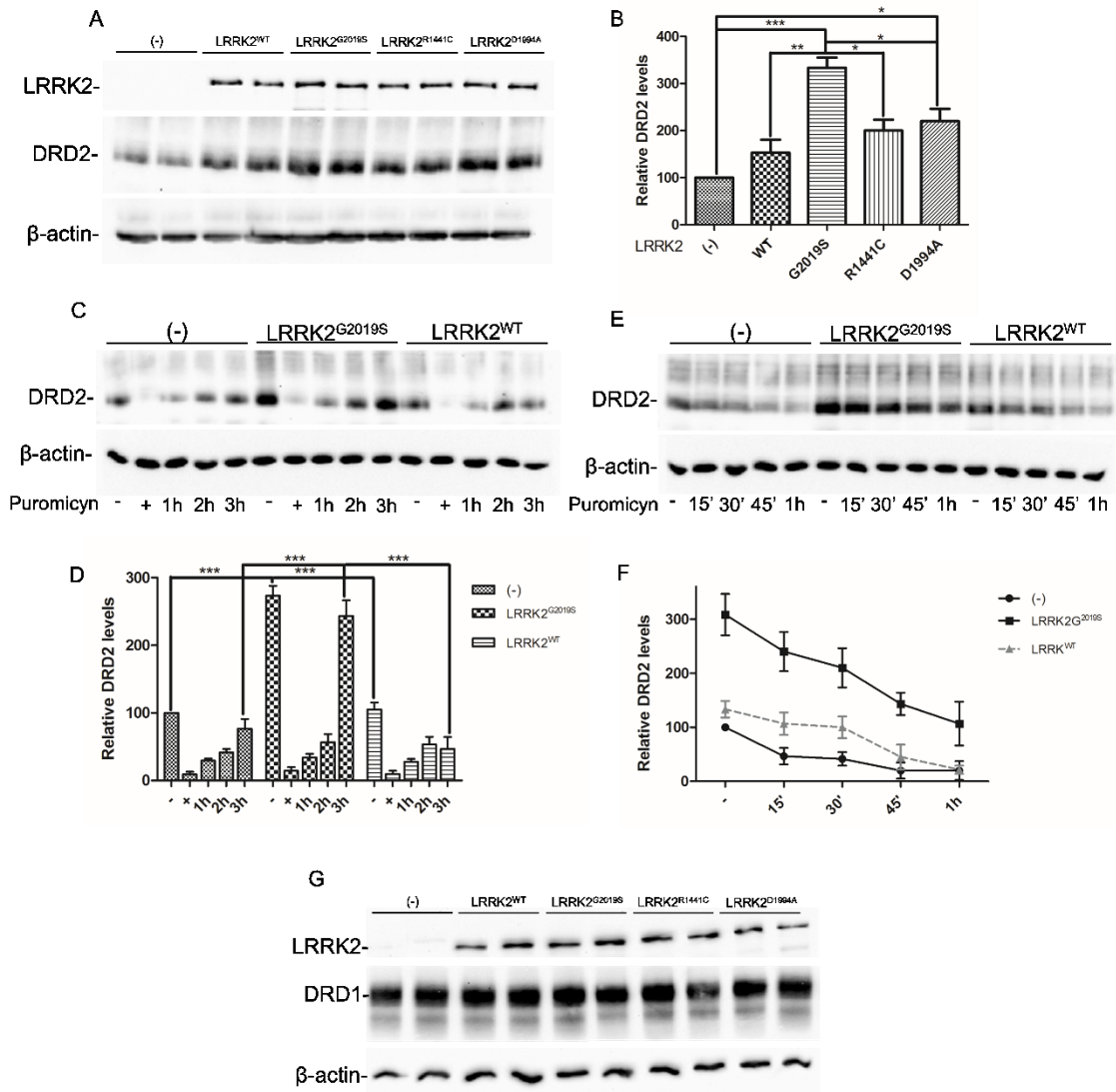
Figure 21. Analysis of LRRK2 effect on DRD2 total protein level. (A) SH-SY5Y cells stably expressing FLAG-tagged DRD2 were transduced by the different LRRK2 isoforms. 48h after transduction, protein extracts were prepared and subjected to SDS-PAGE and western blot. The indicated proteins were visualized by western blot using specific antibody. β-actin serves as controls for equal loading of samples. (B) Quantification of data obtained in (A) and one-way ANOVA test analysis **p<0,05, ***<0,0001. (C) SH-SY5Y-DRD2 transduced as in (A) were treated for 2 hours by puromycin (+), then the compound was removed and the new DRD2L protein synthesis was analyzed at 1h, 2h and 3h. Cell lysates were prepared and analyzed by western blot. (D) Relative band densitometry of data obtained in (C) normalized by the untransduced cells, and two-way ANOVA analysis test were performed as statistical analysis. (E) SH-SY5Y-DRD2 transduced as in (A) were treated for different time points (15', 30', 45', 60') by puromycin, then cell lysates were prepared and analyzed by western blot. DRD2 decrease was visualized by specific anti-FLAG antibody. (F) Relative band densitometry of data obtained in (D) normalized by the untransduced cells and two-way ANOVA analysis test were performed as statistical analysis. (G) SH-SY5Y-DRD1 were transduced and analyzed as in (A).

3.4 LRRK2 expression alters both DRD1 and DRD2 signalling

To study whether the DRD1 and DRD2 trafficking dysregulation due to LRRK2 mutant expression may influence the DA receptor signalling pathways the phosphorylation of Extracellular signal Regulated Kinases 1 and 2 (ERK1 and ERK2) was analysed. As mentioned in the introduction, data obtained from different cell culture systems suggest that both D1- and D2-class dopamine receptors can regulate ERK phosphorylation/activation[256-259].

DRD1- or DRD2-SH-SY5Y cells were transduced by recombinant adenovirus expressing WT or G2019S LRRK2. Forty-eight hours after transduction, cells were incubated for 2 hours without serum and then dopamine was added at different time points (15, 30 or 60 minutes). Subsequently, protein extracts were analysed by western blot using an anti-phospho-ERK antibody. As shown in figures 22 A-B, the presence of G2019S LRRK2 determines a strong ERK activation upon DA treatment in the SH-SY5Y-DRD1 cells and this activation is more persistent than in untransduced cells or in cells transduced by WT LRRK2 that show an intermediate phenotype. Similar results were obtained on ERK phosphorylation, in SH-SY5Y cells stable expressing DRD2, transduced by the different LRRK2 isoforms upon dopamine stimulation (figure 22 C-D). These results suggest that the overexpression of WT and G2019S LRRK2 modifies the DRD1 and DRD2 signalling, most likely through an alteration of receptor trafficking. To further explore the DRD1 signalling in cells overexpressing LRRK2, cAMP generation upon dopamine treatment in SH-SY5Y-DRD1 was analysed (figure 22 E). In SH-SY5Y-DRD1, upon dopamine treatment, G2019S LRRK2 determines a significant decrease of ATP level (that indicates an increase in cAMP generation) compared to cells transduced with WT LRRK2 or untransduced cells.
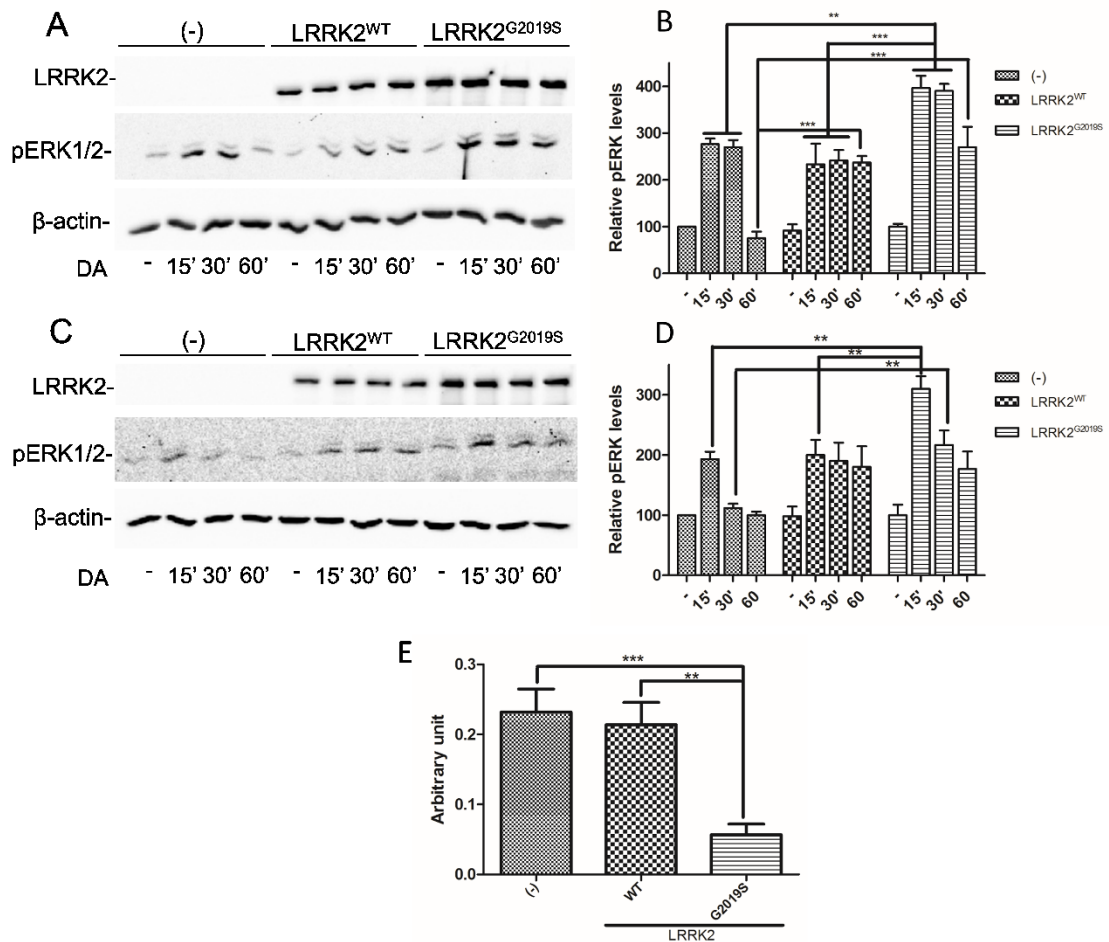
Figure 22. Analysis of DRD1 and DRD2 signaling upon dopamine treatment in SH-SY5Y-DRD1 or -DRD2 stable lines untransduced or transduced by WT or G2019S LRRK2. (A) Cells stably expressing FLAG-tagged DRD1 were transduced by the different LRRK2 isoforms. 48h after transduction the cell were treated for different time points (15', 30', 60') by dopamine. Cell lysates subjected to western blot using specific antibody for the indicated proteins. β-actin serves as controls for equal loading of samples. (B) Relative band densitometry for DRD1 of data obtained in (A) normalized by untransduced and untreated cells. (C) Cells stably expressing FLAG-tagged DRD2 were treated as before and analyzed by western blot. (D) Relative band densitometry for DRD2 of data obtained in (C) normalized by untransduced and untreated cells. (E) The SH-SY5Y-DRD1 were treated as before and analyzed for cAMP level at upon 15 minutes of dopamine treatment. The assay is measuring the ATP decrease due cAMP generation. Two-way ANOVA as statistical test were performed **p<0,01; ***p<0,001.

3.5   Analysis of DRD1 trafficking in LRRK2 animal models

Before performing any experimental analysis in animal models, commercial anti-DRD1 or anti-DRD2 antibodies were tested. The commercial anti-DRD1 antibody (Sigma D2944) was able to detect the DRD1 protein either by western blot or by immunofluorescence. Unfortunately, in the same experimental conditions, no commercial anti-DRD2 antibodies were able to detect the DRD2 either by western blot or by immunofluorescence. Therefore, mice tissues were analysed only for DRD1 expression.

The DRD1 trafficking was analysed in the striatum of 4-month old male mice knock-in for G2019S LRRK2 and 4-month old male mice WT LRRK2 as a control. Western blot analysis showed no difference in DRD1 level in total, membrane or vesicle fraction between WT or G2019S LRRK2 knock-in mice, either in basal conditions or after treatment with apomorphine (3 mg/Kg) for 20 or 60 minutes to stimulate dopamine receptors trafficking (data not shown). However, immunofluorescence analysis on striatal sections highlighted significant differences between the two genotypes. In particular, after 25 minutes of apomorphine treatment is detectable a relevant dotted DRD1 staining (likely in vesicle structures) in WT compared to G2019S knock-in mice (Figure 23 A-B). No significant differences were visible in saline treated animals between the two different genotypes.
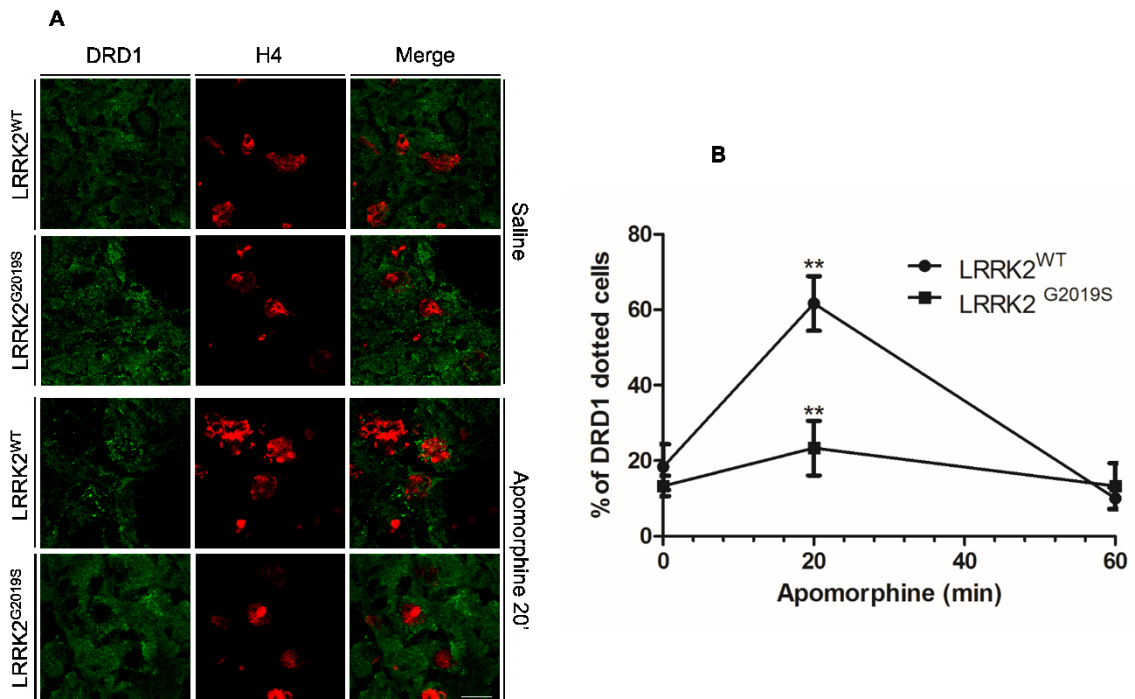

Figure 23. Analysis of DRD1 internalization in G2019S LRRK2 knock-in mice. (A) DRD1 localization/internalization upon 20 minutes of saline (saline) or apomorphine treatment (apomorphine) of G2019S LRRK2 knock-in mice or WT. After agonist treatment the mouse brain were dissected and frozen in embedding medium. Cryostat sections were incubated with the different primary antibodies (anti-DRD1 or histone H4) and with Alexa488-conjugated secondary antibody (green) or Alexa647-conjugated secondary antibody (red) for DRD1 or H4 respectively. Scale bars = 10µm. (B) Quantification of the data obtained in (A). Two-way ANOVA as statistical test were performed **p<0,01.

Chapter 4

Discussion

Parkinson's disease is a common, progressive neurodegenerative disorder, affecting 3% of people over 75 years of age. Until now, the aetiology of PD is largely unknown. In the majority, PD cases are sporadic however in a small percentage PD are hereditary. Mutations in the LRRK2 gene (PARK8; OMIM #609007) are the major genetic causes of PD. Furthermore, LRRK2 has been identified as a risk factor in PD onset. Phenotypically, LRRK2 PD linked is indistinguishable from sporadic PD, mid to late onset, slow progression and a good response to levodopa therapy. LRRK2 appears to be involved in different cellular pathways such as mitochondrial function, vesicular trafficking, cytoskeletal dynamics, protein aggregation, autophagy, neurite morphology. The most important symptoms of PD are related to movement disorders and are caused by a progressive and profound loss of dopaminergic neurons in the SNpc[100, 260].

Five subtype of dopamine receptors have been identified (D1, D2, D3, D4 and D5) and mediate all physiological functions of the catecholaminergic neurotransmitter dopamine. Among them, dopamine receptors D1 and D2 are the most abundant. Dopamine receptors belong to G protein-coupled receptors (GPCRs) family. In a canonical mechanism of action, they are stimulated by agonist binding, desensitized, internalized into vesicles and degraded or recycled to the plasma membrane. At the same time, they evoke a signal transduction cascade that is typical of each receptor subtype[25]. It has been demonstrated that dopamine receptor D1 is rapidly internalized in response to dopamine and recycles *in vivo*[261, 262], in contrast, dopamine receptor D2 is significantly down regulated *in vivo* after prolonged drug administration[263], either in

animals with increased dopamine level obtained through deletion of the dopamine transporter[264] or after chronic low doses of dopamine receptor D2 agonists[265]. These data parallel those obtained in the majority of experiments using cultured cells stably expressing dopamine receptors D1 or D2[253], although with some differences for dopamine D2 receptor[251]. The SH-SY5Y cells stably expressing dopamine receptors D1 and D2, used in this experimental work, largely summarize the dopamine receptor trafficking observed *in vivo* and *in vitro* in most of experimental models, therefore can be reasonably used to generate in *vitro* data to study the effect of LRRK2 on dopamine receptor physiology.

The main goal of this experimental work was to study the effect of LRRK2 on dopamine receptor trafficking and signalling by different molecular approaches, in fact different experimental evidence suggests that LRRK2 plays an important role in the control of vesicle trafficking. In SH-SY5Y cells stably expressing the dopamine receptor D1 the expression of G2019S LRRK2 causes a strong impairment in dopamine receptor D1 internalization upon dopamine treatment. This effect is not visible in cells transduced of either WT or A53T alpha synuclein, excluding any possible artefact in this assay due to recombinant protein expression or to adenovirus transduction. The reduced internalization of dopamine receptor D1 in cells overexpressing LRRK2 G2019S, even at short time (5 minutes), strongly suggests an alteration in endocytosis more than an increase in recycling/exocytosis pathway. It is interesting to note that this result coincides to the clustering/internalization impairment upon apomorphine treatment in G2019S LRRK2 knock-in mice compared to WT LRRK2 mice as shown by immunofluorescence analysis on brain sections. In animal models it was not possible to confirm these data by western blot analysis, but this incongruity can be reasonably explained by the complexity of the striatal tissue; for instance, striatal neurons differ in terms of firing rate and timing in response to agonist stimulation. The internalization impairment is most probably independent of dopamine receptor D1 phosphorylation, since the receptor band undergoes a similar molecular weight shift when analysed by SDS-PAGE in the absence or presence of WT or G2019S LRRK2. The dopamine receptor D1 trafficking alteration in cells overexpressing G2019S LRRK2 parallels a change in its signalling, with a higher cAMP generation and ERK phosphorylation, strongly

suggesting that the impairment in receptor internalization may alter signalling transduction cascade. Therefore, these results indicate that G2019S LRRK2 is altering some molecular mechanism that mediates the internalization of dopamine receptor D1 following the receptor phosphorylation due to agonist treatment.

An alteration in receptor trafficking is detectable also in SH-SY5Y-DRD2 stable line indicating that the LRRK2 overexpression determines a significant dopamine receptor D2 accumulation into the Golgi apparatus compared to untransduced cells. This phenotype is more evident in the presence of LRRK2 pathological mutants compared to WT. These results are of particular interest since all LRRK2 pathological mutants show similar phenotype suggesting a common pathological pathway for all these mutants. The dopamine receptor D2 accumulation into the Golgi correlates with a significant increase of dopamine receptor total protein levels. The presence of any LRRK2 isoform does not significantly alter the dopamine receptor transcriptional or translational rate. Conversely, expression of mutant LRRK2s determines a significant decrease in dopamine receptor D2 degradation (compared to untransduced or WT LRRK2) likely due to the dopamine receptor D2 accumulation into the Golgi. A general explanation might be that physiologically a certain amount of dopamine receptor D2 is kept into the Golgi apparatus and that mutant LRRK2s affect its vesicle-mediated transport to the cell membrane; in turn, this could affect dopamine receptor trafficking turnover although this last LRRK2 effect may be partially due to the suggested role of LRRK2 pathological mutants in autophagy-lysosomal pathways. As mentioned, two independent studies showed a genetic interaction between LRRK2 and Rab7L1; The LRRK2-Rab7L1 pathway cause abnormal Golgi clearance defects[239] and alterated lysosomal structure and retromer complex function[238]. The DRD2 vesicular trafficking alteration may be likely due to defects connecting Golgi apparatus to the endolysosomal protein degradation system. It is possible speculate that LRRK2 is part of a protein complex that regulates the Golgi-membrane trafficking by different protein-protein interaction/modification such as Rab GTPases proteins. Overexpression of WT LRRK2 and even more the pathological mutant is likely increasing the formation/activity of this complex that may partially lock the DRD2 into the Golgi apparatus. Different LRRK2 interactors belong to protein families involved in

the regulation of vesicle trafficking[233, 238, 246-249] or involved in the regulation of the cytoskeleton dynamics that in turn may modulate vesicle trafficking[195, 266-268]. Any of these LRRK2 interactions may be responsible for dopamine receptor D1 and D2 trafficking alteration that were observed in the presence of mutant forms of LRRK2. These data are in agreement with those obtained, to a different extent, to the alteration of dopamine receptor level or signalling observed in LRRK2 mouse models. In particular, the PKA-dependent phosphorylation of GluR1 is aberrantly enhanced in the striatum of young and aged LRRK2-null mice after treatment with a dopamine receptor D1 agonist[266] and the total dopamine receptor D2 protein level is higher in mice over-expressing WT LRRK2[269]. Moreover, the results illustrated in this thesis correlate with accumulating evidences that demonstrate a critical role of LRRK2 in the vesicle trafficking machinery that transports proteins from dendritic ER exit sites to Golgi outpost and to dendritic surface[248]. In particular, it has been reported that either LRRK2 loss or R1441C missense mutation impair the activity-dependent trafficking of NMDRs in neurons[248]. Different PD causative genes have been related to dysregulation in vesicular trafficking such as *SNCA, LRRK2, VPS35* and the risk factor *RAB7L1*[100]. It is possible to speculate that alteration in vesicle trafficking may a starting point of neuronal alteration in PD patients. Alteration in dopamine receptor or dopamine itself trafficking, both regulated by vesicle dynamics, may alter the neuronal physiology leading in the long term to neuronal toxicity/dead. In fact both in animal models and in PD patients the density of D1 and D2 receptors changes[269] as well as, up to date, dysregulation of dopamine and DA metabolite level is still considered one of the most likely hypothesis of dopaminergic neuronal toxicity[270].

Figure 23 summarizes a general view of this work on the involvement of LRRK2 in the regulation of dopamine receptor trafficking. Mutant LRRK2s modulate the DRD2 protein level likely affecting the trafficking from Golgi to cell membrane. G2019S LRRK2 also impairs DRD1 internalization upon dopamine treatment. Further experiments are required to better understand the molecular mechanisms of LRRK2 action and to understand if this effect is specific for the dopaminergic receptors or it is a general mechanism regulating a large number of neuronal membrane receptors.
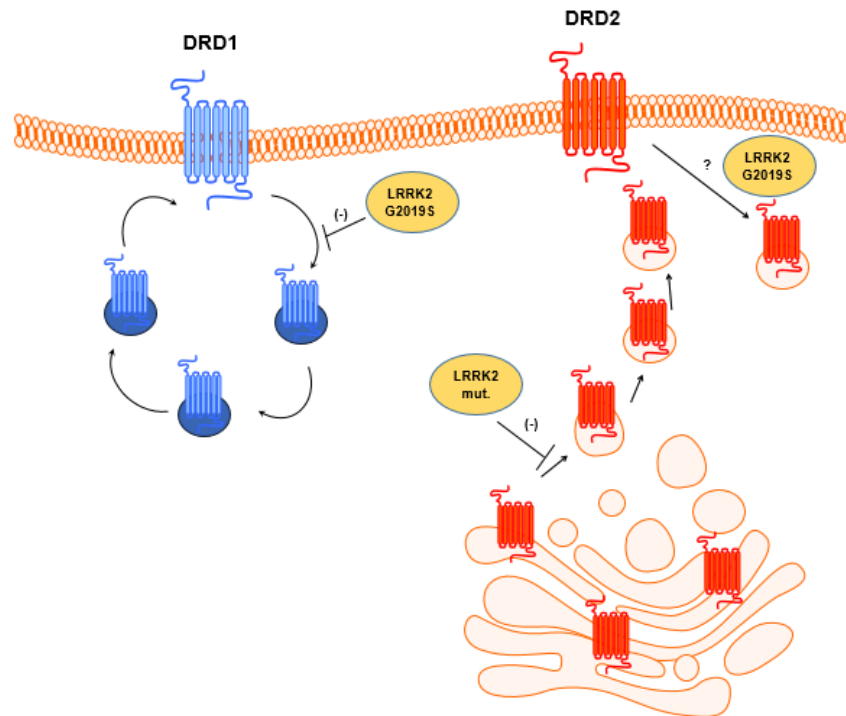
Figure 23. Model for mutant LRRK2 action in the alteration of dopamine receptor trafficking.

Publications

The main topic of this Ph.D. thesis, as extensively previously discussed, was to elucidate the role of LRRK2 in dopamine receptor trafficking/signaling and its implications in Parkinson disease. The results obtained in this work are under review in Plos One journal. During these three years of Ph.D. in parallel with the research activity above described, I was involved in other projects of different topics. In particular, in collaboration with Prof. Mario Sechi (Department of Chemistry and Pharmacy, University of Sassari), different molecular screenings of various compounds were performed to study their biological activity. Specifically, the biological activity of gold-conjugated polyphenol nanoparticles (in particular epigallocatechin-3-gallate gold-conjugated) and heteroaryl-pyrazole carboxylic acid derivatives were evaluated in different cellular models. The results of this experimental work have been published in International Journal of Nanomedicine (see attached paper) and another manuscript is under review of Chemical Communications Journal.

- *Sanna V, Pala N, Dessì G, Manconi P, Mariani A, Dedola S, **Rassu M.**, Crosio C, Iaccarino C, Sechi M (2014). Single-step green synthesis and characterization of gold-conjugated polyphenol nanoparticles with antioxidant and biological activities. International Journal of Nanomedicine, vol. 9; p. 4935-4951, ISSN: 1176-9114, doi: 10.2147/IJN.S70648.*
- *Cadoni R, Pala N, Lomelino C, Mahon BP, McKenna R, Dallocchio R, Dessì A, Carcelli M, Rogolino D, Sanna V, **Rassu M**, Iaccarino C, Vullo D, Supuran C, and Sechi M (2017). Exploring heteroaryl-pyrazole carboxylic acids as human carbonic anhydrase XII inhibitors. Molecular Pharmaceutics. Submitted.*

62

Mauro Rassu: "LRRK2 effect on dopamine receptor trafficking – implication in Parkinson's disease".
Ph.D. Course in Life Sciences and Biotechnologies – University of Sassari.

International Journal of Nanomedicine

Dovepress

open access to scientific and medical research

Open Access Full Text Article

ORIGINAL RESEARCH

Single-step green synthesis and characterization of gold-conjugated polyphenol nanoparticles with antioxidant and biological activities

This article was published in the following Dove Press journal:
International Journal of Nanomedicine
23 October 2014
Number of times this article has been viewed

Vanna Sanna[1,2]
Nicolino Pala[1]
Giuseppina Dessì[1]
Paola Manconi[1]
Alberto Mariani[1]
Sonia Dedola[3]
Mauro Rassu[3]
Claudia Crosio[3]
Ciro Iaccarino[3]
Mario Sechi[1,2]

[1]Department of Chemistry and Pharmacy, University of Sassari, Sassari, Italy; [2]Laboratory of Nanomedicine, Department of Chemistry and Pharmacy, University of Sassari, c/o Porto Conte Ricerche, Tramariglio, Alghero, Italy; [3]Department of Biomedical Sciences, University of Sassari, Sassari, Italy

Correspondence: Mario Sechi
Department of Chemistry and Pharmacy,
Laboratory of Nanomedicine,
University of Sassari, Via Vienna 2,
07100, Sassari, Italy
Tel +39 079 228 753
Fax +39 079 229 559
Email mario.sechi@uniss.it

Vanna Sanna
Department of Chemistry and Pharmacy,
Laboratory of Nanomedicine,
University of Sassari, c/o Porto Conte
Ricerche, Località Tramariglio,
07041 Alghero (SS), Italy
Tel +39 079 998 616
Fax +39 079 229 559
Email vsanna@uniss.it

Background: Gold nanoparticles (GNPs) are likely to provide an attractive platform for combining a variety of biophysicochemical properties into a unified nanodevice with great therapeutic potential. In this study we investigated the capabilities of three different natural polyphenols, epigallocatechin-3-gallate (EGCG), resveratrol (RSV), and fisetin (FS), to allow synergistic chemical reduction of gold salts to GNPs and stabilization in a single-step green process. Moreover, antioxidant properties of the nanosystems, as well as preliminary antiproliferative activity and apoptotic process investigation of model EGCG-GNPs on stable clones of neuroblastoma SH-SY5Y cells expressing CFP-DEVD-YFP reporter, were examined.

Methods: The GNPs were characterized by physicochemical techniques, polyphenol content, and in vitro stability. The antioxidant activity of the GNPs was also determined by 2,2-diphenyl-1-picrylhydrazyl (DPPH) and 2,2′-azinobis(3-ethylbenzothiazoline-6-sulfonic acid) cation (ABTS) radical-scavenging assays. Stable clones of neuronal SH-SY5Y-CFP-DEVD-YFP were generated and characterized, and cell viability after treatment with EGCG-GNPs was assessed after 72 hours through a 3(4,5-dimethylthiazol-2yl)-5-(3-carboxymethoxyphenyl)-2-(4-sulfophenyl)-2H-tetrazolium assay. Activation of the apoptotic pathways was also investigated by Western blot analysis.

Results: With a diameter in the size range of 10–25 nm, the obtained nanoparticles (NPs) were found to contain 2.71%, 3.23%, and 5.47% of EGCG, RSV, and FS, respectively. Nanoprototypes exhibited remarkable in vitro stability in various media, suggesting that NP surface coating with phytochemicals prevents aggregation in different simulated physiological conditions. The scavenging activities for DPPH and ABTS were highly correlated with EGCG, RSV, and FS content. Moreover, high correlation coefficients between the ABTS and DPPH values were found for the prepared nanosystems. EGCG-GNPs induce a dose-dependent reduction on SH-SY5Y-CFP-DEVD-YFP cell viability that is likely to involve the activation of the apoptotic pathways, similarly to free EGCG, as suggested by the processing of the CFP-DEVD-YFP reporter.

Conclusion: These results prompted us to propose the ecofriendly synthesized EGCG-, RSV-, and FS-based nanogold conjugates as suitable carriers for bioactive polyphenols to be used for the treatment of disorders associated with oxidative stress, including neurodegenerative disorders, cardiovascular disease, and cancer.

Keywords: gold nanoparticles, epigallocatechin-3-gallate, resveratrol, fisetin, antioxidant activity, SH-SY5Y-CFP-DEVD-YFP cells

Introduction

In recent years, the synthesis and biofunctionalization of water-dispersible gold nanoparticles (GNPs) have attracted intense interest due to their potential use in biology and medicine.[1–4] Some of the major biomedical applications of GNPs include gene

63

Mauro Rassu: "LRRK2 effect on dopamine receptor trafficking – implication in Parkinson's disease".
Ph.D. Course in Life Sciences and Biotechnologies – University of Sassari.

therapy,[5] protein delivery,[6] cancer diagnosis,[7,8] photothermal and photodynamic therapy,[1] and delivery of antitumor agents.[1-4,9]

The most commonly used method for the synthesis of GNPs is the reduction of chloroauric acid by trisodium citrate.[10] Other chemical and physical techniques involve the use of powerful and highly toxic reducing agents such as hydrazine and sodium borohydride, as well as high temperature and pressure conditions.[11] Moreover, the synthesis of the GNPs can be performed in the presence of a stabilizer in order to modify the surface by physisorption, specific recognition, and electrostatic interactions to ensure stability,[12,13] which is an important determinant for the potential use of gold nano-conjugated as therapeutic agents.[14] In order to minimize or eliminate further chemical interventions and to improve the sustainability of the process, alternative biosynthetic green methods that utilize plant-based phytochemicals for reduction of metal ions provide an inherently green approach to nanotechnology, also referred to as "green nanotechnology".[15]

Recently, several studies have demonstrated the dual role of whole plant extracts and pure compounds isolated from plants as effective reducing agents and as stabilizers, to provide a robust coating on the biocompatible GNPs.[16-20] The reactive phytochemical species include polyphenols such as flavonoids and nonflavonoids, the most abundant antioxidants in human diets, usually found in some fruits, vegetables, and beverages.[21,22]

In this study we investigated the capability of three different natural polyphenols, epigallocatechin-3-gallate (EGCG), resveratrol (RSV), and fisetin (FS), to provide synergistic chemical reduction of gold salts to GNPs, as well as stabilization in a single-step green process (Figure 1).
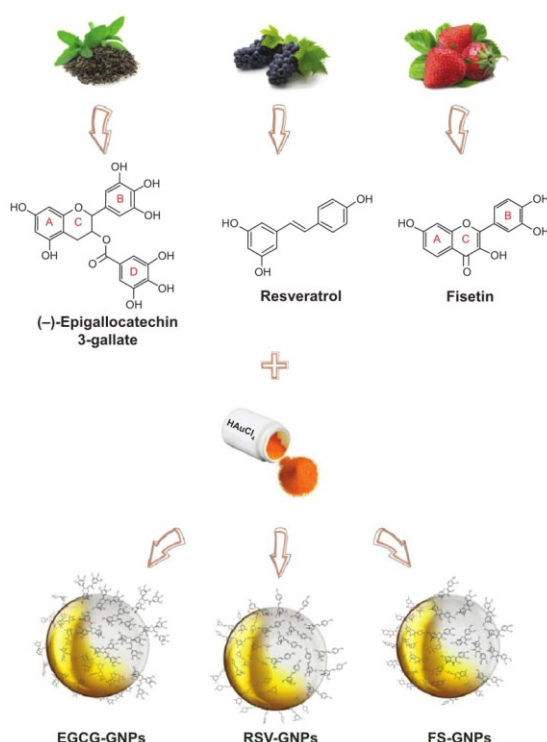

Figure 1 The work plan: from polyphenols to nanogolds. Chemical structures of EGCG, RSV, and FS are included.
Abbreviations: EGCG, epigallocatechin-3-gallate; RSV, resveratrol; FS, fisetin; GNPs, gold nanoparticles.

These polyphenols, with different chemical structures, have been selected because they have received a great deal of interest worldwide as potent bioactive substances endowed with chemopreventive/therapeutic activities because of their anti-invasive and antiproliferative effects in a wide variety of tumor cells,[23–26] with an increased effectiveness when formulated into a variety of nanosystems.[27–31]

On the other hand, the functionalization of GNPs' surface with these bioactive substances might provide a new useful approach as delivery and therapeutic tools, in particular by improving the biopharmaceutical properties of these polyphenols, such as their poor bioavailability and stability, as well as their resistance to specific/nonspecific metabolic processes.

As far as the chemical structure is concerned, EGCG (ie, [−]-epigallocatechin-3-gallate) is a flavonoid constituted by a dihydroxybenzopyran scaffold carrying a pyrogallol-type structure on the B-ring and a galloyl moiety in the D-ring (Figure 1). RSV (ie, trans-3,5,4′-trihydroxystilbene) is a triphenolic phytoalexin having the trans-stilbene skeleton, while FS (ie, 3,3′,4′,7-tetrahydroxyflavone) is a flavone-3-ol that bears a catecholic structural unit in the B-ring and the two hydroxyl groups located in the C- and A-rings (Figure 1).

To date, few examples of EGCG-conjugated nanogold have been reported. In a pioneering work, Nune et al[32] investigated the role of phytochemicals present in black tea leaves and commercially available catechins to provide GNPs with therapeutic potential. More recently, they demonstrated that biocompatible radioactive GNPs stabilized by EGCG bind with excellent affinity to laminin receptors overexpressed in prostate tumor cells, and reduce prostate tumor volumes in vivo.[33] Furthermore, Hsieh et al[34] reported on the synthesis, characterization, antioxidant activity, cytotoxicity in vitro, as well as anticancer activity in vivo of EGCG-conjugated nanogold.

The reaction mechanism for the formation of GNPs in aqueous solution by polyphenols reduction has been proposed in several reports.[35–37] Polyphenols such as EGCG demonstrated to be efficient ligands for metal ions and multiple phenolic hydroxyls are able to bind Au^{3+} ions by forming stable chelating rings. As a consequence of complexation, a redox reaction occurs, and the chelated Au^{3+} ions are reduced to Au^0 atoms in situ, while a part of the phenolic hydroxyls is simultaneously oxidized to corresponding quinone. Thus, polyphenolic molecules result in being physically attached onto the surface of nanogold particles, and the binding of an O atom of the polyphenol molecule to the GNPs' surfaces is presumably due to the electron transfer from O atoms to Au^{3+} ions, as confirmed by computational studies.[38] On the other hand, the high density of free hydroxyl groups,

especially in EGCG-GNPs, could lead to extensive inter- and intramolecular hydrogen bonding, which favors formation of unique supramolecular assemblies.

However, so far, the potential of RSV and FS as reducing agents for the synthesis of GNPs, as well as on their putative effectiveness when attached on the GNPs' surface, has not been explored yet. Therefore, it could also be interesting to preliminarily explore the behaviour of GNPs decorated with these polyphenols (ie, EGCG, RSV, and FS).

More specifically, we sought to test whether or not the intrinsic antioxidant activity displayed by the free compounds was retained when they are adsorbed to the nanoparticles (NPs) surface. Moreover, we wanted to investigate the ability of these engineered capped GNPs in regulating and modulating cellular responses, by evaluating their antiproliferative activity and induction of apoptosis on stable clones of neuroblastoma SH-SY5Y cells expressing CFP-DEVD-YFP reporter.

Herein, we report on "green nanosynthesis" and characterization, in terms of physicochemical properties and polyphenols content, of novel prototypes of polyphenol-capped GNPs (Figure 1) suitable for biomedical finalization. In vitro stability of the colloidal suspensions in various physiological media was also investigated. Furthermore, the capability of obtained GNPs for scavenging free radicals was demonstrated in vitro by following the reaction with stable 2,2-diphenyl-1-picrylhydrazyl (DPPH) and 2,2′-azinobis (3-ethylbenzothiazoline-6-sulfonic acid) cation (ABTS) radicals. Finally, cell viability after treatment with an EGCG-GNP model was evaluated through a 3(4,5-dimethylthiazol-2yl)-5-(3-carboxymethoxyphenyl)-2-(4-sulfophenyl)-2H-tetrazolium (MTS) assay, and activation of the apoptotic pathways was investigated by Western blot analysis.

Materials and methods
Chemicals and reagents
Tetrachloroauric acid (III) trihydrate ($HAuCl_4 \cdot 3H_2O$, >99.5% purity), DPPH, ABTS, and GNPs (15 nm diameter, stabilized suspension in citrate buffer) were purchased from Sigma–Aldrich (Steinheim, Germany). EGCG (≥99% purity) and RSV (≥98% purity) were purchased from Zhejiang Yixin Pharmaceutical Co., Ltd. (Zhejiang, People's Republic of China). FS (>98% purity) was purchased from Shaanxi Taiji Huaqing Technology Co., Ltd. (Shaanxi, People's Republic of China).

Synthesis of GNPs
The synthesis of GNPs was carried out by modification of a method previously reported.[32] Aqueous solution of

HAuCl$_4$·3H$_2$O (10 mM, 1.0 mL) and polyphenol (EGCG, RSV, or FS) solution (1.0 mM, 5.0 mL) was mixed under gentle stirring at room temperature. EGCG was solubilized in water, while RSV and FS were solubilized in ethanol:water mixture (1:4, v/v). The color of the mixture containing EGCG and RSV turned purple–red from pale yellow within a few minutes, indicating the formation of GNPs. For the solution containing FS the color appeared orange then yellow and purple–red after about 10 minutes. The reaction mixture was stirred for an additional 30 minutes. The GNPs were collected by centrifugation (20,000 rpm, 10 minutes, 15°C) and washed three times with water to ensure that no unbound EGCG, RSV, or FS molecules remained in the NP dispersion.

Characterization

The ultraviolet-visible (UV-vis) absorbance spectrum of diluted aqueous NP suspensions was recorded using a Cary 3 UV-vis spectrophotometer (Varian Medical Systems, Inc., Palo Alto, CA, USA).

The morphology and size of the GNPs were characterized by transmission electron microscopy (TEM) (FEI Tecnai G12; FEI, Hillsboro, OR, USA). A drop of sample was placed on a formvar-coated 400 mesh copper grid, followed by drying the sample at ambient conditions before it was attached to the sample holder on the microscope.

The phase characteristics of the as-prepared products were examined by powder X-ray diffraction (XRD; Bruker D8 Advance diffractometer) using Cu Kα radiation (λ=1.54056 Å), operating at 40 kV and 40 mA. Results were recorded in the 2θ range from 20° to 80° with a scanning step of 0.02° per step and 2 seconds per point.

Infrared spectra were collected on a Fourier transform infrared (FT-IR) spectrometer (Bruker Optics, Ettlingen, Germany) at a resolution of 4 cm^{-1} in KBr pellets. The measurements were performed on EGCG, RSV, and FS raw materials as well as on GNPs produced.

Determination of polyphenol content

The polyphenol content was determined by spectrophotometry, using EGCG, RSV, and FS as standard, with some modifications of the method described.[39,40] Briefly, 0.1 mg of the GNPs was transferred to separate tubes containing 0.5 mL of a 1/10 dilution of Folin–Ciocalteu's reagent in water. Then, 1.0 mL of a sodium carbonate solution (7.5% w/v) was added. The tubes were then allowed to stand at 30°C for 30 minutes before absorbance at 760 nm was measured. The polyphenol content was expressed as EGCG, RSV, and FS equivalents in µg/100 µg GNPs. The concentration of polyphenol in samples was derived from the standard curve of EGCG, RSV,

and FS raw materials ranging from 0.1 to 10 µg/mL (EGCG: y=0.0563x+0.0101; R^2=0.9993; RSV: y=0.0765x+0.0086; R^2=0.9990; FS: y=0.0649x+0.0104; R^2=0.9991) (Figure S1).

In vitro stability

In vitro stability studies of GNPs were performed in different media as previously reported.[32] Typically, colloidal NP solution was added to glass vials containing 1.5 mL of 0.5% bovine serum albumin (BSA), 0.5% cysteine, 5.0% sodium chloride (NaCl), and phosphate-buffered solution (PBS) pH 5, pH 7, and pH 9, respectively, and incubated for 3 hours at room temperature. The stability of GNPs was measured by monitoring UV absorbance at 30-minute intervals. A negligible change in UV-vis plasmon band confirmed the retention of nanoparticulate composition in all mixtures.

Antioxidant test: DPPH assay

The capacity of plant materials to catalyze the decomposition of free radicals can be determined by their ability to reduce the concentration of the stable free radical DPPH.[41] The method previously described by Gülçin[42] was used with slight modifications. Stock solutions of DPPH were prepared at 0.1 mmol/L in ethanol and stored at −20°C until needed. An appropriate amount of GNPs dispersed in ethanol (500 µL) was added to 1.0 mL DPPH solution in a test tube to give different final concentrations of NPs (25, 50, 100, and 200 µg/mL). The mixture was sonicated for 5 minutes and then left to stand in the dark. The supernatant containing only DPPH was obtained by centrifuging at 20,000 rpm for 5 minutes. Nonfunctionalized GNPs commercially available were tested as comparison at the same concentration.

The absorption of the supernatant was measured at 517 nm against blank samples lacking scavenger using a UV-vis spectrophotometer. The decrease in absorbance was determined at 5-minute intervals up to 30 minutes. The scavenging percentage was calculated using the following formula:

$$\text{DPPH-scavenging effect (\%)} = \left[\frac{(\text{ABS}_{\text{Control}} - \text{ABS}_{\text{Sample}})}{\text{ABS}_{\text{Control}}} \right] \times 100 \quad (1)$$

where $\text{ABS}_{\text{Control}}$ and $\text{ABS}_{\text{Sample}}$ are absorption of control DPPH and sample applied DPPH at 517 nm, respectively.

Antioxidant test: ABTS assay

The ABTS radical cation decolorization test is a spectrophotometric method widely used for the assessment of antioxidant activity of various substances. The experiment was carried out by adapting a method previously reported.[43]

In brief, a mixture containing 99 mL of ABTS solution (5.0×10^{-4} M) and 1.0 mL of sodium persulfate (6.89×10^{-3} M) was stored in the dark at room temperature for 16 hours before use. The produced ABTS•+ solution was diluted with ethanol to obtain an absorbance of approximately 0.85 at 734 nm. After the addition of 900 μL of diluted ABTS• solution to 100 μL of sample, the absorbance reading was taken at 1-minute intervals up to 5 minutes. Nonfunctionalized GNPs commercially available were used as comparison. A sample blank was run in each assay. All determinations were carried out in triplicate after centrifugation at 20,000 rpm for 1 minute. The percentage radical-scavenging activity was calculated as follows:

$$\text{ABTS•+-scavenging effect (\%)} = \left[\frac{(\text{ABS}_{\text{Control}} - \text{ABS}_{\text{Sample}})}{\text{ABS}_{\text{Control}}}\right] \times 100 \tag{2}$$

where $\text{ABS}_{\text{Control}}$ is absorbance of a control lacking any radical scavenger and $\text{ABS}_{\text{Sample}}$ is absorbance of the remaining ABTS•+ in the presence of a scavenger.[44]

Cell culture

Human neuroblastoma SH-SY5Y cells (American Type Culture Collection number CRL-2266) were cultured in Dulbecco's Modified Eagle Medium F-12 (DMEM/F12) ground (Life Technologies, Carlsbad, CA, USA) in the presence of 10% fetal calf serum (Life Technologies) inactivated at 56°C for 30 minutes. The cells are grown in an incubator at 37°C in a humidified atmosphere containing 5% CO_2. Stable clones expressing CFP-DEVD-YFP (Addgene company code 24537) were obtained by transfecting cells with LipofectAMINE LTX and PLUS reagent (Life Technologies) using 1.5 μg DNA/$5-7 \times 10^5$ cells according to the manufacturer's protocol. The different SH-SY5Y clones were maintained under selection by 400 μg/mL of G418. Individual clones expressing antibiotic resistance were picked after 14 days of selection, moved into a 48-well plate, and maintained in selective medium until confluence growth. Different individual clones were analyzed for CFP-DEVD-YFP expression upon treatment with the caspase-3 activator staurosporine (1 μg/mL).

Assessment of cell viability

The viability of control SH-SY5Y-CFP-DEVD-YFP cells was calculated after 72 hours through an MTS assay. Cell viability was assessed by a colorimetric assay using the MTS assay (CellTiter 96 Aqueous One Solution Assay; Promega Corporation, Madison, WI, USA), according to

the manufacturer's instructions. Absorbance at 490 nm was measured in a multilabel counter (Victor X5; Perkin Elmer, Waltham, MA, USA).

Immunofluorescence

One$\times 10^5$ cells were grown on a cover-glass for 24 hours and treated with staurosporine (1.0 μM) for 2 hours. Cells were washed twice with PBS 1X and then fixed with 1 mL of 4% paraformaldehyde/PBS 1X for 10 minutes. Before analysis, cells were mounted using Mowiol mounting medium[45] and fluorescence was revealed with a Leica TCS SP5 confocal microscope with LAS lite 170 image software.

Western blot analysis

Western blot analysis was performed as previously described.[46] Briefly, protein content was determined using the Bradford protein assay. Equal amounts of protein extracts were resolved by standard sodium dodecyl sulfate-polyacrylamide gel electrophoresis. Samples were electroblotted onto Protan nitrocellulose (Schleicher and Schuell BioScience GmbH, Dassel, Germany). Membranes were incubated with 3% low-fat milk in 1X PBS-Tween 0.05% solution with rabbit anti-green fluorescent protein (anti-GFP; Enzo Life Science, Farmingdale, NY, USA; 1:1,000 final dilution) or mouse anti-β-actin (Sigma-Aldrich; 1:1,000 final dilution) for 16 hours at 4°C. Goat antimouse immunoglobulin G (IgG) peroxidase-conjugated antibody (Millipore Corporation, Billerica, MA, USA; 1:2,500 final dilution) or goat antirabbit IgG peroxidase-conjugated antibody (Millipore; 1:2,500 final dilution) were used to reveal immunocomplexes by enhanced chemiluminescence (Pierce Biotechnology, Rockford, IL, USA).

Statistical analysis

Data are expressed as the mean ± standard deviation of experiments carried out in triplicate. The significance of differences was assessed by one-way analysis of variance. Individual differences were evaluated using a nonparametric post hoc test (Tukey's test) and considered statistically significant at $P < 0.05$.

Results and discussion
Synthesis and characterization of GNPs

In this study, green reduction of Au^{3+} to GNPs by bioactive polyphenols EGCG, RSV, and FS was performed by simply mixing polyphenol and metal gold salt solutions at room temperature. The reaction was complete within minutes and the formation of EGCG-, RSV-, and FS-capped GNPs could be followed by color change from yellow to reddish violet
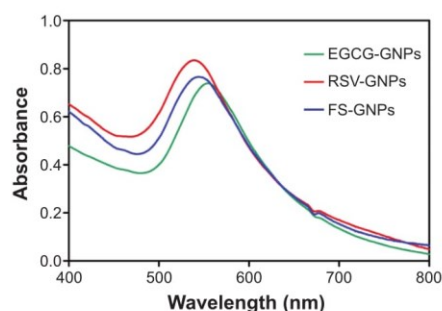
Figure 2 Ultraviolet-visible spectra of stable GNPs synthesized by EGCG, RSV, and FS polyphenols.
Notes: Wavelength expressed in nm. EGCG-GNPs, RSV-GNPs, and FS-GNPs indicate polyphenol-capped nanogold.
Abbreviations: EGCG, epigallocatechin-3-gallate; RSV, resveratrol; FS, fisetin; GNPs, gold nanoparticles.

(Figure S1), due to excitation of surface plasmon resonance (SPR) vibration of GNPs.

In UV-vis absorbance spectra (Figure 2), synthesis of GNPs was confirmed by characteristic SPR peak centered at 554, 540, and 544 nm for EGCG-, RSV-, and FS-capped GNPs, respectively. The significant SPR shift to higher wavelengths observed for EGCG-GNPs suggests an increase in particle size compared with NP batches prepared using RSV and FS.[47]

The size and shape of the GNPs were investigated with TEM. The images reported in Figure 3 show that EGCG-GNPs (Figure 3A) are in variable shapes. Most of them are spherical in nature, followed by occasionally triangular and rarely hexagonal.

On the other hand, a more uniform size distribution and homogeneous spherical shape of RSV and FS-GNPs were
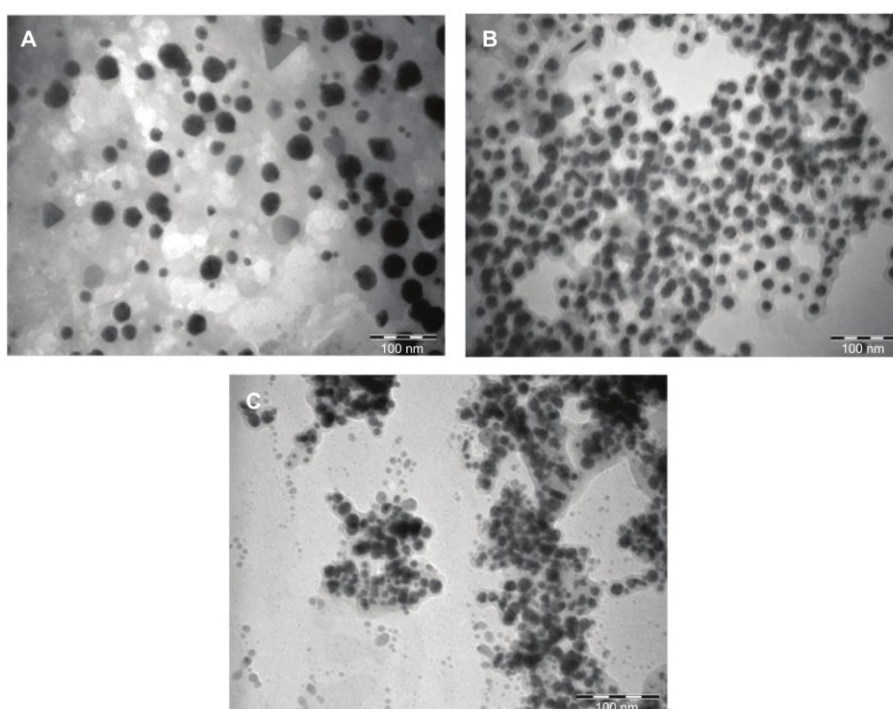

Figure 3 Transmission electron microscopy micrographs of (**A**) EGCG-, (**B**) RSV-, and (**C**) FS-capped GNPs.
Note: Distances expressed in nanometers (nm).
Abbreviations: EGCG, epigallocatechin-3-gallate; RSV, resveratrol; FS, fisetin; GNPs, gold nanoparticles.

Table 1 Mean diameter of EGCG-, RSV-, and FS-capped GNPs

Polyphenol-capped GNPs	Mean diameter ± standard deviation (nm)
EGCG-GNPs	25.55±7.26*
RSV-GNPs	14.55±2.20
FS-GNPs	9.76±1.56*

Notes: Diameter expressed in nanometers (nm). *Significantly different from other GNP-polyphenols. EGCG-GNPs, RSV-GNPs, and FS-GNPs indicate polyphenol-capped nanogold.
Abbreviations: EGCG, epigallocatechin-3-gallate; RSV, resveratrol; FS, fisetin; GNPs, gold nanoparticles.

observed (Figure 3B and C, respectively). As reported in Table 1, the size of the NPs was in the range of 10–25 nm and was influenced by the polyphenol used in the synthetic procedure.

These findings suggest that EGCG, RSV, and FS could be successfully used as reducing and stabilizing agents to produce GNPs with a narrow size distribution. Significant differences ($P<0.05$) were found in mean diameter of EGCG-GNPs with respect to FS-GNPs.

The powder XRD patterns (Figure 4) showed that synthesized GNPs were crystalline. The pattern presents four distinct diffraction peaks at 38.17, 44.33, 64.70, and 77.70, which are assigned to (1 1 1), (2 0 0), (2 2 0), and (3 1 1) crystalline plane diffraction peaks of cubic GNPs, respectively, in agreement with the database of the Joint Committee on Powder Diffraction Standards (JCPDS No 04-0784). The absence of any other crystallographic impurities peaks in the XRD spectrum confirmed the high purity of synthesized GNPs, in accordance with that reported earlier for similar prototypes.[48]
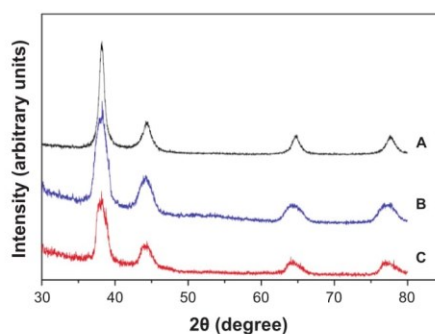
The average particle size was estimated using the Scherrer equation:

$$d = (k\lambda/\beta 1/2 \cos \theta) \quad (3)$$

where k is the Scherrer constant (0.89), λ is the X-ray wavelength of Cu Kα1 radiation, $\beta 1/2$ is the width of the XRD peak at half-height, and θ is the Bragg angle.

The average size of the NPs, calculated from the width of the diffraction peak, was about 19.49, 12.16, and 9.90 nm for EGCG-GNPs, RSV-GNPs, and FS-GNPs, respectively, which were in line with the results obtained from TEM measurements.

To acquire further information about the presence of polyphenols coating in the NP surface, FT-IR measurements of both free polyphenols and the corresponding gold-capped derivatives were assessed.

The analysis of FT-IR spectrum of free compounds and corresponding capped GNPs evidenced an overlapping behavior between all three couples of samples (Figure 5). In particular, the spectra of EGCG and EGCG-GNPs are characterized by the typical C=O ester band at about 1,700 cm^{-1} (Figure 5A). Moreover, aromatic double-bond stretching at about 1,610 cm^{-1}, aromatic C–C stretching at 1,450 cm^{-1}, O–H bending vibration centered at 1,375 cm^{-1}, and C–O stretching at 1,210 cm^{-1} were also detected in both samples. Spectra of RSV and RSV-GNPs (Figure 5B) revealed four intense bands at about 1,610, 1,590, 1,450, and 1,150 cm^{-1}, corresponding to C–C aromatic double-bond stretching, C–C olefinic stretching, aromatic C–H stretching, and C–C aromatic bending vibration, respectively. Finally, FS and its nanogold derivative showed similar pattern signals (Figure 5C), which are constituted by C=O stretching of the ketone functionality located on the chromen-4-one ring (1,725–1,690 cm^{-1}), C=C stretching (1,605 cm^{-1}), C–C stretching (1,260 cm^{-1}), and C–OH bending vibration (1,110 cm^{-1}).

Determination of polyphenol content

Since GNPs can be proposed as suitable carriers for the delivery of bioactive EGCG, RSV, and FS, as well as for other related phytochemicals, it is important to determine the amount of polyphenols adsorbed on the NPs' surface.

To evaluate the EGCG, RSV, and FS content in gold nanosystems, the rapid colorimetric Folin–Ciocalteu method, frequently used for quantification of total phenolic content in natural products, was considered in this study.[49] We derived the concentration of each polyphenol in NPs from the standard curve prepared using EGCG, RSV, and FS raw materials

Figure 4 X-ray diffraction pattern of (**A**) EGCG-, (**B**) RSV-, and (**C**) FS-capped GNPs.
Note: Diffraction angle 2θ expressed in degrees.
Abbreviations: EGCG, epigallocatechin-3-gallate; RSV, resveratrol; FS, fisetin; GNPs, gold nanoparticles.
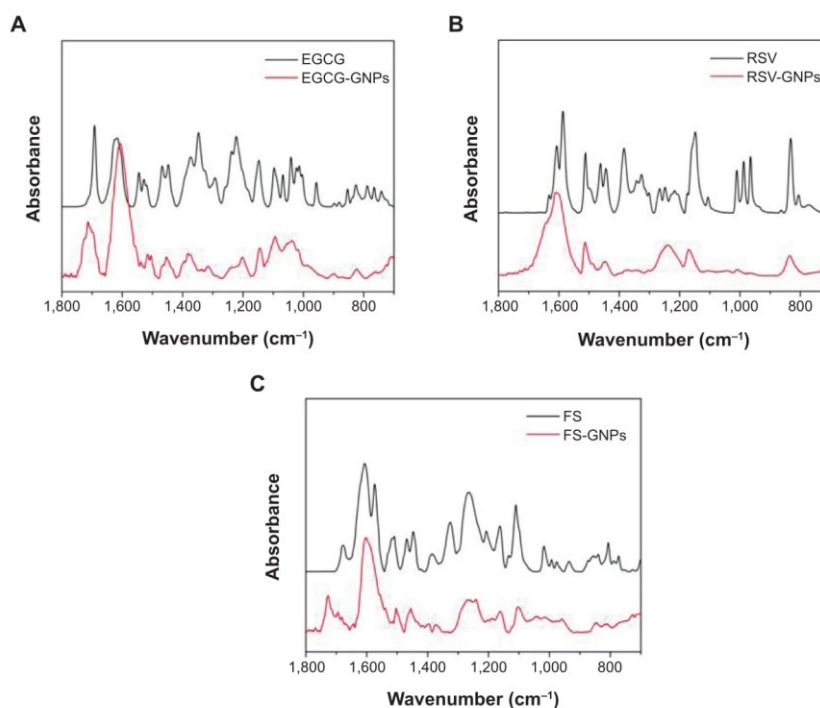
Figure 5 Fourier transform infrared spectra of (**A**) EGCG-GNPs, (**B**) RSV-GNPs, and (**C**) FS-GNPs, compared with pure EGCG, RSV, and FS, respectively.
Note: Wavenumber expressed in cm⁻¹.
Abbreviations: EGCG, epigallocatechin-3-gallate; RSV, resveratrol; FS, fisetin; GNPs, gold nanoparticles.

(Figure S2). The percentage of polyphenol content resulted as 2.71%, 3.23%, and 5.47% (w/w) for GNPs synthesized using EGCG, RSV, and FS, respectively.

In vitro stability

One of the most important aspects to be taken into account for various biomedical applications of GNPs is their stability in physiological media, in order to prevent aggregation.[32] In fact, it represents a key issue that underlies multiple deleterious effects in many therapeutics, including loss of efficacy, altered pharmacokinetics, and induction of unwanted immunogenicity.

The stability of polyphenol-capped GNPs was monitored using absorption spectroscopy in 0.5% BSA, 0.5% cysteine, and 5.0% NaCl solutions over 3 hours. We have also investigated the stability of GNPs in PBS at pH 5, 7, and 9.

On the whole, the plasmon wavelengths in all the tested GNPs (Figure 6A–C) show minimal shifts of 1–5 nm, confirming that the NPs are intact, thus demonstrating good in vitro stability in simulated biological fluids. These results confirm that EGCG, RSV, and FS are acting in stabilizing gold nanoparticulate systems from agglomerations in solution. It was also observed that at pH 9 all GNPs are characterized by a more remarkable (7–12 nm) blue shift in SPR band. As previously reported, the shift in SPR can be correlated with NPs' surface charge at different pH.[50] In alkaline pH, the presence of a high concentration of hydroxyl ions on the surface of NPs might maximize their repulsive electrostatic and electrosteric interactions, thus reducing particles aggregation, as detected by the hypsochromic shift of UV-vis peak.[48]

On the other hand, when colloidal gold solution was added into BSA, the position of the peak of colloidal gold

Mauro Rassu: "LRRK2 effect on dopamine receptor trafficking – implication in Parkinson's disease".
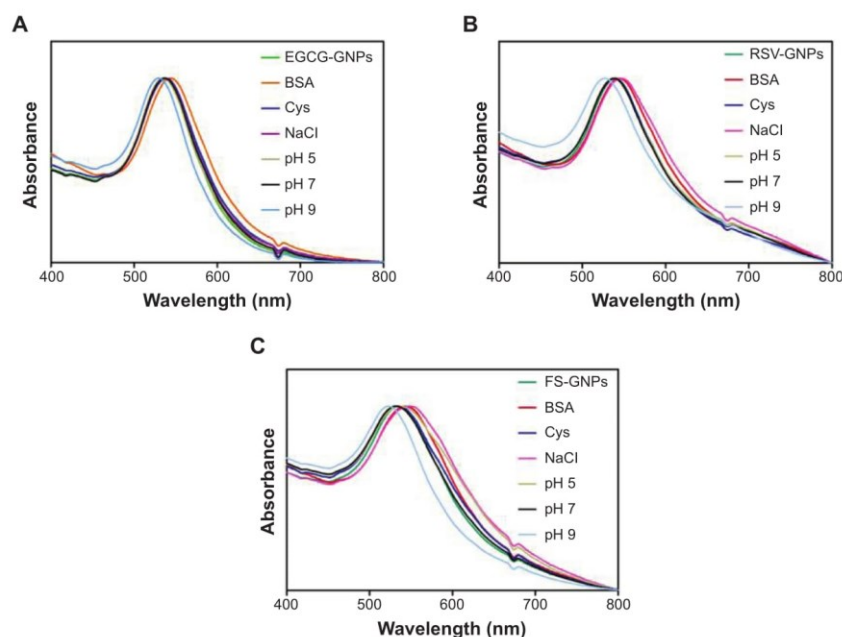Ph.D. Course in Life Sciences and Biotechnologies – University of Sassari.

Figure 6 In vitro stability ultraviolet-visible studies of GNPs capped with (**A**) EGCG, (**B**) RSV, and (**C**) FS in different media.
Notes: Wavelength expressed in nm. EGCG-GNPs, RSV-GNPs, and FS-GNPs indicate polyphenol-capped nanogold.
Abbreviations: EGCG, epigallocatechin-3-gallate; RSV, resveratrol; FS, fisetin; GNPs, gold nanoparticles; BSA, bovine serum albumin; Cys, cysteine; NaCl, sodium chloride.

slightly shifted red (~7 nm). These results could be attributed to the possible formations of BSA–colloidal gold complex, probably due to the interaction with free thiol groups of protein.[51]

Concerning RSV-GNPs and FS-GNPs, a slight red shift (7 and 10 nm, respectively) was also observed when the strong electrolyte (ie, NaCl) was added at 5.0% concentration; the high concentration of ions presumably shielded the repulsive electrostatic forces between NPs, allowing them to form small aggregates. Considering that in physiological conditions the concentration of NaCl corresponds to 0.9% (150 mM), all produced GNPs can be considered stable.

Antioxidant activity: DPPH assay

Measurement of radical-scavenging activity using discoloration of DPPH has been widely used due to its stability, simplicity, and reproducibility.[42]

As shown in Figure 7A, all GNPs scavenged DPPH radicals in a dose-dependent manner and shared a good linear correlation between the percentage inhibition of the DPPH

and the amount of GNPs used (ECGG-GNPs: $R^2=0.9534$; RSV-GNPs: $R^2=0.9295$; FS-GNPs: $R^2=0.9880$).

At all tested concentrations, EGCG-GNPs and FS-GNPs exhibited a similar DPPH-scavenging activity. Percentage inhibition of DPPH ranged from about 16% and 19% at a lower concentration (25 µg/mL) to 60% and 66% obtained at higher concentration (200 µg/mL) for EGCG-GNPs and FS-GNPs, respectively. On the contrary, the RSV-GNPs showed a significantly lower ($P<0.05$) free radical-scavenging effect when compared with EGCG-GNPs and FS-GNPs, with only 26% of scavenging activity at 200 µg/mL.

Moreover, the kinetics of DPPH• radicals-scavenging activity of all GNPs increased with an increase in the concentration, and the decrease in absorbance reached a plateau within the 5-minute sampling period, which indicated that the reaction had reached completion (data not shown).

Antioxidant activity: ABTS assay

The ABTS assay is another commonly used method available to evaluate antioxidant activities of natural compounds

Mauro Rassu: "LRRK2 effect on dopamine receptor trafficking – implication in Parkinson's disease".
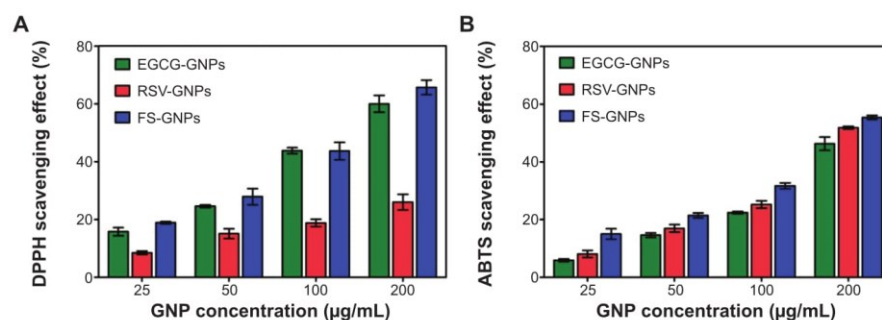Ph.D. Course in Life Sciences and Biotechnologies – University of Sassari.

Figure 7 Antioxidant activities of EGCG-GNPs, RSV-GNPs, and FS-GNPs at various concentrations assessed by percentage inhibition of DPPH (**A**) and ABTS (**B**) radicals.
Notes: GNP concentration expressed in µg/mL. EGCG-GNPs, RSV-GNPs, and FS-GNPs indicate polyphenol-capped nanogold.
Abbreviations: EGCG, epigallocatechin-3-gallate; RSV, resveratrol; FS, fisetin; GNPs, gold nanoparticles; DPPH, 2,2-diphenyl-1-picrylhydrazyl; ABTS, 2,2'-azinobis (3-ethylbenzothiazoline-6-sulfonic acid).

based on their ability to scavenge the long-life radical cation ABTS•+.[52]

The results reported in Figure 7B show that radical-scavenging activities of all the GNPs increased linearly with increasing concentration, exhibiting their dose-dependent nature (EGCG-GNPs: R^2=0.9921; RSV-GNPs: R^2=0.9924; FS-GNPs: R^2=0.9993). The antioxidant activity was found to be stronger for FS-GNPs, followed by the RSV-GNPs and then EGCG-GNPs.

The scavenging percentages range from 6%, 8%, and 15% at 25 µg/mL to 46%, 51%, and 55% at higher concentration (200 µg/mL) for EGCG-GNPs, RSV-GNPs, and FS-GNPs, respectively. Interestingly, at all tested concentrations, the reaction reaches steady state conditions after the first 2 minutes (data not shown), suggesting that polyphenols on the surface of GNPs maintained a high antioxidant efficiency.

To elucidate in more detail the antioxidant activity differences detected for the obtained GNPs, the DPPH- and ABTS-scavenging effects of EGCG, RSV, and FS raw materials at different concentrations were also evaluated.

As shown in Figure S3, the percentage of inhibition for DPPH of all polyphenols showed a good linearity at the tested concentrations. EGCG exhibited the highest antioxidant capacity with a percentage of DPPH inhibition that ranged from 9.5% (0.25 µg/mL) to 66% (2.5 µg/mL). At the same concentrations, values found for FS were decreased and ranged from 8.5% to 60%. On the other hand, RSV showed the lowest antioxidant potential with comparable activity at higher concentrations (62.1% inhibition of DPPH at 20 µg/mL).

These findings are in agreement with previous reports and suggest that the DPPH antioxidant activity of polyphenolic compounds is closely associated with their chemical structure, such as the number and position of phenolic hydrogen, which influences the accessibility to the radical centre of DPPH•. Thus, the greater number of hydroxyl groups, especially O-dihydroxy group on B-ring of EGCG and FS with respect to RSV, are potentially able to quench more efficiently the free radicals by forming resonance-stabilized phenoxyl radicals.[52]

As concerns ABTS-scavenging activity (Figure S4), no significant differences were found for EGCG and RSV, with the percentage of inhibition of about 20% at lower concentration (0.5 µg/mL) and 65% at higher concentration (10 µg/mL). In contrast, the ABTS antioxidant activity of FS, at the same concentrations, decreased significantly, ranging from 16% to 53%.

The different behavior of polyphenols, and in particular of RSV, observed in DPPH and ABTS assays suggests that the reaction mechanisms involved in both methods are influenced by the chemical structure of the antioxidants, and that the two assay cations react by using different active chemical groups. In particular, in contrast to the oxidation of polyphenols by DPPH radicals that occur at B-ring, forming the corresponding O-quinone, or even at the C-2 position of the C-ring, the oxidation of polyphenols by ABTS radical cations occurs at the A-ring.[53]

Additionally, no significant DPPH and ABTS antioxidant activities were detected by using as control the nonfunctionalized GNPs at the same concentration of polyphenols-capped GNPs, thus confirming that radical-scavenging activities are due to the presence of polyphenols on the GNPs' surface (data not shown).

Correlations between polyphenol content and antioxidant activity

The correlation coefficients (R^2) were used to evaluate the correlation between each polyphenol content in GNPs and the methods used to determine their antioxidant capacity. As reported in Figure S5, the R^2 values between DPPH and polyphenolic content were 0.9654, 0.9578, and 0.9944 for EGCG-GNPs, RSV-GNPs, and FS-GNPs, respectively. High correlation was also demonstrated between ABTS and polyphenolic content (R^2=0.9944, 0.9923, and 0.9961 for EGCG-GNPs, RSV-GNPs, and FS-GNPs, respectively).

These results suggest that the higher DPPH and ABTS antioxidant activities are correlated to the high EGCG, RSV, and FS content in GNPs. The R^2 values for correlations between DPPH and ABTS assays were R^2=0.9335, 0.9374, and 0.9843 for EGCG-GNPs, RSV-GNPs, and FS-GNPs, respectively (Figure S6).

Antiproliferative activity and apoptosis activation in SH-SY5Y-CFP-DEVD-YFP cells

Several polyphenols have shown remarkable cancer-preventive and some cancer-therapeutic effects, partially due to their ability to induce apoptosis in cancer cells without affecting normal cells.

In this scenario, growth-suppressive effect on cell proliferation demonstrated by polyphenols such as EGCG is mediated through programmed cell death or apoptosis by interfering with many cellular processes, including nuclear condensation, caspase-3 activation, and poly-ADP ribose polymerase cleavage, as well as eliciting the production of intracellular reactive oxygen species.[54] The essential role of caspases (in particular, the key caspase-3 protein) in EGCG-mediated inhibition of NF-kB and its subsequent apoptosis has also been demonstrated.[55]

To assess whether the engineered GNPs may alter cell proliferation and induce apoptosis, we took advantage of the neuronal SH-SY5Y cells stably expressing CFP-DEVD-YFP reporter.[56] In this reporter the sequence coding for CFP (CFP: GFP with mutations Y66W, F64L, S65T, N146I, M153T, and V163A) is fused to the one coding for YPF (YFP: a particular GFP variant called Venus with mutations F64L, M153T, V163A, and S175G) via the aminoacidic sequence DEVD, which is the substrate for active caspase-3. Different stable cell lines were generated and characterized for the first time. Figure 8 shows the SH-SY5Y stable cell line used in the following experiments. The expression levels of CFP-DEVD-YFP were evaluated by Western blot (Figure 8A) and immunofluorescence (Figure 8B) experiments after induction of

apoptosis by staurosporine treatment. As shown in Figure 8A, treatment with staurosporine determined the cleavage of DEVD target sequence and the resulting separation of two fluorescent proteins, indicating the activation of caspase-3.

Next, SH-SY5Y-CFP-DEVD-YFP cells were treated for 72 hours with EGCG-GNPs at different concentrations and cell viability was measured by MTS assay (Figure 8C). At the end of 72 hours of exposure, EGCG-GNPs decreased cell viability approximately in a dose-dependent manner, displaying an overlapping behavior with that of free EGCG. More specifically, both EGGC-GNPs and free EGCG exhibited similar cytotoxicity profiles, showing a dose-dependent antiproliferative effect and inhibition values in the overall cell growth. With respect to control, at 1 µg/mL concentration, EGCG-GNPs determined a growth inhibition of SH-SY5Y-CFP-DEVD-YFP cells of ~10%, similarly to an equivalent amount of free EGCG (ie, cells resulted in being exposed to equimolar amounts of free and capped EGCG). At 5 µg/mL, 10 µg/mL, and 25 µg/mL concentration exposure, tested EGCG-GNPs showed a reduction of cell viability of about 20%–30%, and, finally, treatment of SH-SY5Y-CFP-DEVD-YFP cells with 50 µg/mL of EGCG-GNPs proved the highest cytotoxicity, showing a cell growth inhibition of ~40% (Figure 8C).

Moreover, treatment of cells with EGCG-GNPs (and free ECGG) shared increased CFP-DEVD-YFP reporter cleavage (Figure 8D) due to caspase-3 activation, thus supporting an apoptotic mechanism of action.

In summary, EGCG-GNPs induce a dose-dependent reduction on cell viability that is likely to involve the activation of the apoptotic pathways.

Of course, to evaluate whether these activities may have an in vivo relevance when providing a reasonable dose of these NPs, further studies are in progress to explore a large panel of more responsive tumor cells. However, for comparative purposes, in a previous in vivo study on polymeric NP-mediated delivery of bioactive catechins administered at concentrations ranging 5–20 µg/mouse, the polyphenols loading of NPs resulted in 3.38% and 5.76% of the polymer weight, similar to the concentration of polyphenols found in our prototypes.[57]

Conclusion

In this work, green synthesis of GNPs using natural polyphenols EGCG, RSV, and FS was successfully investigated and proposed as a simple, reproducible, low-cost, and nontoxic method. Stable nanogolds were uniformly generated and fully characterized for their physicochemical properties. Overall, enhanced antioxidant properties were detected for all three
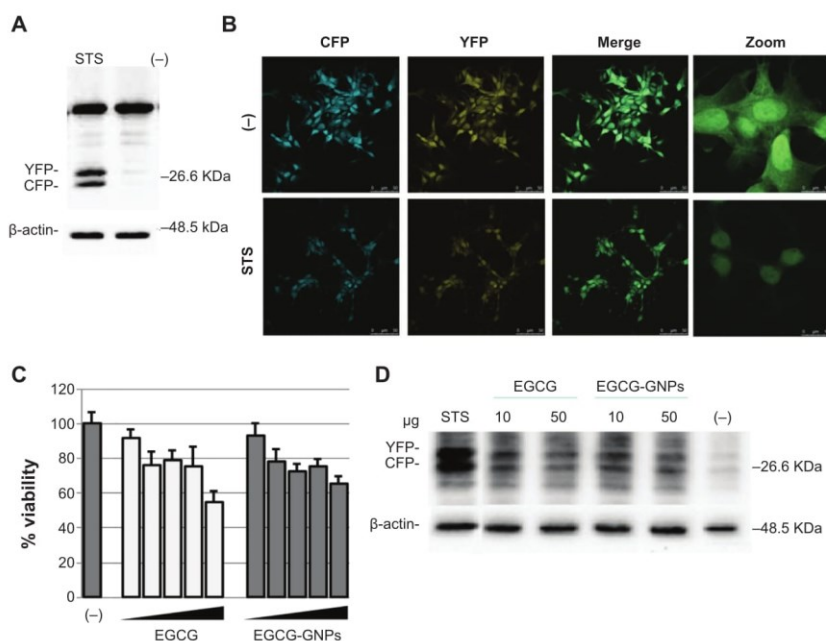
Figure 8 Effect of EGCG-GNPs on CFP-DEVD-YFP reporter gene. (**A**) SH-SY5Y-derived cells expressing CFP-DEVD-YFP reporter gene were left untreated (−) or treated (+) for 2 hours with 1 μM staurosporine to induce caspase-3 activation. Cell lysates were subjected to reducing sodium dodecyl sulfate-polyacrylamide gel electrophoresis. The anti-GFP antibody was used to visualize CFP-DEVD-YFP reporter and anti-β-actin serves as control for equal loading of samples. (**B**) Autofluorescence analysis of cells as in (**A**). (**C**) Effect EGCG-GNPs at 1, 5, 10, 25, and 50 μg/mL on SH-SY5Y-CFP-DEVD-YFP cells. (**D**) Western blots on protein extracts from cells treated as in (**C**) were performed using anti-GFP antibody and anti-β-actin as controls for equal EGCG loading of samples (EGCG-GNPs concentration =10 and 50 μg/mL).
Notes: Results for MTS assays are the means ± SEM of three experiments performed in triplicate. Concentration of free EGCG and EGCG capped in GNPs is the same.
Abbreviations: EGCG, epigallocatechin-3-gallate; RSV, resveratrol; FS, fisetin; GNPs, gold nanoparticles; GFP, green fluorescent protein; MTS, 3(4,5-dimethylthiazol-2yl)-5-(3-carboxymethoxyphenyl)-2-(4-sulfophenyl)-2H-tetrazolium; SEM, standard error of the mean.

prototypes, and this correlates well with the high EGCG, RSV, and FS content in GNPs. However, some differences in free radical-scavenging action between the three nanosystems have been observed, due to their peculiar chemical structure. Moreover, a high degree of correlation among the antioxidant activities measured by DPPH and ABTS assays has been found in these polyphenol-capped GNPs. Our data on the antiproliferative activity of EGCG-GNPs in a neuroblastoma cell model demonstrated that these constructs induce a concentration-dependent reduction on cell viability by involving the activation of the apoptotic pathways. Moreover, the effectiveness of EGCG in terms of antiproliferative efficacy can be retained in EGCG-capped GNPs and supports the antioxidant capacity of these polyphenols and their ability to catalyze the decomposition/scavenging of free radicals.

These results would make these stable polyphenol-capped gold nanoprototypes suitable as functional and promising candidates for the treatment of disorders associated with oxidative stress, and extensive preclinical studies are warranted.

Disclosure
The authors report no conflicts of interest in this work.

References

1. Sperling RA, Rivera-Gil P, Zhang F, Zanella M, Parak WJ. Biological applications of gold nanoparticles. *Chem Soc Rev.* 2008;37(9):1896–1908.
2. Dykman L, Khlebtsov N. Gold nanoparticles in biomedical applications: recent advances and perspectives. *Chem Soc Rev.* 2012;41(6):2256–2282.
3. Dreaden EC, Alkilany AM, Huang X, Murphy CJ, El-Sayed MA. The golden age: gold nanoparticles for biomedicine. *Chem Soc Rev.* 2012;41(7):2740–2779.
4. Vigderman L, Zubarev ER. Therapeutic platforms based on gold nanoparticles and their covalent conjugates with drug molecules. *Adv Drug Deliv Rev.* 2013;65(5):663–676.
5. Thomas M, Klibanov AM. Conjugation to gold nanoparticles enhances polyethylenimine's transfer of plasmid DNA into mammalian cells. *Proc Natl Acad Sci U S A.* 2003;100(16):9138–9143.
6. Du J, Jin J, Yan M, Lu Y. Synthetic nanocarriers for intracellular protein delivery. *Curr Drug Metab.* 2012;13(1):82–92.
7. Giljohann DA, Seferos DS, Daniel WL, Massich MD, Patel PC, Mirkin CA. Gold nanoparticles for biology and medicine. *Angew Chem Int Ed Engl.* 2010;49(19):3280–3294.
8. Llevot A, Astruc D. Applications of vectorized gold nanoparticles to the diagnosis and therapy of cancer. *Chem Soc Rev.* 2012;41(1):242–257.
9. Cai W, Gao T, Hong H, Sun J. Applications of gold nanoparticles in cancer nanotechnology. *Nanotechnol Sci Appl.* 2008;1:17–32.
10. Turkevich J, Stevenson PC, Hillier J. A study of the nucleation and growth processes in the synthesis of colloidal gold. *Discuss Faraday Soc.* 1951;11:55–75.
11. Daniel MC, Astruc D. Gold nanoparticles: assembly, supramolecular chemistry, quantum-size-related properties, and applications toward biology, catalysis, and nanotechnology. *Chem Rev.* 2004;104:293–346.
12. Corbierre MK, Cameron NS, Lennox RB. Polymer-stabilized gold nanoparticles with high grafting densities. *Langmuir.* 2004;20(7):2867–2873.
13. DeLong RK, Reynolds CM, Malcolm Y, Schaeffer A, Severs T, Wanekaya A. Functionalized gold nanoparticles for the binding, stabilization, and delivery of therapeutic DNA, RNA, and other biological macromolecules. *Nanotechnol Sci App.* 2010;3(1):53–63.
14. Chompoosor A, Han G, Rotello VM. Charge dependence of ligand release and monolayer stability of gold nanoparticles by biogenic thiols. *Bioconjug Chem.* 2008;19(7):1342–1345.
15. Katti K, Chanda N, Shukla R, et al. Green nanotechnology from cumin phytochemicals: generation of biocompatible gold nanoparticles. *Int J Green Nanotechnol Biomed.* 2009;1(1):B39–B52.
16. Menon D, Basanth A, Retnakumari A, Manzoor K, Nair SV. Green synthesis of biocompatible gold nanocrystals with tunable surface plasmon resonance using garlic phytochemicals. *J Biomed Nanotechnol.* 2012;8(6):901–911.
17. Mukherjee S, Sushma V, Patra S, et al. Green chemistry approach for the synthesis and stabilization of biocompatible gold nanoparticles and their potential applications in cancer therapy. *Nanotechnology.* 2012;23(45):455103.
18. Das S, Roy P, Mondal S, Bera T, Mukherjee A. One pot synthesis of gold nanoparticles and application in chemotherapy of wild and resistant type visceral leishmaniasis. *Colloids Surf B Biointerfaces.* 2013;107:27–34.
19. Arunachalam KD, Annamalai SK, Hari S. One-step green synthesis and characterization of leaf extract-mediated biocompatible silver and gold nanoparticles from Memecylon umbellatum. *Int J Nanomedicine.* 2013;8:1307–1315.
20. Arunachalam KD, Annamalai SK. Chrysopogon zizanioides aqueous extract mediated synthesis, characterization of crystalline silver and gold nanoparticles for biomedical applications. *Int J Nanomedicine.* 2013;8:2375–2384.
21. Han X, Shen T, Lou H. Dietary polyphenols and their biological significance. *Int J Mol Sci.* 2007;8(9):950–988.
22. Scalbert A, Johnson IT, Saltmarsh M. Polyphenols: antioxidants and beyond. *Am J Clin Nutr.* 2005;81(1 Suppl):215S–217S.
23. Higdon JV, Frei B. Tea catechins and polyphenols: health effects, metabolism, and antioxidant functions. *Crit Rev Food Sci Nutr.* 2003;43(1):89–143.
24. Khan N, Mukhtar H. Tea polyphenols for health promotion. *Life Sci.* 2007;81(7):519–533.
25. Pervaiz S, Holme AL. Resveratrol: its biologic targets and functional activity. *Antioxid Redox Signal.* 2009;11(11):2851–2897.
26. Khan N, Asim M, Afaq F, Abu Zaid M, Mukhtar H. A novel dietary flavonoid fisetin inhibits androgen receptor signaling and tumor growth in athymic nude mice. *Cancer Res.* 2008;68(20):8555–8563.
27. Siddiqui IA, Adhami VM, Bharali DJ, et al. Introducing nanochemoprevention as a novel approach for cancer control: proof of principle with green tea polyphenol epigallocatechin-3-gallate. *Cancer Res.* 2009;69(5):1712–1716.
28. Sanna V, Pintus G, Roggio AM, et al. Targeted biocompatible nanoparticles for the delivery of (–)-epigallocatechin 3-gallate to prostate cancer cells. *J Med Chem.* 2011;54(5):1321–1332.
29. Sanna V, Sechi M. Nanoparticle therapeutics for prostate cancer treatment. *Nanomedicine.* 2012;8:S31–S36.
30. Sanna V, Roggio AM, Siliani S, et al. Development of novel cationic chitosan- and anionic alginate-coated poly(D,L-lactide-co-glycolide) nanoparticles for controlled release and light protection of resveratrol. *Int J Nanomedicine.* 2012;7:5501–5516.
31. Sanna V, Siddiqui IA, Sechi M, Mukhtar H. Nanoformulation of natural products for prevention and therapy of prostate cancer. *Cancer Lett.* 2013;334:142–151.
32. Nune SK, Chanda N, Shukla R, et al. Green nanotechnology from tea: phytochemicals in tea as building blocks for production of biocompatible gold nanoparticles. *J Mater Chem.* 2009;19(19):2912–2920.
33. Shukla R, Chanda N, Zambre A, et al. Laminin receptor specific therapeutic gold nanoparticles (198AuNP-EGCg) show efficacy in treating prostate cancer. *Proc Natl Acad Sci U S A.* 2012;109(31):12426–12431.
34. Hsieh DS, Lu HC, Chen CC, Wu CJ, Yeh MK. The preparation and characterization of gold-conjugated polyphenol nanoparticles as a novel delivery system. *Int J Nanomedicine.* 2012;7:1623–1633.
35. Huang X, Wu H, Liao X, Shi B. One-step, size-controlled synthesis of gold nanoparticles at room temperature using plant tannin. *Green Chem.* 2010;12:395–399.
36. Wu H, Huang X, Gao M, Liao X, Shi B. Polyphenol-grafted collagen fiber as reductant and stabilizer for one-step synthesis of size-controlled gold nanoparticles and their catalytic application to 4-nitrophenol reduction. *Green Chem.* 2011;13:651–658.
37. Zhu H, Du ML, Zou ML, Xu CS, Li N, Fu YQ. Facile and green synthesis of well-dispersed Au nanoparticles in PAN nanofibers by tea polyphenols. *J Mater Chem.* 2012;22:9301–9307.
38. Singh DK, Jagannathan R, Khandelwal P, Abraham PM, Poddar P. In situ synthesis and surface functionalization of gold nanoparticles with curcumin and their antioxidant properties: an experimental and density functional theory investigation. *Nanoscale.* 2013;5:1882–1893.
39. Lowry OH, Rosebrough NJ, Farr AL, Randall RJ. Protein measurement with the folin phenol reagent. *J Biol Chem.* 1951;193:265–275.
40. George S, Brat P, Alter P, Amiot MJ. Rapid determination of polyphenols and vitamin C in plant-derived products. *J Agric Food Chem.* 2005;53(5):1370–1373.
41. Blois MS. Antioxidant determinations by the use of a stable free radical. *Nature.* 1958;181:1199–1200.
42. Gülçin I. Antioxidant properties of resveratrol: a structure-activity insight. *Innov Food Sci Emerg Technol.* 2010;11(1):210–218.
43. Re R, Pellegrini N, Proteggente A, Pannala A, Yang M, Rice-Evans C. Antioxidant activity applying an improved ABTS radical cation decolorization assay. *Free Radic Biol Med.* 1999;26(9–10):1231–1237.
44. Gülçin I, Elias R, Gepdiremen A, Boyer L. Antioxidant activity of lignans from fringe tree (chionanthus virginicus L.). *Eur Food Res Technol.* 2006;223(6):759–767.

Reprinted from: Single-step green synthesis and characterization of gold-conjugated polyphenol nanoparticles with antioxidant and biological activities. Sanna V, Pala N, Dessì G, Manconi P, Mariani A, Dedola S, Rassu M., Crosio C, Iaccarino C, Sechi M. Single-step green synthesis and characterization of gold-conjugated polyphenol nanoparticles with antioxidant and biological activities. Volume No 9, Pages No 4935-4951. Copyright (2014), with permission from Dove Medical Press Ltd.

75

Mauro Rassu: "LRRK2 effect on dopamine receptor trafficking – implication in Parkinson's disease".
Ph.D. Course in Life Sciences and Biotechnologies – University of Sassari.

Sanna et al   **Dove**press

45. Baschong W, Suetterlin R, Laeng RH. Control of autofluorescence of archival formaldehyde-fixed, paraffin-embedded tissue in confocal laser scanning microscopy (CLSM). *J Histochem Cytochem.* 2001;49:1565–1572.
46. Iaccarino C, Mura ME, Esposito S, et al. Bcl2-A1 interacts with pro-caspase-3: implications for amyotrophic lateral sclerosis. *Neurobiol Dis.* 2011;43:642–650.
47. Philip D. Synthesis and spectroscopic characterization of gold nanoparticles. *Spectrochim Acta A Mol Biomol Spectrosc.* 2008;71(1):80–85.
48. Philip D. Green synthesis of gold and silver nanoparticles using hibiscus rosa sinensis. *Phys E.* 2010;42(5):1417–1424.
49. Singleton VL, Orthofer R, Lamuela-Raventós RM. Analysis of total phenols and other oxidation substrates and antioxidants by means of folin-ciocalteu reagent. *Methods Enzymol.* 1998;299:152–178.
50. Dauthal P, Mukhopadhyay M. In-vitro free radical scavenging activity of biosynthesized gold and silver nanoparticles using prunus armeniaca (apricot) fruit extract nanomaterials in energy, health and environment. *J Nanopart Res.* 2013;1:15.
51. Gao D, Tian Y, Bi S, Chen Y, Yu A, Zhang H. Studies on the interaction of colloidal gold and serum albumins by spectral methods. *Spectrochim Acta A Mol Biomol Spectrosc.* 2005;62(4–5):1203–1208.
52. Rice-Evans CA, Miller NJ, Paganga G. Structure-antioxidant activity relationships of flavonoids and phenolic acids. *Free Radic Biol Med.* 1996;20(7):933–956.
53. Osman AM, Wong KKY, Fernyhough A. ABTS radical-driven oxidation of polyphenols: isolation and structural elucidation of covalent adducts. *Biochem Biophys Res Comm.* 2006;346:321–329.

54. Qanungo S, Das M, Haldar S, Basu A. Epigallocatechin-3-gallate induces mitochondrial membrane depolarization and caspase-dependent apoptosis in pancreatic cancer cells. *Carcinogenesis.* 2005;26:958–967.
55. Islam S, Islam N, Kermode T, et al. Involvement of caspase-3 in epigallocatechin-3-gallate-mediated apoptosis of human chondrosarcoma cells. *Biochem Biophys Res Commun.* 2000;270:793–797.
56. Tyas L, Brophy VA, Pope A, Rivett AJ, Tavaré JM. Rapid caspase-3 activation during apoptosis revealed using fluorescence-resonance energy transfer. *EMBO Rep.* 2000;3:267–270.
57. Srivastava AK, Bhatnagar P, Singh M, et al. Synthesis of PLGA nanoparticles of tea polyphenols and their strong in vivo protective effect against chemically induced DNA damage. *Int J Nanomedicine.* 2013;8:1451–1462.

Reprinted from: Single-step green synthesis and characterization of gold-conjugated polyphenol nanoparticles with antioxidant and biological activities. Sanna V, Pala N, Dessì G, Manconi P, Mariani A, Dedola S, Rassu M., Crosio C, Iaccarino C, Sechi M. Single-step green synthesis and characterization of gold-conjugated polyphenol nanoparticles with antioxidant and biological activities. Volume No 9, Pages No 4935-4951. Copyright (2014), with permission from Dove Medical Press Ltd.

Mauro Rassu: "LRRK2 effect on dopamine receptor trafficking – implication in Parkinson's disease".
Ph.D. Course in Life Sciences and Biotechnologies – University of Sassari.

Bibliography

1. Dauer, W. & Przedborski, S. Parkinson's disease: mechanisms and models. *Neuron* **39**, 889-909 (2003).
2. Forno, L.S., DeLanney, L.E., Irwin, I. & Langston, J.W. Electron microscopy of Lewy bodies in the amygdala-parahippocampal region. Comparison with inclusion bodies in the MPTP-treated squirrel monkey. *Adv Neurol* **69**, 217-28 (1996).
3. Spillantini, M.G., Crowther, R.A., Jakes, R., Hasegawa, M. & Goedert, M. alpha-Synuclein in filamentous inclusions of Lewy bodies from Parkinson's disease and dementia with lewy bodies. *Proc Natl Acad Sci U S A* **95**, 6469-73 (1998).
4. Gibb, W.R. & Lees, A.J. The relevance of the Lewy body to the pathogenesis of idiopathic Parkinson's disease. *J Neurol Neurosurg Psychiatry* **51**, 745-52 (1988).
5. Farrer, M.J. Genetics of Parkinson disease: paradigm shifts and future prospects. *Nat Rev Genet* **7**, 306-18 (2006).
6. Eisenhofer, G. et al. Substantial production of dopamine in the human gastrointestinal tract. *J Clin Endocrinol Metab* **82**, 3864-71 (1997).
7. Carlsson, A., Lindqvist, M. & Magnusson, T. 3,4-Dihydroxyphenylalanine and 5-hydroxytryptophan as reserpine antagonists. *Nature* **180**, 1200 (1957).
8. Hiroi, T., Imaoka, S. & Funae, Y. Dopamine formation from tyramine by CYP2D6. *Biochem Biophys Res Commun* **249**, 838-43 (1998).
9. Bromek, E., Haduch, A., Golembiowska, K. & Daniel, W.A. Cytochrome P450 mediates dopamine formation in the brain in vivo. *J Neurochem* **118**, 806-15 (2011).
10. Sanchez-Ferrer, A., Rodriguez-Lopez, J.N., Garcia-Canovas, F. & Garcia-Carmona, F. Tyrosinase: a comprehensive review of its mechanism. *Biochim Biophys Acta* **1247**, 1-11 (1995).
11. Chaudhry, F.A., Edwards, R.H. & Fonnum, F. Vesicular neurotransmitter transporters as targets for endogenous and exogenous toxic substances. *Annu Rev Pharmacol Toxicol* **48**, 277-301 (2008).
12. Miesenbock, G., De Angelis, D.A. & Rothman, J.E. Visualizing secretion and synaptic transmission with pH-sensitive green fluorescent proteins. *Nature* **394**, 192-5 (1998).
13. Vergo, S., Johansen, J.L., Leist, M. & Lotharius, J. Vesicular monoamine transporter 2 regulates the sensitivity of rat dopaminergic neurons to disturbed cytosolic dopamine levels. *Brain Res* **1185**, 18-32 (2007).
14. Werkman, T.R., Glennon, J.C., Wadman, W.J. & McCreary, A.C. Dopamine receptor pharmacology: interactions with serotonin receptors and significance for the aetiology and treatment of schizophrenia. *CNS Neurol Disord Drug Targets* **5**, 3-23 (2006).
15. Zhang, H. & Sulzer, D. Regulation of striatal dopamine release by presynaptic auto- and heteroreceptors. *Basal Ganglia* **2**, 5-13 (2012).

Mauro Rassu: "LRRK2 effect on dopamine receptor trafficking – implication in Parkinson's disease".
Ph.D. Course in Life Sciences and Biotechnologies – University of Sassari.

16. Eriksen, J., Jorgensen, T.N. & Gether, U. Regulation of dopamine transporter function by protein-protein interactions: new discoveries and methodological challenges. *J Neurochem* **113**, 27-41 (2010).

17. Eisenhofer, G., Kopin, I.J. & Goldstein, D.S. Catecholamine metabolism: a contemporary view with implications for physiology and medicine. *Pharmacol Rev* **56**, 331-49 (2004).

18. Myohanen, T.T., Schendzielorz, N. & Mannisto, P.T. Distribution of catechol-O-methyltransferase (COMT) proteins and enzymatic activities in wild-type and soluble COMT deficient mice. *J Neurochem* **113**, 1632-43 (2010).

19. Meiser, J., Weindl, D. & Hiller, K. Complexity of dopamine metabolism. *Cell Commun Signal* **11**, 34 (2013).

20. Anden, N.E. et al. Demonstration and Mapping out of Nigro-Neostriatal Dopamine Neurons. *Life Sci* **3**, 523-30 (1964).

21. Dahlstroem, A. & Fuxe, K. Evidence for the Existence of Monoamine-Containing Neurons in the Central Nervous System. I. Demonstration of Monoamines in the Cell Bodies of Brain Stem Neurons. *Acta Physiol Scand Suppl*, SUPPL 232:1-55 (1964).

22. Snyder, S.H., Taylor, K.M., Coyle, J.T. & Meyerhoff, J.L. The role of brain dopamine in behavioral regulation and the actions of psychotropic drugs. *Am J Psychiatry* **127**, 199-207 (1970).

23. Missale, C., Nash, S.R., Robinson, S.W., Jaber, M. & Caron, M.G. Dopamine receptors: from structure to function. *Physiol Rev* **78**, 189-225 (1998).

24. Iversen, S.D. & Iversen, L.L. Dopamine: 50 years in perspective. *Trends Neurosci* **30**, 188-93 (2007).

25. Beaulieu, J.M. & Gainetdinov, R.R. The physiology, signaling, and pharmacology of dopamine receptors. *Pharmacol Rev* **63**, 182-217 (2011).

26. Andersen, P.H. et al. Dopamine receptor subtypes: beyond the D1/D2 classification. *Trends Pharmacol Sci* **11**, 231-6 (1990).

27. Niznik, H.B. & Van Tol, H.H. Dopamine receptor genes: new tools for molecular psychiatry. *J Psychiatry Neurosci* **17**, 158-80 (1992).

28. Vallone, D., Picetti, R. & Borrelli, E. Structure and function of dopamine receptors. *Neurosci Biobehav Rev* **24**, 125-32 (2000).

29. Sokoloff, P. et al. The dopamine D3 receptor: a therapeutic target for the treatment of neuropsychiatric disorders. *CNS Neurol Disord Drug Targets* **5**, 25-43 (2006).

30. Rankin, M.L. et al. The D1 dopamine receptor is constitutively phosphorylated by G protein-coupled receptor kinase 4. *Mol Pharmacol* **69**, 759-69 (2006).

31. Rondou, P., Haegeman, G. & Van Craenenbroeck, K. The dopamine D4 receptor: biochemical and signalling properties. *Cell Mol Life Sci* **67**, 1971-86 (2010).

32. Wu, J., Xiao, H., Sun, H., Zou, L. & Zhu, L.Q. Role of dopamine receptors in ADHD: a systematic meta-analysis. *Mol Neurobiol* **45**, 605-20 (2012).

33. Gerfen, C.R. Molecular effects of dopamine on striatal-projection pathways. *Trends Neurosci* **23**, S64-70 (2000).

34. Beischlag, T.V. et al. The human dopamine D5 receptor gene: cloning and characterization of the 5'-flanking and promoter region. *Biochemistry* **34**, 5960-70 (1995).

35. Bergson, C. et al. Regional, cellular, and subcellular variations in the distribution of D1 and D5 dopamine receptors in primate brain. *J Neurosci* **15**, 7821-36 (1995).

36. Gerfen, C.R. Dopamine-mediated gene regulation in models of Parkinson's disease. *Ann Neurol* **47**, S42-50; discussion S50-2 (2000).

37. Seeman, P. Targeting the dopamine D2 receptor in schizophrenia. *Expert Opin Ther Targets* **10**, 515-31 (2006).

38. Sokoloff, P. et al. Localization and function of the D3 dopamine receptor. *Arzneimittelforschung* **42**, 224-30 (1992).

39. Sharples, S.A., Koblinger, K., Humphreys, J.M. & Whelan, P.J. Dopamine: a parallel pathway for the modulation of spinal locomotor networks. *Front Neural Circuits* **8**, 55 (2014).

40. Sibley, D.R. New insights into dopaminergic receptor function using antisense and genetically altered animals. *Annu Rev Pharmacol Toxicol* **39**, 313-41 (1999).

41. Wolf, M.E. & Roth, R.H. Autoreceptor regulation of dopamine synthesis. *Ann N Y Acad Sci* **604**, 323-43 (1990).

42. Usiello, A. et al. Distinct functions of the two isoforms of dopamine D2 receptors. *Nature* **408**, 199-203 (2000).

43. De Mei, C., Ramos, M., Iitaka, C. & Borrelli, E. Getting specialized: presynaptic and postsynaptic dopamine D2 receptors. *Curr Opin Pharmacol* **9**, 53-8 (2009).

44. Gainetdinov, R.R., Sotnikova, T.D., Grekhova, T.V. & Rayevsky, K.S. Simultaneous monitoring of dopamine, its metabolites and trans-isomer of atypical neuroleptic drug carbidine concentrations in striatal dialysates of conscious rats. *Prog Neuropsychopharmacol Biol Psychiatry* **20**, 291-305 (1996).

45. Zapata, A. & Shippenberg, T.S. D(3) receptor ligands modulate extracellular dopamine clearance in the nucleus accumbens. *J Neurochem* **81**, 1035-42 (2002).

46. Joseph, J.D. et al. Dopamine autoreceptor regulation of release and uptake in mouse brain slices in the absence of D(3) receptors. *Neuroscience* **112**, 39-49 (2002).

47. White, F.J., Bednarz, L.M., Wachtel, S.R., Hjorth, S. & Brooderson, R.J. Is stimulation of both D1 and D2 receptors necessary for the expression of dopamine-mediated behaviors? *Pharmacol Biochem Behav* **30**, 189-93 (1988).

48. Thompson, R.H., Menard, A., Pombal, M. & Grillner, S. Forebrain dopamine depletion impairs motor behavior in lamprey. *Eur J Neurosci* **27**, 1452-60 (2008).

49. Thompson, M.D., Burnham, W.M. & Cole, D.E. The G protein-coupled receptors: pharmacogenetics and disease. *Crit Rev Clin Lab Sci* **42**, 311-92 (2005).

50. Palczewski, K., Hofmann, K.P. & Baehr, W. Rhodopsin--advances and perspectives. *Vision Res* **46**, 4425-6 (2006).

51. Moreira, I.S. Structural features of the G-protein/GPCR interactions. *Biochim Biophys Acta* **1840**, 16-33 (2014).

52. Hanyaloglu, A.C. & von Zastrow, M. Regulation of GPCRs by endocytic membrane trafficking and its potential implications. *Annu Rev Pharmacol Toxicol* **48**, 537-68 (2008).

53. Ritter, S.L. & Hall, R.A. Fine-tuning of GPCR activity by receptor-interacting proteins. *Nat Rev Mol Cell Biol* **10**, 819-30 (2009).

54. Volume 202, number 2 (1998), in article no. DB989010, "FREAC-1 contains a cell-type-specific transcriptional activation domain and is expressed in epithelial-mesenchymal Interfaces," by margit mahlapuu, markku pelto-huikko, marjo aitola, sven Enerback, and peter carlsson, pages 183-195. *Dev Biol* **207**, 476 (1999).

55. Violin, J.D. & Lefkowitz, R.J. Beta-arrestin-biased ligands at seven-transmembrane receptors. *Trends Pharmacol Sci* **28**, 416-22 (2007).

56. Urban, J.D. et al. Functional selectivity and classical concepts of quantitative pharmacology. *J Pharmacol Exp Ther* **320**, 1-13 (2007).

57. Svenningsson, P. et al. DARPP-32: an integrator of neurotransmission. *Annu Rev Pharmacol Toxicol* **44**, 269-96 (2004).

58. Girault, J.A. Signaling in striatal neurons: the phosphoproteins of reward, addiction, and dyskinesia. *Prog Mol Biol Transl Sci* **106**, 33-62 (2012).

59. Beaulieu, J.M. et al. An Akt/beta-arrestin 2/PP2A signaling complex mediates dopaminergic neurotransmission and behavior. *Cell* **122**, 261-73 (2005).

60. Park, S.K. et al. Par-4 links dopamine signaling and depression. *Cell* **122**, 275-87 (2005).

61. Bouvier, M. Oligomerization of G-protein-coupled transmitter receptors. *Nat Rev Neurosci* **2**, 274-86 (2001).

62. Marshall, F.H. Heterodimerization of G-protein-coupled receptors in the CNS. *Curr Opin Pharmacol* **1**, 40-4 (2001).

63. Milligan, G. & White, J.H. Protein-protein interactions at G-protein-coupled receptors. *Trends Pharmacol Sci* **22**, 513-8 (2001).

64. Fuxe, K. et al. Intramembrane receptor-receptor interactions: a novel principle in molecular medicine. *J Neural Transm (Vienna)* **114**, 49-75 (2007).

65. Agnati, L.F. et al. Possible role of intramembrane receptor-receptor interactions in memory and learning via formation of long-lived heteromeric complexes: focus on motor learning in the basal ganglia. *J Neural Transm Suppl*, 1-28 (2003).

66. Agnati, L.F., Fuxe, K., Zoli, M., Rondanini, C. & Ogren, S.O. New vistas on synaptic plasticity: the receptor mosaic hypothesis of the engram. *Med Biol* **60**, 183-90 (1982).

67. Rashid, A.J., O'Dowd, B.F., Verma, V. & George, S.R. Neuronal Gq/11-coupled dopamine receptors: an uncharted role for dopamine. *Trends Pharmacol Sci* **28**, 551-5 (2007).

68. Perreault, M.L., Jones-Tabah, J., O'Dowd, B.F. & George, S.R. A physiological role for the dopamine D5 receptor as a regulator of BDNF and Akt signalling in rodent prefrontal cortex. *Int J Neuropsychopharmacol* **16**, 477-83 (2013).

69. O'Dowd, B.F., Ji, X., Nguyen, T. & George, S.R. Two amino acids in each of D1 and D2 dopamine receptor cytoplasmic regions are involved in D1-D2 heteromer formation. *Biochem Biophys Res Commun* **417**, 23-8 (2012).

70. Perreault, M.L., Hasbi, A., O'Dowd, B.F. & George, S.R. Heteromeric dopamine receptor signaling complexes: emerging neurobiology and disease relevance. *Neuropsychopharmacology* **39**, 156-68 (2014).

71. Verma, V., Hasbi, A., O'Dowd, B.F. & George, S.R. Dopamine D1-D2 receptor Heteromer-mediated calcium release is desensitized by D1 receptor occupancy with or without signal activation: dual functional regulation by G protein-coupled receptor kinase 2. *J Biol Chem* **285**, 35092-103 (2010).

72. Ng, J., Rashid, A.J., So, C.H., O'Dowd, B.F. & George, S.R. Activation of calcium/calmodulin-dependent protein kinase IIalpha in the striatum by the heteromeric D1-D2 dopamine receptor complex. *Neuroscience* **165**, 535-41 (2010).

73. Perreault, M.L., Fan, T., Alijaniaram, M., O'Dowd, B.F. & George, S.R. Dopamine D1-D2 receptor heteromer in dual phenotype GABA/glutamate-coexpressing striatal medium spiny neurons: regulation of BDNF, GAD67 and VGLUT1/2. *PLoS One* **7**, e33348 (2012).

74. Rashid, A.J. et al. D1-D2 dopamine receptor heterooligomers with unique pharmacology are coupled to rapid activation of Gq/11 in the striatum. *Proc Natl Acad Sci U S A* **104**, 654-9 (2007).

75. Hasbi, A. et al. Calcium signaling cascade links dopamine D1-D2 receptor heteromer to striatal BDNF production and neuronal growth. *Proc Natl Acad Sci U S A* **106**, 21377-82 (2009).

76. Lidow, M.S. Calcium signaling dysfunction in schizophrenia: a unifying approach. *Brain Res Brain Res Rev* **43**, 70-84 (2003).

77. Fiorentini, C. et al. Reciprocal regulation of dopamine D1 and D3 receptor function and trafficking by heterodimerization. *Mol Pharmacol* **74**, 59-69 (2008).

78. Marcellino, D. et al. Identification of dopamine D1-D3 receptor heteromers. Indications for a role of synergistic D1-D3 receptor interactions in the striatum. *J Biol Chem* **283**, 26016-25 (2008).

79. Bordet, R., Ridray, S., Schwartz, J.C. & Sokoloff, P. Involvement of the direct striatonigral pathway in levodopa-induced sensitization in 6-hydroxydopamine-lesioned rats. *Eur J Neurosci* **12**, 2117-23 (2000).

80. Stern, M.B. & Freese, A. Parkinson's disease: the case for novel treatment strategies. *Exp Neurol* **144**, 2-3 (1997).

81. Ferre, S. et al. Neurotransmitter receptor heteromers and their integrative role in 'local modules': the striatal spine module. *Brain Res Rev* **55**, 55-67 (2007).

82. Oertel, W. & Schulz, J.B. Current and experimental treatments of Parkinson disease: A guide for neuroscientists. *J Neurochem* **139 Suppl 1**, 325-337 (2016).

83. Poewe, W., Antonini, A., Zijlmans, J.C.M., Burkhard, P.R. & Vingerhoets, F. Levodopa in the treatment of Parkinson's disease: an old drug still going strong. *Clinical Interventions in Aging* **5**, 229-238 (2010).

84. Muller, T. Drug therapy in patients with Parkinson's disease. *Transl Neurodegener* **1**, 10 (2012).

85. Ossig, C. & Reichmann, H. Treatment of Parkinson's disease in the advanced stage. *J Neural Transm* **120**, 523-9 (2013).

86. Gray, R. et al. Long-term effectiveness of dopamine agonists and monoamine oxidase B inhibitors compared with levodopa as initial treatment for Parkinson's disease (PD MED): a large, open-label, pragmatic randomised trial. *Lancet* **384**, 1196-205 (2014).

87. Fox, S.H. et al. The Movement Disorder Society Evidence-Based Medicine Review Update: Treatments for the motor symptoms of Parkinson's disease. *Mov Disord* **26 Suppl 3**, S2-41 (2011).

88. Poewe, W. When a Parkinson's disease patient starts to hallucinate. *Pract Neurol* **8**, 238-41 (2008).

89. Lai, B.C., Marion, S.A., Teschke, K. & Tsui, J.K. Occupational and environmental risk factors for Parkinson's disease. *Parkinsonism Relat Disord* **8**, 297-309 (2002).

90. Langston, J.W., Ballard, P., Tetrud, J.W. & Irwin, I. Chronic Parkinsonism in humans due to a product of meperidine-analog synthesis. *Science* **219**, 979-80 (1983).

91. Liu, Y., Roghani, A. & Edwards, R.H. Gene transfer of a reserpine-sensitive mechanism of resistance to N-methyl-4-phenylpyridinium. *Proc Natl Acad Sci U S A* **89**, 9074-8 (1992).

92. Ramsay, R.R., Dadgar, J., Trevor, A. & Singer, T.P. Energy-driven uptake of N-methyl-4-phenylpyridine by brain mitochondria mediates the neurotoxicity of MPTP. *Life Sci* **39**, 581-8 (1986).

93. Klaidman, L.K., Adams, J.D., Jr., Leung, A.C., Kim, S.S. & Cadenas, E. Redox cycling of MPP+: evidence for a new mechanism involving hydride transfer with xanthine oxidase, aldehyde dehydrogenase, and lipoamide dehydrogenase. *Free Radic Biol Med* **15**, 169-79 (1993).

94. Dawson, T.M., Ko, H.S. & Dawson, V.L. Genetic animal models of Parkinson's disease. *Neuron* **66**, 646-61 (2010).

95. Priyadarshi, A., Khuder, S.A., Schaub, E.A. & Priyadarshi, S.S. Environmental risk factors and Parkinson's disease: a metaanalysis. *Environ Res* **86**, 122-7 (2001).

96. Poskanzer, D.C. & Schwab, R.S. Cohort Analysis of Parkinson's Syndrome: Evidence for a Single Etiology Related to Subclinical Infection About 1920. *J Chronic Dis* **16**, 961-73 (1963).

97. Gamboa, E.T. et al. Influenza virus antigen in postencephalitic parkinsonism brain. Detection by immunofluorescence. *Arch Neurol* **31**, 228-32 (1974).

98. Thomas, B. & Beal, M.F. Parkinson's disease. *Hum Mol Genet* **16 Spec No. 2**, R183-94 (2007).

99.   Wirdefeldt, K., Adami, H.O., Cole, P., Trichopoulos, D. & Mandel, J. Epidemiology and etiology of Parkinson's disease: a review of the evidence. *Eur J Epidemiol* **26 Suppl 1**, S1-58 (2011).

100. Hernandez, D.G., Reed, X. & Singleton, A.B. Genetics in Parkinson disease: Mendelian versus non-Mendelian inheritance. *J Neurochem* **139 Suppl 1**, 59-74 (2016).

101. Polymeropoulos, M.H. et al. Mutation in the alpha-synuclein gene identified in families with Parkinson's disease. *Science* **276**, 2045-7 (1997).

102. Ki, C.S. et al. The Ala53Thr mutation in the alpha-synuclein gene in a Korean family with Parkinson disease. *Clin Genet* **71**, 471-3 (2007).

103. Puschmann, A. et al. A Swedish family with de novo alpha-synuclein A53T mutation: evidence for early cortical dysfunction. *Parkinsonism Relat Disord* **15**, 627-32 (2009).

104. Spillantini, M.G. et al. Alpha-synuclein in Lewy bodies. *Nature* **388**, 839-40 (1997).

105. Klein, C. & Schlossmacher, M.G. The genetics of Parkinson disease: Implications for neurological care. *Nat Clin Pract Neurol* **2**, 136-46 (2006).

106. Singleton, A.B. et al. alpha-Synuclein locus triplication causes Parkinson's disease. *Science* **302**, 841 (2003).

107. Farrer, M. et al. Comparison of kindreds with parkinsonism and alpha-synuclein genomic multiplications. *Ann Neurol* **55**, 174-9 (2004).

108. Ibanez, P. et al. Alpha-synuclein gene rearrangements in dominantly inherited parkinsonism: frequency, phenotype, and mechanisms. *Arch Neurol* **66**, 102-8 (2009).

109. Spillantini, M.G., Divane, A. & Goedert, M. Assignment of human alpha-synuclein (SNCA) and beta-synuclein (SNCB) genes to chromosomes 4q21 and 5q35. *Genomics* **27**, 379-81 (1995).

110. Ueda, K. et al. Molecular cloning of cDNA encoding an unrecognized component of amyloid in Alzheimer disease. *Proc Natl Acad Sci U S A* **90**, 11282-6 (1993).

111. Chandra, S., Chen, X., Rizo, J., Jahn, R. & Sudhof, T.C. A broken alpha -helix in folded alpha -Synuclein. *J Biol Chem* **278**, 15313-8 (2003).

112. Giasson, B.I., Murray, I.V., Trojanowski, J.Q. & Lee, V.M. A hydrophobic stretch of 12 amino acid residues in the middle of alpha-synuclein is essential for filament assembly. *J Biol Chem* **276**, 2380-6 (2001).

113. George, J.M. The synucleins. *Genome Biol* **3**, REVIEWS3002 (2002).

114. Lashuel, H.A., Overk, C.R., Oueslati, A. & Masliah, E. The many faces of alpha-synuclein: from structure and toxicity to therapeutic target. *Nat Rev Neurosci* **14**, 38-48 (2013).

115. Fortin, D.L. et al. Lipid rafts mediate the synaptic localization of alpha-synuclein. *J Neurosci* **24**, 6715-23 (2004).

116. Gitler, A.D. et al. The Parkinson's disease protein alpha-synuclein disrupts cellular Rab homeostasis. *Proc Natl Acad Sci U S A* **105**, 145-50 (2008).

117. Burre, J. et al. Alpha-synuclein promotes SNARE-complex assembly in vivo and in vitro. *Science* **329**, 1663-7 (2010).

118. Thayanidhi, N. et al. Alpha-synuclein delays endoplasmic reticulum (ER)-to-Golgi transport in mammalian cells by antagonizing ER/Golgi SNAREs. *Mol Biol Cell* **21**, 1850-63 (2010).

119. Kitada, T. et al. Mutations in the parkin gene cause autosomal recessive juvenile parkinsonism. *Nature* **392**, 605-8 (1998).

120. Hedrich, K. et al. The importance of gene dosage studies: mutational analysis of the parkin gene in early-onset parkinsonism. *Hum Mol Genet* **10**, 1649-56 (2001).

121. Pirkevi, C., Lesage, S., Brice, A. & Basak, A.N. From genes to proteins in mendelian Parkinson's disease: an overview. *Anat Rec (Hoboken)* **292**, 1893-901 (2009).

122. Scuderi, S., La Cognata, V., Drago, F., Cavallaro, S. & D'Agata, V. Alternative splicing generates different parkin protein isoforms: evidences in human, rat, and mouse brain. *Biomed Res Int* **2014**, 690796 (2014).

123. Farrer, M. et al. Lewy bodies and parkinsonism in families with parkin mutations. *Ann Neurol* **50**, 293-300 (2001).

124. van de Warrenburg, B.P. et al. Clinical and pathologic abnormalities in a family with parkinsonism and parkin gene mutations. *Neurology* **56**, 555-7 (2001).

125. Mori, H., Hattori, N. & Mizuno, Y. Genotype-phenotype correlation: familial Parkinson disease. *Neuropathology* **23**, 90-4 (2003).

126. Doherty, K.M. & Hardy, J. Parkin disease and the Lewy body conundrum. *Mov Disord* **28**, 702-4 (2013).

127. Shimura, H. et al. Familial Parkinson disease gene product, parkin, is a ubiquitin-protein ligase. *Nat Genet* **25**, 302-5 (2000).

128. Narendra, D., Tanaka, A., Suen, D.F. & Youle, R.J. Parkin is recruited selectively to impaired mitochondria and promotes their autophagy. *J Cell Biol* **183**, 795-803 (2008).

129. Narendra, D.P. et al. PINK1 is selectively stabilized on impaired mitochondria to activate Parkin. *PLoS Biol* **8**, e1000298 (2010).

130. Valente, E.M. et al. Localization of a novel locus for autosomal recessive early-onset parkinsonism, PARK6, on human chromosome 1p35-p36. *Am J Hum Genet* **68**, 895-900 (2001).

131. Valente, E.M. et al. Hereditary early-onset Parkinson's disease caused by mutations in PINK1. *Science* **304**, 1158-60 (2004).

132. Bekris, L.M., Mata, I.F. & Zabetian, C.P. The genetics of Parkinson disease. *J Geriatr Psychiatry Neurol* **23**, 228-42 (2010).

133. Pridgeon, J.W., Olzmann, J.A., Chin, L.S. & Li, L. PINK1 protects against oxidative stress by phosphorylating mitochondrial chaperone TRAP1. *PLoS Biol* **5**, e172 (2007).

134. Kane, L.A. et al. PINK1 phosphorylates ubiquitin to activate Parkin E3 ubiquitin ligase activity. *J Cell Biol* **205**, 143-53 (2014).

135. Winklhofer, K.F. Parkin and mitochondrial quality control: toward assembling the puzzle. *Trends Cell Biol* **24**, 332-41 (2014).

136. Kondapalli, C. et al. PINK1 is activated by mitochondrial membrane potential depolarization and stimulates Parkin E3 ligase activity by phosphorylating Serine 65. *Open Biol* **2**, 120080 (2012).

137. Gegg, M.E. et al. Mitofusin 1 and mitofusin 2 are ubiquitinated in a PINK1/parkin-dependent manner upon induction of mitophagy. *Hum Mol Genet* **19**, 4861-70 (2010).

138. Zhang, L. et al. TRAP1 rescues PINK1 loss-of-function phenotypes. *Hum Mol Genet* **22**, 2829-41 (2013).

139. Bonifati, V. et al. DJ-1(PARK7), a novel gene for autosomal recessive, early onset parkinsonism. *Neurol Sci* **24**, 159-60 (2003).

140. Nagakubo, D. et al. DJ-1, a novel oncogene which transforms mouse NIH3T3 cells in cooperation with ras. *Biochem Biophys Res Commun* **231**, 509-13 (1997).

141. Pankratz, N. et al. Mutations in DJ-1 are rare in familial Parkinson disease. *Neurosci Lett* **408**, 209-13 (2006).

142. Klein, C. & Westenberger, A. Genetics of Parkinson's disease. *Cold Spring Harb Perspect Med* **2**, a008888 (2012).

143. Canet-Aviles, R.M. et al. The Parkinson's disease protein DJ-1 is neuroprotective due to cysteine-sulfinic acid-driven mitochondrial localization. *Proc Natl Acad Sci U S A* **101**, 9103-8 (2004).

144. Junn, E. et al. Interaction of DJ-1 with Daxx inhibits apoptosis signal-regulating kinase 1 activity and cell death. *Proc Natl Acad Sci U S A* **102**, 9691-6 (2005).

145. Macedo, M.G. et al. The DJ-1L166P mutant protein associated with early onset Parkinson's disease is unstable and forms higher-order protein complexes. *Hum Mol Genet* **12**, 2807-16 (2003).

Mauro Rassu: "LRRK2 effect on dopamine receptor trafficking – implication in Parkinson's disease".
Ph.D. Course in Life Sciences and Biotechnologies – University of Sassari.

146. Takahashi-Niki, K., Niki, T., Taira, T., Iguchi-Ariga, S.M. & Ariga, H. Reduced anti-oxidative stress activities of DJ-1 mutants found in Parkinson's disease patients. *Biochem Biophys Res Commun* **320**, 389-97 (2004).

147. Anderson, P.C. & Daggett, V. Molecular basis for the structural instability of human DJ-1 induced by the L166P mutation associated with Parkinson's disease. *Biochemistry* **47**, 9380-93 (2008).

148. Malgieri, G. & Eliezer, D. Structural effects of Parkinson's disease linked DJ-1 mutations. *Protein Sci* **17**, 855-68 (2008).

149. Requejo-Aguilar, R. et al. DJ1 represses glycolysis and cell proliferation by transcriptionally up-regulating Pink1. *Biochem J* **467**, 303-10 (2015).

150. Zimprich, A. et al. A mutation in VPS35, encoding a subunit of the retromer complex, causes late-onset Parkinson disease. *Am J Hum Genet* **89**, 168-75 (2011).

151. Vilarino-Guell, C. et al. VPS35 mutations in Parkinson disease. *Am J Hum Genet* **89**, 162-7 (2011).

152. Lesage, S. et al. Identification of VPS35 mutations replicated in French families with Parkinson disease. *Neurology* **78**, 1449-50 (2012).

153. Kumar, K.R. et al. Frequency of the D620N mutation in VPS35 in Parkinson disease. *Arch Neurol* **69**, 1360-4 (2012).

154. Seaman, M.N., McCaffery, J.M. & Emr, S.D. A membrane coat complex essential for endosome-to-Golgi retrograde transport in yeast. *J Cell Biol* **142**, 665-81 (1998).

155. Hierro, A. et al. Functional architecture of the retromer cargo-recognition complex. *Nature* **449**, 1063-7 (2007).

156. Haft, C.R. et al. Human orthologs of yeast vacuolar protein sorting proteins Vps26, 29, and 35: assembly into multimeric complexes. *Mol Biol Cell* **11**, 4105-16 (2000).

157. Funayama, M. et al. A new locus for Parkinson's disease (PARK8) maps to chromosome 12p11.2-q13.1. *Ann Neurol* **51**, 296-301 (2002).

158. Haubenberger, D. et al. A novel LRRK2 mutation in an austrian cohort of patients with Parkinson's disease. *Movement Disorders* **22**, 1640-1643 (2007).

159. Paisan-Ruiz, C. et al. Cloning of the gene containing mutations that cause PARK8-linked Parkinson's disease. *Neuron* **44**, 595-600 (2004).

160. Nalls, M.A. et al. Large-scale meta-analysis of genome-wide association data identifies six new risk loci for Parkinson's disease. *Nat Genet* **46**, 989-93 (2014).

161. Li, C.J. & Beal, M.F. Leucine-rich repeat kinase 2: A new player with a familiar theme for Parkinson's disease pathogenesis. *Proc Natl Acad Sci U S A* **102**, 16535-16536 (2005).

162. Rideout, H.J. & Stefanis, L. The Neurobiology of LRRK2 and its Role in the Pathogenesis of Parkinson's Disease. *Neurochem Res* (2013).

163. Guaitoli, G. et al. Structural model of the dimeric Parkinson's protein LRRK2 reveals a compact architecture involving distant interdomain contacts. *Proc Natl Acad Sci U S A* **113**, E4357-66 (2016).

164. Tewari, R., Bailes, E., Bunting, K.A. & Coates, J.C. Armadillo-repeat protein functions: questions for little creatures. *Trends Cell Biol* **20**, 470-81 (2010).

165. Mosavi, L.K., Cammett, T.J., Desrosiers, D.C. & Peng, Z.Y. The ankyrin repeat as molecular architecture for protein recognition. *Protein Sci* **13**, 1435-48 (2004).

166. Mata, I.F., Wedemeyer, W.J., Farrer, M.J., Taylor, J.P. & Gallo, K.A. LRRK2 in Parkinson's disease: protein domains and functional insights. *Trends Neurosci* **29**, 286-93 (2006).

167. Bella, J., Hindle, K.L., McEwan, P.A. & Lovell, S.C. The leucine-rich repeat structure. *Cell Mol Life Sci* **65**, 2307-33 (2008).

168. Xu, C. & Min, J. Structure and function of WD40 domain proteins. *Protein Cell* **2**, 202-14 (2011).

169.   Gilsbach, B.K. et al. Roco kinase structures give insights into the mechanism of Parkinson disease-related leucine-rich-repeat kinase 2 mutations. *Proc Natl Acad Sci U S A* **109**, 10322-7 (2012).

170.   Gilsbach, B.K. & Kortholt, A. Structural biology of the LRRK2 GTPase and kinase domains: implications for regulation. *Front Mol Neurosci* **7**, 32 (2014).

171.   Deng, J. et al. Structure of the ROC domain from the Parkinson's disease-associated leucine-rich repeat kinase 2 reveals a dimeric GTPase. *Proc Natl Acad Sci U S A* **105**, 1499-504 (2008).

172.   Gotthardt, K., Weyand, M., Kortholt, A., Van Haastert, P.J. & Wittinghofer, A. Structure of the Roc-COR domain tandem of C. tepidum, a prokaryotic homologue of the human LRRK2 Parkinson kinase. *EMBO J* **27**, 2239-49 (2008).

173.   Greggio, E. et al. The Parkinson disease-associated leucine-rich repeat kinase 2 (LRRK2) is a dimer that undergoes intramolecular autophosphorylation. *J Biol Chem* **283**, 16906-14 (2008).

174.   Sen, S., Webber, P.J. & West, A.B. Dependence of leucine-rich repeat kinase 2 (LRRK2) kinase activity on dimerization. *J Biol Chem* **284**, 36346-56 (2009).

175.   Civiero, L. et al. Biochemical characterization of highly purified leucine-rich repeat kinases 1 and 2 demonstrates formation of homodimers. *PLoS One* **7**, e43472 (2012).

176.   Biosa, A. et al. GTPase activity regulates kinase activity and cellular phenotypes of Parkinson's disease-associated LRRK2. *Hum Mol Genet* **22**, 1140-56 (2013).

177.   James, N.G. et al. Number and brightness analysis of LRRK2 oligomerization in live cells. *Biophys J* **102**, L41-3 (2012).

178.   Cookson, M.R. Structure, function, and leucine-rich repeat kinase 2: On the importance of reproducibility in understanding Parkinson's disease. *Proc Natl Acad Sci U S A* **113**, 8346-8 (2016).

179.   Taymans, J.M. The GTPase function of LRRK2. *Biochem Soc Trans* **40**, 1063-9 (2012).

180.   Rosenbusch, K.E. & Kortholt, A. Activation Mechanism of LRRK2 and Its Cellular Functions in Parkinson's Disease. *Parkinsons Dis* **2016**, 7351985 (2016).

181.   Rubio, J.P. et al. Deep sequencing of the LRRK2 gene in 14,002 individuals reveals evidence of purifying selection and independent origin of the p.Arg1628Pro mutation in Europe. *Hum Mutat* **33**, 1087-98 (2012).

182.   Healy, D.G. et al. Phenotype, genotype, and worldwide genetic penetrance of LRRK2-associated Parkinson's disease: a case-control study. *Lancet Neurol* **7**, 583-90 (2008).

183.   Aasly, J.O. et al. Novel pathogenic LRRK2 p.Asn1437His substitution in familial Parkinson's disease. *Mov Disord* **25**, 2156-63 (2010).

184.   Nuytemans, K., Theuns, J., Cruts, M. & Van Broeckhoven, C. Genetic etiology of Parkinson disease associated with mutations in the SNCA, PARK2, PINK1, PARK7, and LRRK2 genes: a mutation update. *Hum Mutat* **31**, 763-80 (2010).

185.   Bardien, S., Lesage, S., Brice, A. & Carr, J. Genetic characteristics of leucine-rich repeat kinase 2 (LRRK2) associated Parkinson's disease. *Parkinsonism Relat Disord* **17**, 501-8 (2011).

186.   Lorenzo-Betancor, O. et al. LRRK2 haplotype-sharing analysis in Parkinson's disease reveals a novel p.S1761R mutation. *Mov Disord* **27**, 146-51 (2012).

187.   Haugarvoll, K. & Wszolek, Z.K. Clinical features of LRRK2 parkinsonism. *Parkinsonism Relat Disord* **15 Suppl 3**, S205-8 (2009).

188.   Correia Guedes, L. et al. Worldwide frequency of G2019S LRRK2 mutation in Parkinson's disease: a systematic review. *Parkinsonism Relat Disord* **16**, 237-42 (2010).

189.   Greggio, E. Role of LRRK2 kinase activity in the pathogenesis of Parkinson's disease. *Biochem Soc Trans* **40**, 1058-62 (2012).

190.   Greggio, E. et al. Kinase activity is required for the toxic effects of mutant LRRK2/dardarin. *Neurobiol Dis* **23**, 329-41 (2006).

191.   West, A.B. et al. Parkinson's disease-associated mutations in LRRK2 link enhanced GTP-binding and kinase activities to neuronal toxicity. *Hum Mol Genet* **16**, 223-32 (2007).

192.   Funayama, M. et al. An LRRK2 mutation as a cause for the parkinsonism in the original PARK8 family. *Ann Neurol* **57**, 918-21 (2005).

193.   Gloeckner, C.J. et al. The Parkinson disease causing LRRK2 mutation I2020T is associated with increased kinase activity. *Hum Mol Genet* **15**, 223-32 (2006).

194.   Ray, S. et al. The Parkinson disease-linked LRRK2 protein mutation I2020T stabilizes an active state conformation leading to increased kinase activity. *J Biol Chem* **289**, 13042-53 (2014).

195.   Jaleel, M. et al. LRRK2 phosphorylates moesin at threonine-558: characterization of how Parkinson's disease mutants affect kinase activity. *Biochem J* **405**, 307-17 (2007).

196.   Greggio, E. & Cookson, M.R. Leucine-rich repeat kinase 2 mutations and Parkinson's disease: three questions. *ASN Neuro* **1** (2009).

197.   Gorostidi, A., Ruiz-Martinez, J., Lopez de Munain, A., Alzualde, A. & Marti Masso, J.F. LRRK2 G2019S and R1441G mutations associated with Parkinson's disease are common in the Basque Country, but relative prevalence is determined by ethnicity. *Neurogenetics* **10**, 157-9 (2009).

198.   Wallings, R., Manzoni, C. & Bandopadhyay, R. Cellular processes associated with LRRK2 function and dysfunction. *FEBS J* **282**, 2806-26 (2015).

199.   Khan, N.L. et al. Mutations in the gene LRRK2 encoding dardarin (PARK8) cause familial Parkinson's disease: clinical, pathological, olfactory and functional imaging and genetic data. *Brain* **128**, 2786-96 (2005).

200.   Lewis, P.A. et al. The R1441C mutation of LRRK2 disrupts GTP hydrolysis. *Biochem Biophys Res Commun* **357**, 668-71 (2007).

201.   Liao, J. et al. Parkinson disease-associated mutation R1441H in LRRK2 prolongs the "active state" of its GTPase domain. *Proc Natl Acad Sci U S A* **111**, 4055-60 (2014).

202.   Daniels, V. et al. Insight into the mode of action of the LRRK2 Y1699C pathogenic mutant. *J Neurochem* **116**, 304-15 (2011).

203.   Biskup, S. et al. Localization of LRRK2 to membranous and vesicular structures in mammalian brain. *Ann Neurol* **60**, 557-69 (2006).

204.   West, A.B. et al. Differential LRRK2 expression in the cortex, striatum, and substantia nigra in transgenic and nontransgenic rodents. *J Comp Neurol* **522**, 2465-80 (2014).

205.   Su, A.I. et al. A gene atlas of the mouse and human protein-encoding transcriptomes. *Proc Natl Acad Sci U S A* **101**, 6062-7 (2004).

206.   Larsen, K. & Madsen, L.B. Sequence conservation between porcine and human LRRK2. *Mol Biol Rep* **36**, 237-43 (2009).

207.   Thevenet, J., Pescini Gobert, R., Hooft van Huijsduijnen, R., Wiessner, C. & Sagot, Y.J. Regulation of LRRK2 expression points to a functional role in human monocyte maturation. *PLoS One* **6**, e21519 (2011).

208.   Hakimi, M. et al. Parkinson's disease-linked LRRK2 is expressed in circulating and tissue immune cells and upregulated following recognition of microbial structures. *J Neural Transm (Vienna)* **118**, 795-808 (2011).

209.   Dubey, J., Ratnakaran, N. & Koushika, S.P. Neurodegeneration and microtubule dynamics: death by a thousand cuts. *Front Cell Neurosci* **9**, 343 (2015).

210.   MacLeod, D. et al. The familial Parkinsonism gene LRRK2 regulates neurite process morphology. *Neuron* **52**, 587-93 (2006).

211.   Kawakami, F. et al. LRRK2 phosphorylates tubulin-associated tau but not the free molecule: LRRK2-mediated regulation of the tau-tubulin association and neurite outgrowth. *PLoS One* **7**, e30834 (2012).

212. Parisiadou, L. et al. Phosphorylation of ezrin/radixin/moesin proteins by LRRK2 promotes the rearrangement of actin cytoskeleton in neuronal morphogenesis. *J Neurosci* **29**, 13971-80 (2009).

213. Gillardon, F. Leucine-rich repeat kinase 2 phosphorylates brain tubulin-beta isoforms and modulates microtubule stability--a point of convergence in parkinsonian neurodegeneration? *J Neurochem* **110**, 1514-22 (2009).

214. Esteves, A.R. & Cardoso, S.M. LRRK2 at the Crossroad Between Autophagy and Microtubule Trafficking: Insights into Parkinson's Disease. *Neuroscientist* (2016).

215. Pellegrini, L., Wetzel, A., Granno, S., Heaton, G. & Harvey, K. Back to the tubule: microtubule dynamics in Parkinson's disease. *Cell Mol Life Sci* (2016).

216. Plowey, E.D., Cherra, S.J., 3rd, Liu, Y.J. & Chu, C.T. Role of autophagy in G2019S-LRRK2-associated neurite shortening in differentiated SH-SY5Y cells. *J Neurochem* **105**, 1048-56 (2008).

217. Tong, Y. et al. Loss of leucine-rich repeat kinase 2 causes impairment of protein degradation pathways, accumulation of alpha-synuclein, and apoptotic cell death in aged mice. *Proc Natl Acad Sci U S A* **107**, 9879-84 (2010).

218. Hinkle, K.M. et al. LRRK2 knockout mice have an intact dopaminergic system but display alterations in exploratory and motor co-ordination behaviors. *Mol Neurodegener* **7**, 25 (2012).

219. Manzoni, C. et al. mTOR independent regulation of macroautophagy by Leucine Rich Repeat Kinase 2 via Beclin-1. *Sci Rep* **6**, 35106 (2016).

220. Mortiboys, H., Johansen, K.K., Aasly, J.O. & Bandmann, O. Mitochondrial impairment in patients with Parkinson disease with the G2019S mutation in LRRK2. *Neurology* **75**, 2017-20 (2010).

221. Cherra, S.J., 3rd, Steer, E., Gusdon, A.M., Kiselyov, K. & Chu, C.T. Mutant LRRK2 elicits calcium imbalance and depletion of dendritic mitochondria in neurons. *Am J Pathol* **182**, 474-84 (2013).

222. Wang, X. et al. LRRK2 regulates mitochondrial dynamics and function through direct interaction with DLP1. *Hum Mol Genet* **21**, 1931-44 (2012).

223. Niu, J., Yu, M., Wang, C. & Xu, Z. Leucine-rich repeat kinase 2 disturbs mitochondrial dynamics via Dynamin-like protein. *J Neurochem* **122**, 650-8 (2012).

224. Su, Y.C. & Qi, X. Inhibition of excessive mitochondrial fission reduced aberrant autophagy and neuronal damage caused by LRRK2 G2019S mutation. *Hum Mol Genet* **22**, 4545-61 (2013).

225. Stafa, K. et al. Functional interaction of Parkinson's disease-associated LRRK2 with members of the dynamin GTPase superfamily. *Hum Mol Genet* **23**, 2055-77 (2014).

226. Ryan, B.J., Hoek, S., Fon, E.A. & Wade-Martins, R. Mitochondrial dysfunction and mitophagy in Parkinson's: from familial to sporadic disease. *Trends Biochem Sci* **40**, 200-10 (2015).

227. Iaccarino, C. et al. Apoptotic mechanisms in mutant LRRK2-mediated cell death. *Hum Mol Genet* **16**, 1319-26 (2007).

228. Lin, X. et al. Leucine-rich repeat kinase 2 regulates the progression of neuropathology induced by Parkinson's-disease-related mutant alpha-synuclein. *Neuron* **64**, 807-27 (2009).

229. Stafa, K. et al. GTPase activity and neuronal toxicity of Parkinson's disease-associated LRRK2 is regulated by ArfGAP1. *PLoS Genet* **8**, e1002526 (2012).

230. Sanna, G., Del Giudice, M.G., Crosio, C. & Iaccarino, C. LRRK2 and vesicle trafficking. *Biochem Soc Trans* **40**, 1117-22 (2012).

231. Esposito, G., Ana Clara, F. & Verstreken, P. Synaptic vesicle trafficking and Parkinson's disease. *Dev Neurobiol* **72**, 134-44 (2012).

232. Shin, N. et al. LRRK2 regulates synaptic vesicle endocytosis. *Exp Cell Res* **314**, 2055-65 (2008).

233. Matta, S. et al. LRRK2 controls an EndoA phosphorylation cycle in synaptic endocytosis. *Neuron* **75**, 1008-21 (2012).

234. Arranz, A.M. et al. LRRK2 functions in synaptic vesicle endocytosis through a kinase-dependent mechanism. *J Cell Sci* **128**, 541-52 (2015).

235. Piccoli, G. et al. LRRK2 controls synaptic vesicle storage and mobilization within the recycling pool. *J Neurosci* **31**, 2225-37 (2011).

236. Yun, H.J. et al. LRRK2 phosphorylates Snapin and inhibits interaction of Snapin with SNAP-25. *Exp Mol Med* **45**, e36 (2013).

237. Migheli, R. et al. LRRK2 affects vesicle trafficking, neurotransmitter extracellular level and membrane receptor localization. *PLoS One* **8**, e77198 (2013).

238. MacLeod, D.A. et al. RAB7L1 interacts with LRRK2 to modify intraneuronal protein sorting and Parkinson's disease risk. *Neuron* **77**, 425-39 (2013).

239. Beilina, A. et al. Unbiased screen for interactors of leucine-rich repeat kinase 2 supports a common pathway for sporadic and familial Parkinson disease. *Proc Natl Acad Sci U S A* **111**, 2626-31 (2014).

240. Seaman, M.N., Harbour, M.E., Tattersall, D., Read, E. & Bright, N. Membrane recruitment of the cargo-selective retromer subcomplex is catalysed by the small GTPase Rab7 and inhibited by the Rab-GAP TBC1D5. *J Cell Sci* **122**, 2371-82 (2009).

241. Beccano-Kelly, D.A. et al. Synaptic function is modulated by LRRK2 and glutamate release is increased in cortical neurons of G2019S LRRK2 knock-in mice. *Front Cell Neurosci* **8**, 301 (2014).

242. Li, X. et al. Enhanced striatal dopamine transmission and motor performance with LRRK2 overexpression in mice is eliminated by familial Parkinson's disease mutation G2019S. *J Neurosci* **30**, 1788-97 (2010).

243. Tong, Y. et al. R1441C mutation in LRRK2 impairs dopaminergic neurotransmission in mice. *Proc Natl Acad Sci U S A* **106**, 14622-7 (2009).

244. Zhou, H. et al. Temporal expression of mutant LRRK2 in adult rats impairs dopamine reuptake. *Int J Biol Sci* **7**, 753-61 (2011).

245. Melrose, H.L. et al. Impaired dopaminergic neurotransmission and microtubule-associated protein tau alterations in human LRRK2 transgenic mice. *Neurobiol Dis* **40**, 503-17 (2010).

246. Yun, H.J. et al. An early endosome regulator, Rab5b, is an LRRK2 kinase substrate. *J Biochem* **157**, 485-95 (2015).

247. Beilina, A. et al. Unbiased screen for interactors of leucine-rich repeat kinase 2 supports a common pathway for sporadic and familial Parkinson disease. *Proc Natl Acad Sci U S A* **111**, 2626-31 (2014).

248. Cho, H.J. et al. Leucine-rich repeat kinase 2 regulates Sec16A at ER exit sites to allow ER-Golgi export. *EMBO J* **33**, 2314-31 (2014).

249. Steger, M. et al. Phosphoproteomics reveals that Parkinson's disease kinase LRRK2 regulates a subset of Rab GTPases. *Elife* **5** (2016).

250. Sambrook, J. & Russell, D.W. Molecular Cloning: A Laboratory Manual (2001).

251. Vickery, R.G. & von Zastrow, M. Distinct dynamin-dependent and -independent mechanisms target structurally homologous dopamine receptors to different endocytic membranes. *J Cell Biol* **144**, 31-43 (1999).

252. Takeuchi, Y. & Fukunaga, K. Dopamine D2 receptor activates extracellular signal-regulated kinase through the specific region in the third cytoplasmic loop. *J Neurochem* **89**, 1498-507 (2004).

253. Bartlett, S.E. et al. Dopamine responsiveness is regulated by targeted sorting of D2 receptors. *Proc Natl Acad Sci U S A* **102**, 11521-6 (2005).

Mauro Rassu: "LRRK2 effect on dopamine receptor trafficking – implication in Parkinson's disease".
Ph.D. Course in Life Sciences and Biotechnologies – University of Sassari.

254. Kim, O.J. et al. The role of phosphorylation in D1 dopamine receptor desensitization: evidence for a novel mechanism of arrestin association. *J Biol Chem* **279**, 7999-8010 (2004).

255. Calo, L., Wegrzynowicz, M., Santivanez-Perez, J. & Grazia Spillantini, M. Synaptic failure and alpha-synuclein. *Mov Disord* **31**, 169-77 (2016).

256. Wang, C., Buck, D.C., Yang, R., Macey, T.A. & Neve, K.A. Dopamine D2 receptor stimulation of mitogen-activated protein kinases mediated by cell type-dependent transactivation of receptor tyrosine kinases. *J Neurochem* **93**, 899-909 (2005).

257. Beom, S., Cheong, D., Torres, G., Caron, M.G. & Kim, K.M. Comparative studies of molecular mechanisms of dopamine D2 and D3 receptors for the activation of extracellular signal-regulated kinase. *J Biol Chem* **279**, 28304-14 (2004).

258. Chen, J., Rusnak, M., Luedtke, R.R. & Sidhu, A. D1 dopamine receptor mediates dopamine-induced cytotoxicity via the ERK signal cascade. *J Biol Chem* **279**, 39317-30 (2004).

259. Kim, S.Y. et al. The dopamine D2 receptor regulates the development of dopaminergic neurons via extracellular signal-regulated kinase and Nurr1 activation. *J Neurosci* **26**, 4567-76 (2006).

260. Lewis, P.A. & Manzoni, C. LRRK2 and human disease: a complicated question or a question of complexes? *Sci Signal* **5**, pe2 (2012).

261. Ariano, M.A. et al. Agonist-induced morphologic decrease in cellular D1A dopamine receptor staining. *Synapse* **27**, 313-21 (1997).

262. Dumartin, B., Caille, I., Gonon, F. & Bloch, B. Internalization of D1 dopamine receptor in striatal neurons in vivo as evidence of activation by dopamine agonists. *J Neurosci* **18**, 1650-61 (1998).

263. Volkow, N.D., Fowler, J.S. & Wang, G.J. Imaging studies on the role of dopamine in cocaine reinforcement and addiction in humans. *J Psychopharmacol* **13**, 337-45 (1999).

264. Jones, S.R. et al. Loss of autoreceptor functions in mice lacking the dopamine transporter. *Nat Neurosci* **2**, 649-55 (1999).

265. Jeziorski, M. & White, F.J. Dopamine agonists at repeated "autoreceptor-selective" doses: effects upon the sensitivity of A10 dopamine autoreceptors. *Synapse* **4**, 267-80 (1989).

266. Parisiadou, L. et al. LRRK2 regulates synaptogenesis and dopamine receptor activation through modulation of PKA activity. *Nat Neurosci* **17**, 367-76 (2014).

267. Godena, V.K. et al. Increasing microtubule acetylation rescues axonal transport and locomotor deficits caused by LRRK2 Roc-COR domain mutations. *Nat Commun* **5**, 5245 (2014).

268. Law, B.M. et al. A direct interaction between leucine-rich repeat kinase 2 and specific beta-tubulin isoforms regulates tubulin acetylation. *J Biol Chem* **289**, 895-908 (2014).

269. Beccano-Kelly, D.A. et al. LRRK2 overexpression alters glutamatergic presynaptic plasticity, striatal dopamine tone, postsynaptic signal transduction, motor activity and memory. *Hum Mol Genet* **24**, 1336-49 (2015).

270. Segura-Aguilar, J. et al. Protective and toxic roles of dopamine in Parkinson's disease. *J Neurochem* **129**, 898-915 (2014).